UNIVERSITÄT ZU LÜBECK

From the Institute for Experimental and Clinical Pharmacology and Toxicology

of the University of Lübeck

Director: Prof. Dr. Markus Schwaninger

"The reactive pyruvate metabolite dimethylglyoxal in experimental disease models and the role of *Ilvbl* in its generation in the brain"

Dissertation

for Fulfillment of Requirements

for the Doctoral Degree

of the University of Lübeck

from the Department of Natural Sciences

Submitted by

Riccardo Costalunga

from Casalmaggiore (Italy)

Lübeck 2025

First referee:	Prof. Dr. Markus Schwaninger
Second referee:	Prof. Dr. Charlotte Uetrecht
Date of oral examination:	September 26th, 2025
Approved for printing:	October 2nd, 2025

Table of contents

Table of contents

Summary

Reactive glucose metabolites are involved in neurological complications of diabetes by the generation of advanced glycated end products (AGEs), which are formed by the interaction between α-dicarbonyls and proteins. AGEs induce oxidative stress, inflammation and tissue damage and have been associated with neuropathy, nephropathy and retinopathy. So far, only the α-dicarbonyls 3-deoxyglucosone, glyoxal and methylglyoxal have been recognized as reactive glucose metabolites and associated with complications in diabetes. Only recently, the α-dicarbonyl dimethylglyoxal (DMG) has been categorized as mammal cellular pyruvate metabolite, and its levels were higher in the plasma of type-1 diabetic mice and in the serum of patients with diabetes. In this thesis, I investigated the α-dicarbonyl DMG in mouse models under pathological conditions and its metabolic pathway in mammals using liquid chromatography coupled to tandem mass spectrometry (LC-MS^2).

Here, plasma DMG concentrations were upregulated in mouse experimental models of type-1 and type-2 diabetes. In contrast, high-fat diet did not influence the serum levels of DMG, suggesting that diabetic conditions – but not obesity itself – are associated with plasma DMG upregulation and accumulation. Moreover, DMG levels were enormously augmented in the ipsilateral side of a mouse model of hyperglycemic stroke compared to sham control. Interestingly, DMG levels were also higher in the contralateral hemisphere of the brain of mice with stroke compared to sham controls, showing that the contralateral hemisphere is also affected by ischemic stroke. Furthermore, the current study confirmed that DMG is a post-glycolytic product in mammals and its levels are increased under hypoxic conditions *in vitro*. Then, I investigated the role of the gene ilvB acetolactate synthase-like (*Ilvbl*), the mammal orthologue gene of acetolactate synthase that generates DMG from pyruvate in bacteria, yeast and plants. Importantly, *Ilvbl* knockout reduced DMG levels in the brain of mice with type-1 diabetes or hyperglycemic stroke, showing that *Ilvbl* has conserved its role in DMG generation in mammals. Moreover, DMG interacted with lysine, generating the glycated amino acid Nε-3-hydroxy-2-butanonelysine (HBL), confirming that DMG is a reactive compound and can glycate proteins generating AGEs. Thus, DMG induced oxidative stress and neuroinflammation in mouse hippocampal neuronal (HT-22) cells, probably based on protein glycation.

In conclusion, this study characterizes the α-dicarbonyl DMG in experimental models under pathological conditions, showing that DMG could play a significant role in diabetic complications and ischemic stroke complications. DMG is the only α-dicarbonyl generated after glycolysis, and the current discovery could explain why cells consuming lactate – such as neurons – are not protected by dicarbonyl stress. Importantly, this study shows that ILVBL plays a significant role in the DMG generation from pyruvate in the brain of acute or chronic hyperglycemic mice. Further investigation

on DMG and the attenuation of its concentrations may lead to improvement in diabetic and ischemic stroke complications.

Zusammenfassung

Reaktive Glukosemetabolite sind an den neurologischen Komplikationen von Diabetes beteiligt, indem sie sogenannte Advanced Glycation End Products (AGEs) bilden. Diese entstehen durch die Wechselwirkung zwischen α-Dicarbonylen und Proteinen. AGEs induzieren oxidativen Stress, Entzündungen und Gewebeschäden und werden mit Neuropathie, Nephropathie und Retinopathie in Verbindung gebracht. Bislang wurden nur die α-Dicarbonyle 3-Deoxyglucosone, Glyoxal und Methylglyoxal als reaktive Glukosemetabolite identifiziert, die mit Komplikationen bei Diabetes in Verbindung stehen. Kürzlich wurde auch Dimethylglyoxal (DMG) als α-Dicarbonyl und zellulärer Pyruvat-Metabolit von Säugetieren beschrieben. Seine Konzentrationen waren im Plasma von Mäusen mit Typ-1-Diabetes und im Serum von Diabetes-Patienten erhöht. In dieser Arbeit habe ich das α-Dicarbonyl DMG in Mausmodellen unter pathologischen Bedingungen untersucht und seinen Stoffwechselweg in Säugetieren mithilfe der Flüssigchromatographie, gekoppelt an die Tandem-Massenspektrometrie (LC-MS^2), analysiert.

In experimentellen Mausmodellen für Typ-1- und Typ-2-Diabetes wurden erhöhte DMG-Konzentrationen im Plasma beobachtet. Im Gegensatz dazu hatte eine fettreiche Ernährung keinen Einfluss auf die DMG-Serumspiegel. Dies deutet darauf hin, dass diabetische Erkrankungen, nicht jedoch Adipositas selbst, mit einer Erhöhung und Akkumulation von DMG im Plasma verbunden sind. Darüber hinaus war der DMG-Spiegel auf der ipsilateralen Seite eines Mausmodells für einen hyperglykämischen Schlaganfall enorm erhöht. Interessanterweise waren die DMG-Spiegel auch in der kontralateralen Hemisphäre des Gehirns von Mäusen mit Schlaganfall erhöht, was zeigt, dass auch diese Hemisphäre von dem ischämischen Schlaganfall betroffen ist. Die aktuelle Studie bestätigte zudem, dass DMG ein postglykolytisches Produkt in Säugetieren ist und seine Konzentrationen unter hypoxischen Bedingungen *in vitro* erhöht sind.

Des Weiteren untersuchte ich die Rolle des Gens ilvB acetolactate synthase-like (*Ilvbl*). Diese Enzym ist bei Bakterien, Hefen und Pflanzen für die Erzeugung von DMG aus Pyruvat verantwortlich. Wichtig ist, dass der Knockout von *Ilvbl* den DMG-Spiegel im Gehirn von Mäusen mit Typ-1-Diabetes oder hyperglykämischem Schlaganfall reduziert. Dies zeigt, dass die Rolle von *Ilvbl* bei der DMG-Erzeugung in Säugetieren konserviert wurde. Darüber hinaus konnte gezeigt werden, dass DMG mit Lysin interagiert und die glykierte Aminosäure Nε-3-Hydroxy-2-Butanonelysin (HBL) bildet. Dies bestätigt, dass DMG eine reaktive Verbindung ist, die Proteine unter Bildung von AGEs glykieren kann. Dementsprechend, induzierte DMG oxidativen Stress und Neuroinflammation in neuronalen Zellen des Hippocampus der Maus (HT-22), was wahrscheinlich auf der Glykierung von Proteinen beruht.

Zusammenfassend lässt sich sagen, dass diese Studie das α-Dicarbonyl DMG in experimentellen Modellen unter pathologischen Bedingungen charakterisiert und zeigt, dass DMG eine bedeutende

Zusammenfassung

Rolle bei diabetischen Komplikationen und ischämischen Schlaganfallkomplikationen spielen könnte. DMG ist das einzige α-Dicarbonyl, das nach der Glykolyse entsteht. Die aktuelle Entdeckung könnte erklären, warum Zellen, die Laktat verbrauchen – wie Neuronen – nicht vor Dicarbonylstress geschützt sind. Von Bedeutung ist zudem, dass diese Studie zeigt, dass ILVBL eine bedeutende Rolle bei der DMG-Bildung aus Pyruvat im Gehirn von akut oder chronisch hyperglykämischen Mäusen spielt. Weitere Untersuchungen zu DMG und dessen Konzentration könnten zu einer Verbesserung diabetischer Komplikationen und ischämischer Schlaganfallkomplikationen führen.

1. Introduction

1.1. Glucose metabolism

Glucose is the most important metabolic energy source and is essential for life. Chemically, glucose is a monosaccharide characterized by six carbon atoms ($C_6H_{12}O_6$, **Fig. 1.1**) and is a reducing sugar. In plants, glucose is generated from carbon dioxide and water by photosynthesis and stored as cellulose and starch.

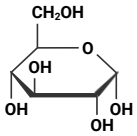

Fig. 1.1 | Glucose
The molecule structure was created with Biorender.com

Generally, humans consume glucose directly or indirectly through diet by sucrose or polysaccharides. Sucrose is a disaccharide composed of glucose and fructose, while polysaccharides (e.g., starch) are long-chained monosaccharide polymers. Some polysaccharides get demolished to glucose and other monosaccharide molecules due to enzymatic actions. For example, sucrose is converted to glucose and fructose by β-fructofuranosidase, and lactose is degraded to glucose and galactose by lactase. Subsequently, glucose is metabolized in cells to produce energy or is stored in liver, fat or muscle cells as glycogen[1].

Glycolysis is an anaerobic metabolic pathway that converts glucose into two pyruvate molecules in the cytosol (**Fig. 1.2**). Glycolysis also produces two molecules of adenosine triphosphate (ATP) and two molecules of reduced nicotinamide adenine dinucleotide (NADH). Glycolysis consists of ten reactions and can be distinguished into two phases: the preparatory phase and the pay-off phase. In the preparatory phase, one glucose molecule is converted to two molecules of glyceraldehyde 3-phosphate (G3P) by consuming two ATP molecules. Therefore, two G3P molecules are metabolized into two pyruvate molecules with the gain of four molecules of ATP and two molecules of NADH. Then, pyruvate is catabolized to L-lactate by lactate dehydrogenase (LDH) or acetyl-CoA by pyruvate dehydrogenase complex (PDC, **Fig. 1.2**). Subsequently, the mitochondrial citrate synthase (CS) catalyzes the condensation of acetyl-CoA with oxaloacetate generating citrate, a Krebs cycle (or citric acid cycle, TCA) and *de novo* lipogenesis substrate (**Fig. 1.2**).

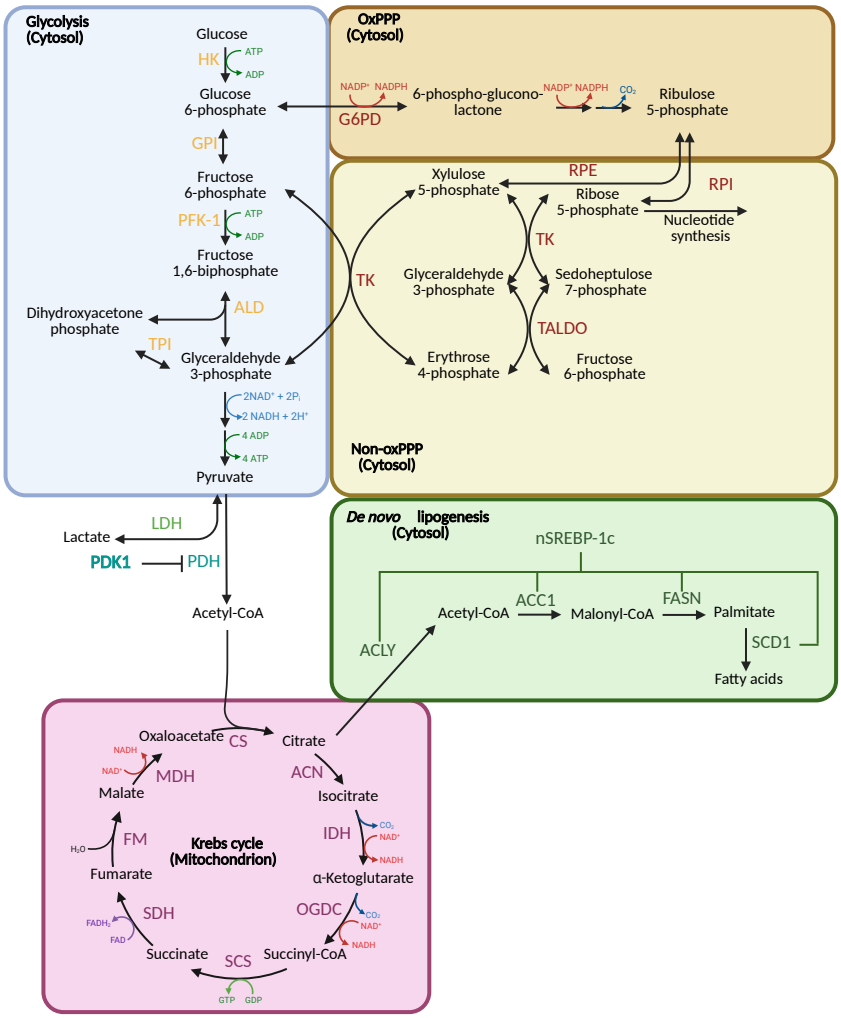

Fig. 1.2 | Schematic illustration of glucose catabolism by glycolysis, oxidative (ox) and non-ox pentose phosphate pathway (PPP), Krebs cycle and de novo lipogenesis.

Detailed abbreviation legend is provided on page 88. The illustration was created with Biorender.com and adapted after TeSlaa, T., Ralser, M., Fan, J., et al., 2023[2]; and Haddad, A., Mohiuddin, S., S., 2023[3].

The Krebs cycle is an aerobic metabolic pathway that generates three molecules of NADH, one equivalent of reduced flavine adenine dinucleotide ($FADH_2$) and one of guanosine triphosphate (GTP) in the mitochondrion (**Fig. 1.2**). Two acetylic carbons are oxidated during the TCA cycle, generating four electron pairs and two carbon dioxide (CO_2) molecules. Lastly, NADH and $FADH_2$ molecules interact with oxygen molecules, producing water, whereas the reducing coenzymes are used to generate ATP by oxidative phosphorylation[4]. The phosphate/oxygen (P/O) ratio estimates the generated chemical energy, calculating 2.73 ATP molecules from NADH oxidation and 1.64 ATP molecules from $FADH_2$ oxidation. Moreover, the TCA metabolite citrate can be converted to fatty acids by *de novo* lipogenesis (**Fig. 1.2**). Glucose is also involved in the generation of nucleotides by the pentose phosphate pathway (PPP, **Fig. 1.2**). Here, the glycolytic product glucose 6-phosphate is converted to ribulose 5-phosphate,

generating two NADPH molecules[2]. Subsequently, ribulose 5-phosphate is isomerized to ribose 5-phosphate, a precursor of nucleotide synthesis. During the non-oxidative part of the pentose phosphate pathway, ribulose 5-phosphate and ribose 5-phosphate are also catabolized to fructose 6-phosphate and G3P, two glycolytic metabolites[2].

Apart from the previously described pathways that show the crucial role of glucose in the generation of chemical energy, glucose also generates toxic compounds during its catabolism. Since these metabolites react quickly with other endogenous molecules, they have been recognized as reactive glucose metabolites.

1.2 α-Dicarbonyls

α-Dicarbonyls are organic compounds containing two adjacent carbonyl groups (**Fig. 1.3**). The nomenclature "α" refers to the position of the carbon directly attached to the functional group. Chemically, α-dicarbonyls can be distinguished into 1,2-dialdehydes, 1,2-ketoaldehydes and 1,2-diketones. Endogenously, they originate from glucose and are highly reactive. The interaction between α-dicarbonyls and proteins or lipids leads to the formation of advanced glycation end products (AGEs)[5,6].

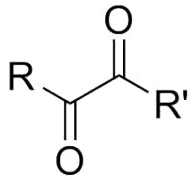

Fig. 1.3 | α-Dicarbonyl
The molecule structure was created by ChemSketch.

1.2.1 3-Deoxyglucosone

3-Deoxyglucosone (3-DG, **Fig. 1.4**) belongs to the group of 1,2-ketoaldehyde, and it is generated from glucose via Maillard reaction[7] (**Fig. 1.6**). The Maillard reaction is a non-enzymatic reaction that consists of the interaction between the carbonyl group of the reducing sugar, such as glucose, and the amino group of amino acids, followed by the rearrangements of the Amadori products to 3-DG[7]. 3-DG interacts with amino acids, generating AGEs and glycated amino acids like pyrraline, 3-deoxyglucosone lysine dimer (DOLD) and glycated 3-DG in histone H1 (3-DG-H1)[8-10]. On the other hand, 3-DG can be catabolized to 3-deoxyfructose by aldoketo reductases[11,12]. In addition to its endogenous formation from glucose, 3-DG has been detected in several foods and drinks, such as yoghurt and red wine[13]. Previous studies showed that 3-DG concentrations are upregulated in the serum of patients with diabetes and plasma of type-1 diabetic rats[14-17].

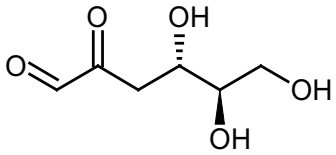

Fig. 1.4 | 3-Deoxyglucosone
The molecule structure was created by ChemSketch.

1.2.2 Glyoxal

Glyoxal (Gx, **Fig. 1.5**) is the smallest dialdehyde and a metabolite generated from glucose degradation, lipid peroxidation and glycated protein degradation. Gx is also a Maillard reaction product (**Fig. 1.6**), during which Gx is generated from both Schiff bases and Amadori products[6]. Moreover, Gx is directly generated from glucose by autooxidation (**Fig. 1.6**) and is also a product of lipid peroxidation of linolenic acid[18]. In addition, Gx is taken up with the diet[13,19,20]. Gx is metabolized to glycolate via the glyoxalase system or to glyoxylate via aldehyde dehydrogenase[21,22]. Subsequently, glyoxylate is catabolized to oxalate[22], and high levels of this metabolite can lead to the formation of calcium oxalate stones in the urinary tract[22,23]. Gx concentrations were higher in the plasma of patients with diabetes[24]. Previous studies showed that Gx induced the generation of reactive oxygen species (ROS) in rat hepatocytes and the expression of the proinflammatory gene cyclooxygenase (COX)-2 in human vascular endothelial cells[25,26]. As 3-DG, Gx can also generate AGEs and glycated amino acids, such as glyoxal-derived lysine dimer (GOLD) and N^{ε}-carboxymethyl-lysine (CML)[27].

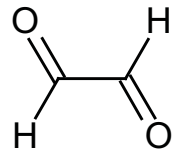

Fig. 1.5 | Glyoxal
The molecule structure was created by ChemSketch.

1.2.3 Methylglyoxal

Methylglyoxal (MG, **Fig. 1.7**) is a 1,2-ketoaldehyde, mainly generated from glucose by glycolysis (**Fig. 1.6**). Specifically, MG is a product of the degradation of the glycolytic isomers G3P and dihydroxyacetone phosphate[28,29].

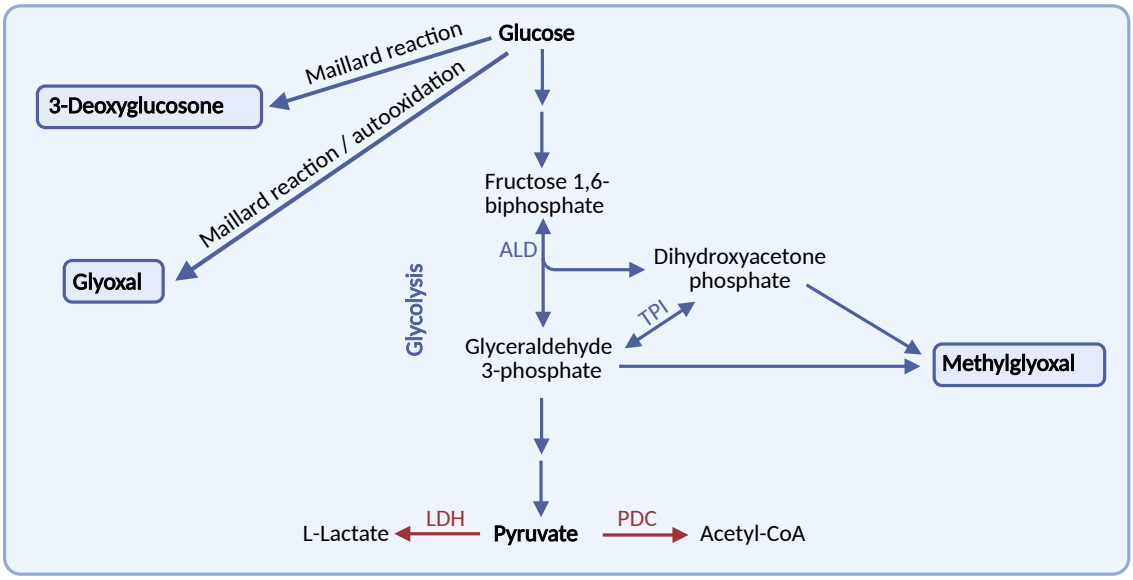

Fig. 1.6 | Schematic illustration of the 3-deoxyglucose, glyoxal and methylglyoxal anabolic pathways.
The illustration was created with Biorender.com. ALD = aldolase, TPI = triose phosphate isomerase, LDH = lactate dehydrogenase, PDC = pyruvate dehydrogenase complex.

Moreover, MG is also generated from fatty acids via the formation of acetone and acetol and from glycine and threonine via aminoacetone[30-32]. In addition, MG is exogenously taken up by the consumption of ordinary food or drinks[13,20,33]. Interestingly, high levels of MG were found in the Australian *Leptospermum* (Manuka) honey and its concentrations were positively associated with the anti-bacterial proprieties of the honey[34,35]. MG generates glycated amino acids, such as methylglyoxal-lysine dimer (MOLD), argpyrimidine, and AGEs, by interacting with lysine or arginine[36,37]. MG induces oxidative stress, inflammation and endothelial dysfunction in type-2 diabetic rats and in control rats treated with MG[38]. MG is mainly catabolized to D-lactate via the glyoxalase system. More specifically, glyoxalase-1 converts methylglyoxal-reduced glutathione hemithioacetal to S-Lactoylglutathione, while the enzyme glyoxalase-2 converts the previous product to D-lactate[39,40].

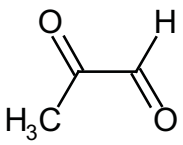

Fig. 1.7 | Methylglyoxal
The molecule structure was created by ChemSketch.

1.2.4 Dimethylglyoxal

The polar α-diketone dimethylglyoxal (or diacetyl, DMG, **Fig. 1.9**) is a yellow liquid compound with a strong odor and an intensive buttery and milky taste[41]. Due to this peculiar taste, DMG has been used as a flavoring agent in food, such as microwave popcorn or cookie dough. However, the occupational exposition to DMG has been associated with developing the irreversible lung disease bronchiolitis obliterans, known as "popcorn workers´ lung"[42]. Nevertheless, DMG is naturally present in drinks or food such as milk, tea, puddings, cheese, butter and yogurt[13,20,43-45]. DMG has been reported as a natural product of fermentation and detected in wine and beer[13,46,47]. In bacteria, plants and yeast, DMG is generated from pyruvate. Pyruvate is converted to α-acetolactate by the enzyme acetolactate synthase (ALS), followed by oxidative decarboxylation to DMG. Lastly, DMG is enzymatically reduced to acetoin and subsequently to 2,3-butanediol (**Fig. 1.8**)[48]. ALS is also involved in the synthesis of the branched-chain amino acids (isoleucine, leucine and valine) in plants and microorganisms[49-51]. However, ilvB acetolactate synthase-like (ILVBL, or 2-hydroxyacyl-CoA lyase 2), the mammal orthologue gene of ALS, lost its function to catalyze the branched-chain amino acids, making isoleucine, leucine and valine essential nutrients for mammals.

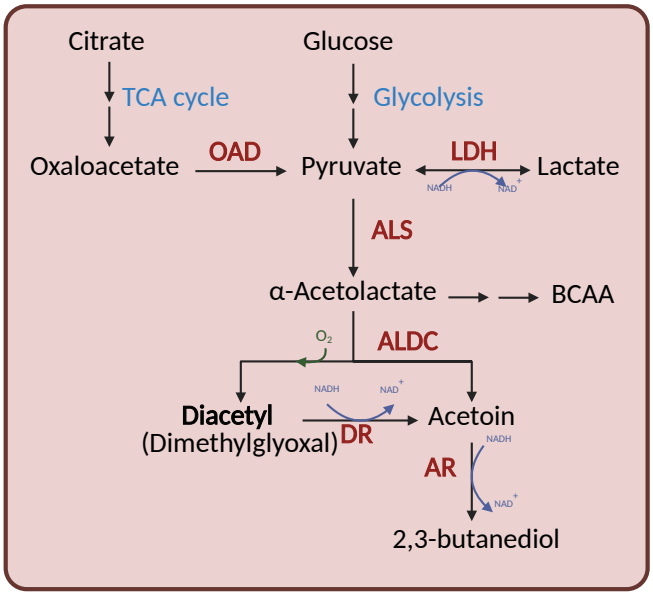

Fig. 1.8 | Schematic illustration of the dimethylglyoxal metabolic pathway in (lactic acid) bacteria.
The Illustration was created with Biorender.com and adapted after Tian, H., *et al.*, 2022[52]; Lerm, E., *et al.*, 2010[53]; and Yu, S., Zheng, B., Chen, Z., *et al.*, 2021[51]. TCA = tricarboxylic acid, OAD = oxaloacetate decarboxylase, LDH = lactate dehydrogenase, ALS: acetolactate synthase, ALDC = acetolactate decarboxylase, DR = diacetyl reductase, AR = acetoin reductase.

Recently, DMG has been recognized as an endogenous product of pyruvate metabolism in mice[54,55]. So far, ILVBL has not been investigated in terms of its role in the formation of DMG in mammals. However, recent studies showed that ILVBL is located in the endoplasmic reticulum and involved in the α-oxidation of 2-hydroxy fatty acids to odd-chain fatty acids in sphingolipids in mammals[56,57]. So far, DMG has not been associated with diabetes or hyperglycemic conditions. Only recently, Rhein *et al.* found higher plasma and brain DMG concentrations in type-1 diabetic mice[54,55].

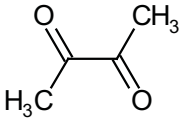

Fig. 1.9 | Dimethylglyoxal
The molecule structure was created by ChemSketch.

1.3 Diabetes mellitus

Diabetes mellitus has been recognized as a disease since antiquity. Based on the high production of urine and the quick passage of water through the body, ancient Greeks coined the term “diabetes” which means “to pass through” to describe this abnormality[58]. Further, the term “mellitus” means “honey”, which refers to the glucose surplus in the urine. In 1889, Minkowski and von Mering, two German physiologists, associated diabetes mellitus with the pancreas because the removal of a dog´s pancreas caused polyuria and higher glucose concentrations in the urine[59]. In 2022, around 830 million people had diabetes and its prevalence has rapidly increased in low- and middle-income countries compared to high-income countries[60]. Diabetes was the 8th leading cause of death in the world in 2021, and the number of deaths almost doubled since 2000[61].

Diabetes mellitus is a chronic disease characterized by high blood glucose levels and is caused by impaired insulin secretion or insulin activity. Insulin is a hormone produced by β-cells of the islets of Langerhans located in the pancreas, and it is generated from preproinsulin. After crossing the membrane of the endoplasmic reticulum, preproinsulin is converted into proinsulin, a stable prohormone due to the generation of intramolecular disulfide bridges. Subsequently, the inactive proinsulin is converted to insulin due to the action of prohormone convertases PC2 and PC3 (**Fig. 1.10**)[62,63]. Insulin is a polypeptide hormone and comprises 51 amino acids with a total molecular weight of 5808 g/mol[64]. In healthy conditions, insulin activates the insulin receptor, a transmembrane receptor tyrosine kinase expressed in adipose tissue, skeletal muscle and other tissues. Insulin receptor activation leads to phosphorylation and activation of the insulin receptor substrate (IRS-1). Then, phosphatidylinositol 3-kinase (PI3K) is activated by phosphorylated IRS-1, inducing the conversion of phosphatidylinositol-4,5-bisphosphate (PIP2) to phosphatidylinositol-3,4,5-bisphosphate (PIP3) and the consequent phosphorylation of protein kinase B (PBK or AKT). The PBK activation leads to the

release and translocation of glucose transporter type 4 (GLUT4) from intracellular vesicles to the cell membrane (**Fig. 1.11**)[65,66]. Thus, GLUT4 allows the uptake of glucose in adipose and striated tissue.

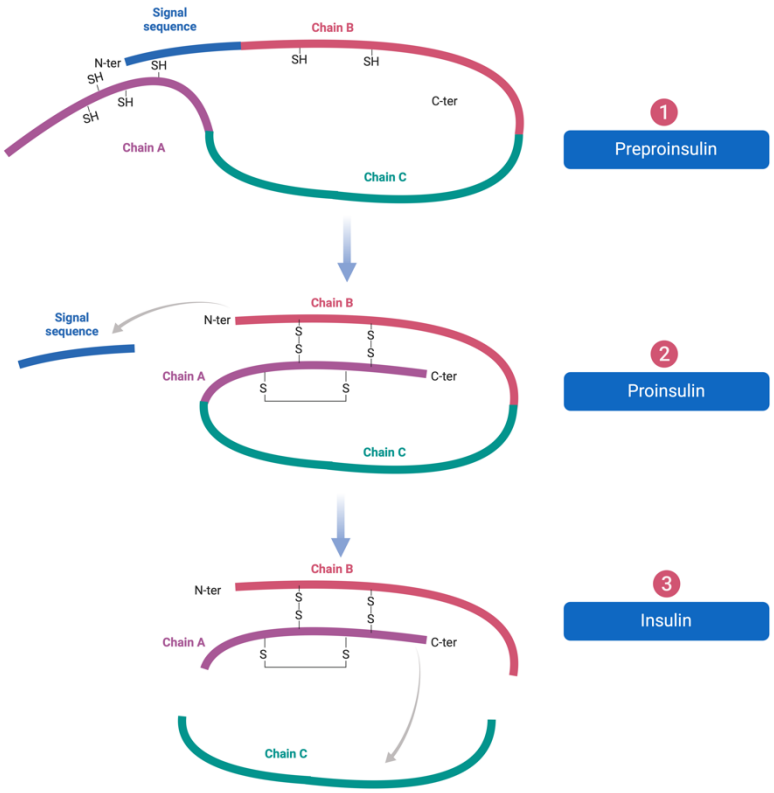

Fig. 1.10 | Schematic illustration of the generation of insulin from preproinsulin.

The illustration was modified after a template with Biorender.com.

The brain, nerve and blood cells take up glucose without insulin mediation[67]. In particular, glucose transporters GLUT1 and GLUT3 are activated independently of insulin concentrations. GLUT 1 is mainly expressed in brain endothelial cells, kidneys, and placenta, and it transports glucose through the blood-brain barrier, whereas GLUT3 is primarily expressed in neurons[68,69]. Thus, peripherical hyperglycemic conditions increase intracellular glucose concentrations in neurons and brain endothelial cells[70,71]. Although neurons metabolize glucose by glycolysis, they also take up extracellular lactate generated from glucose in glial cells[72,73]. In particular, monocarboxylate transporter (MCT)-1 is the carrier of lactate release in the extracellular space, while MCT-2 catalyzes lactate uptake in neurons (**Fig. 1.12**)[74]. According to the World Health Organization (WHO) guidelines, hyperglycemic conditions are characterized by fasting blood glucose concentrations higher than 126 mg/dl (7 mmol/l) on two separate tests[75]. Hyperglycemic conditions can also be diagnosed based on the concentration of glycated hemoglobin (HbA_{1c} > 6.4 %) or by an oral glucose tolerance test (fasting plasma glucose concentrations > 200 mg/dl or 11.1 mM, 2 hours after oral glucose uptake)[76,77].

Diabetes mellitus can be classified into two categories: type-1 and type-2 diabetes. Type-1 diabetes is an autoimmune disease concomitant with the destruction of pancreatic β-cells[78]. The loss of β-cells leads to insulin deficiency and the consequent impediment of GLUT4 release and translocation to the cell membrane (**Fig. 1.11**). Thus, insulin scarcity causes hyperglycemic conditions in the extracellular space. Type-1 diabetes can be diagnosed at any age, with the highest peak of diagnosis during childhood[79]. Patients with type-1 diabetes show a symptomatic picture based on polydipsia, polyuria, higher production of ketone bodies (ketoacidosis) and weight-loss[78,80,81]. Type-1 diabetes-related symptoms and complications can be attenuated by the treatment with exogenous insulin. In addition, diet management and physical activity could improve the management of type-1 diabetes[78].

Type-2 diabetes is a chronic disease characterized by insulin resistance (**Fig. 1.11**), partial dysfunction of β-cells and hyperglycemic conditions[82,83]. Similar to the type-1 diabetic symptoms, type-2 diabetes causes polydipsia, fatigue and polyuria[84]. Type-2 diabetes is related to family history and environmental factors such as a diet rich in sugars and fat, tobacco use and physical inactivity[85]. Thus, obesity is a risk factor for type-2 diabetes, making lifestyle management an important role in the prevention of type-2 diabetes development[86,87]. Moreover, pharmaceutical intervention can prevent or manage type-2 diabetes. For example, metformin, one of the most common type-2 diabetic drugs, was able to reduce fasting glucose concentrations in plasma and HbA1c values in metformin-treated compared to placebo-treated patients with type-2 diabetes[88].

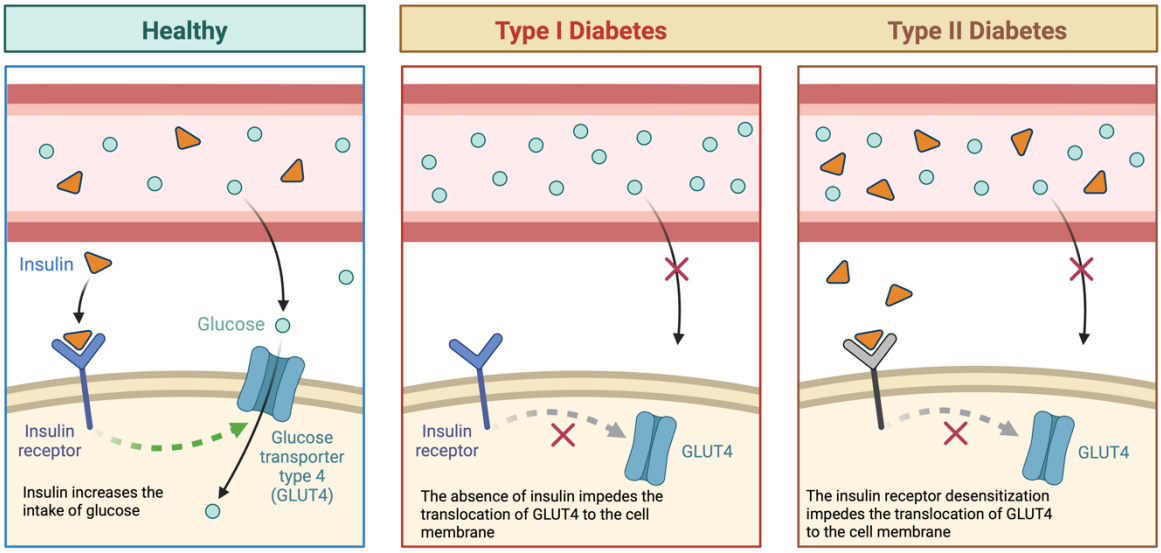

Fig. 1.11 | Schematic illustration of role of insulin in healthy and type-1 and type-2 diabetic organisms.
The illustration was modified after a template with Biorender.com.

Notably, diabetes can lead to macrovascular and microvascular long-term complications[87,89]. Macrovascular complications of diabetes consist in cerebrovascular diseases (e.g. stroke) and

peripherical vascular diseases[87,89]. Diabetic microvascular complications comprise neuropathy, retinopathy and nephropathy[87,90]. In both macro- and microvasculature, protein glycation and AGE formation by α-dicarbonyls causes alteration of normal protein functions, such as enzymatic activity alteration or glycation of low-density lipoproteins (LDLs) involved in diabetic atherosclerosis[91,92]. Furthermore, collagen glycation caused by α-dicarbonyls worsened the arterial wall features in type-1 diabetic rats[93]. Generally, several studies showed that diabetic and hyperglycemic conditions increased levels of glycated amino acids in experimental animal models of type-1 diabetes[94-96]. In particular, upregulation of glycated amino acids was found in peripheral nerves in diabetic animals and patients, suggesting the important role of these adducts in the development of diabetic neuropathy[96,97].

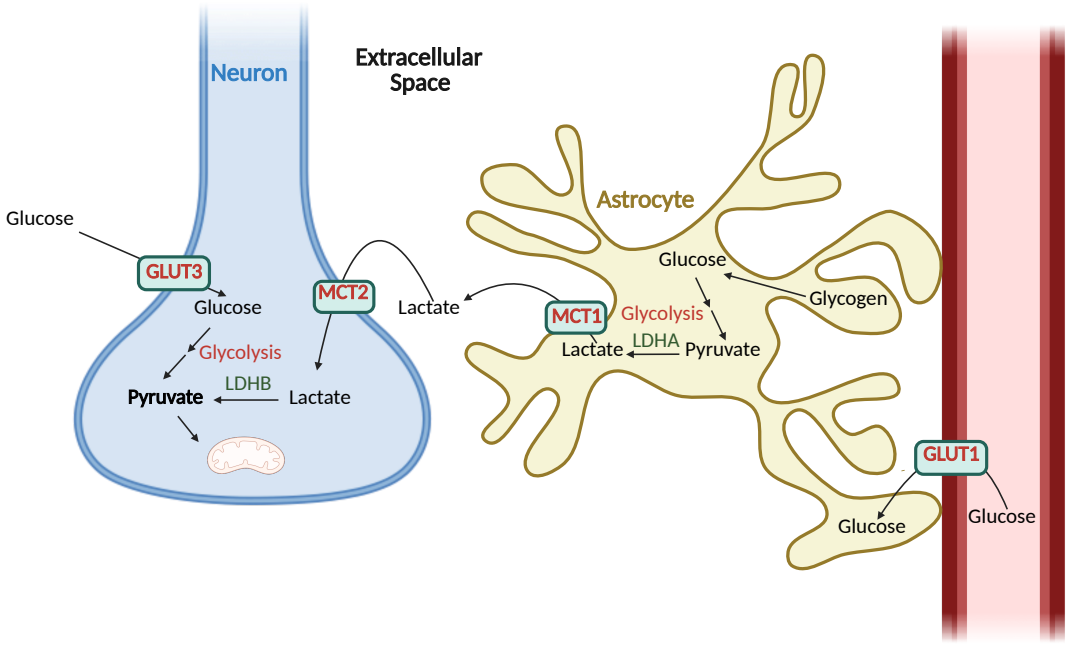

Fig. 1.12 | Schematic illustration of neuron-astrocyte lactate shuttle and lactate consumption in neurons. The illustration was created with Biorender.com and adapted after Allaman, I., *et al.*, 2015[98]; and Newington, J., T., *et al.*, 2013[99]. GLUT = translocating glucose transporter type, LDH = lactate dehydrogenase, MCT = monocarboxylate transporter.

Previous studies showed that AGEs induced apoptosis in rat neuronal and Schwann cells by interacting with the receptor for AGEs (RAGE), indicating that AGEs could cause diabetic neuropathy through demyelination[100,101]. RAGE is also expressed in endothelial cells, whose overexpression negatively affects the endothelial membrane repair[102]. Moreover, the binding of AGEs with RAGE induces the activation of the nuclear factor kappa-light-chain-enhancer of activated B cells (NF-κB) cascade, causing oxidative stress and overexpression of proinflammatory cytokines such as interleukin-1α and tumor necrosis factor-α (TNF) in endothelial cells and activated (M1) macrophages[103-106]. Furthermore,

RAGE is expressed in astrocytes and is associated with the neurodegenerative Huntington´s disease by NF-κB translocation in astrocytic nuclei[107].

Therapeutic strategies can decrease glycation and AGE generation, reducing the development of diabetic complications. A British study found that acetylsalicylic acid can prevent cataract in type-1 diabetic mice, suggesting that acetylsalicylic acid can reduce the protein glycation by acetylation of amino groups[108]. Moreover, pimagedine (also called aminoguanidine) is a relevant drug in diabetic complications. This molecule can interact with 3-DG and Gx, inhibiting the Maillard reaction and preventing the generation of AGEs[109,110]. Moreover, MG and DMG also interact with pimagedine *in vitro*[109,111,112]. However, pimagedine is an investigational drug since the drug approval process was stopped during clinical trials[109].

1.4 Ischemic stroke

Stroke is the second leading cause of death in the world, with the highest incidence in East Asia and East Europe[113]. Stoke can be distinguished in hemorrhagic and ischemic stroke. Hemorrhagic stroke is caused by the rupture of a brain blood vessel and consequent bleeding[114]. However, the majority of strokes globally are classified as ischemic stroke, which consists of an impairment of the blood flow in the brain[113,115]. While age, sex and family history are unmodifiable risk factors, diabetes mellitus, hypertension, physical activity, depression, tobacco and alcohol consumption, and chronic inflammation are modifiable risk factors which can be controlled by targeted interventions[116]. Notably, hyperglycemic conditions were also found in patients without diabetes after ischemic stroke[117,118]. Stress-induced hyperglycemia is caused by increased gluconeogenesis and insulin resistance by the action of several hormones and cytokines. For example, a Danish prospective study showed a positive association between serum cortisol levels and acute stroke injury[119]. Due to the established correlation between cortisol and blood glucose levels by the upregulation of gluconeogenesis, this study suggested that ischemic stroke induces hypothalamic-pituitary-adrenal axis activation and the consequent hyperglycemia in patients without diabetes[119]. Moreover, the α-adrenergic agonist epinephrine and other catecholamines augment gluconeogenesis in the liver and consequently blood glucose concentrations[120]. Furthermore, catecholamines increase glucagon secretion by the agonistic interaction with β-adrenergic receptors, inducing the increase of blood glucose levels by glycogenolysis in the liver[121].

Ischemic stroke triggers a cascade, which consists of a series of biochemical reactions potentially leading to neuronal death[122]. Local hypoxic conditions result from the tissue's lack of oxygen due to the low blood supply. Under hypoxia, the hypoxia-inducible factor (HIF)-1α protein is stabilized based on the inactivation of prolyl hydroxylase[123]. HIF-1 is a transcription factor comprising HIF-1α and HIF-

1β subunits[124]. In particular, HIF-1α increases the expression of the pyruvate dehydrogenase kinase 1 (PDK1), an enzyme that causes the downregulation of pyruvate dehydrogenase (PDH)[125,126]. PDH is the enzyme that catalyzes the generation of pyruvate to acetyl-CoA. Thus, the inhibition of this gene leads to the downregulation of the TCA cycle. Under these conditions, glycolysis becomes the primary ATP source, generating a significantly lower chemical energy than during physoxia[127]. Moreover, hypoxia and lower energy generation cause the increase of ROS and the consequent damage to cell membranes[122,128,129].

Furthermore, the decreased energy production also causes ionic pump damage, leading to the dysregulation of ionic balance with extracellular release of potassium ions (K^+) and intracellular accumulation of sodium ions (Na^+)[122,130]. In addition, ischemia stimulates the synaptic release of glutamate, increasing the activation of α-amino-3-hydroxy-5-methyl-4-isoxazole propionic acid (AMPA) and *N*-methyl-D-aspartate (NMDA) receptors. The activation of AMPA and NMDA receptors leads to membrane depolarization, causing the increase of intracellular calcium ions (Ca^{2+}), inducing excitotoxicity[122,130]. The Ca^{2+} accumulation leads to the stimulation of ROS, phospholipases and proteases[131]. Phospholipases catalyze the hydrolysis of phospholipids to fatty acids. Thus, higher activity of phospholipases leads to cell membrane damage since it mainly consists of phospholipids. In particular, phospholipase A2 generates arachidonic acid, which is metabolized to prostaglandins (PG) by COX-1 (or PTGS1) or COX2 (PTGS2) or to leukotrienes in inflammatory cells by the 5-lipoxygenase pathway[132,133]. Prostaglandins and leukotrienes are eicosanoids involved in inflammation with PGE_2 being one of the most active prostaglandins involved in pain, edema and vasodilatation[132]. On the other hand, Ca^{2+}-dependent protease overactivation may also damage the cell membrane by Ca^{2+}-dependent matrix metalloproteinases - proteases involved in the degradation of extracellular membranes[122,134]. Moreover, intracellular Ca^{2+} accumulation stimulates nitric oxide synthases (NOS), an enzyme class that catalyzes the generation of citrulline and nitric oxide (NO) from L-arginine[135,136]. The interaction of free radicals ($^{\bullet}NO$) with superoxide ($^{\bullet}O_2^-$) generates peroxynitrite ($^{-}OONO$), a reactive nitrogen species (RNS)[136]. RNS lead to lipid peroxidation, deoxyribonucleic acid (DNA) damage and cell apoptosis[137,138]. Consequently, ischemic-induced upregulation of ROS and RNS, proinflammatory molecules, and matrix metalloproteinases causes blood-brain barrier (BBB) damage[134]. The BBB is a selective semi-permeable and protective membrane comprising endothelial cells, microglial cells, pericytes and astrocytic end-feet[139,140]. The BBB plays a critical metabolic and physical role in protecting the central nervous system (CNS) from neurotoxic molecules[140,141]. In particular, occludin and claudins are tight junction proteins between adjacent endothelial cells and are crucial for the protective role of the BBB[142]. Thus, BBB damage leads to neuroinflammation and cerebral edema and worsens the cognitive impairment prognosis[143,144].

1.5 Liquid chromatography – tandem mass spectrometry

During this doctoral research, derivatized α-dicarbonyls and glycated amino acids were investigated using liquid chromatography coupled tandem mass spectrometry (LC-MS^2). The combination of liquid chromatography with mass spectrometry allows the identification of specific analytes in a complex mixture. Liquid chromatography (LC) and mass spectrometry (MS) are not directly linked due to their incompatibilities, such as the necessity of MS to analyze gas-phase ions and different pressures between LC and MS systems. To solve this problem, liquid chromatography and mass spectrometry are connected by an interface.

1.5.1 Liquid chromatography

Chromatography is a physical technique that separates a mixture into singular components based on their distribution between the stationary and mobile phase[145]. The stationary phase may be a solid, liquid or gel. The mobile phase moves in a clear direction and may be a liquid, gas or a supercritical fluid[145]. Thus, liquid chromatography is a physical separation technique characterized by a liquid mobile phase. High-performance liquid chromatography (HPLC, previously an acronym for high-pressure liquid chromatography) is characterized by good chromatographic resolution and high pressure (up to 400 bar)[146]. These conditions allow a constant flow rate and a reproducible and robust chromatographic process[146]. The HPLC system could be illustrated with the following primary apparatus (**Fig. 1.13**):

1. **Mobile phase reservoirs:** An isocratic elution means that the eluent composition stays constant during the chromatographic separation. On the other hand, a gradient elution implies that the mobile phase composition changes gradually or continuously during the elution. Eluents can be distinguished in polar (e.g. water or methanol) or non-polar (e.g. acetonitrile). This is crucial for a proper analyte separation during the elution in this study. Furthermore, eluents can be classified as organic or inorganic. Generally, the inorganic solvent water is mainly used because of its high polarity, safety advantages and costs. In contrast, organic solvents (e.g. methanol) can be preferred to water due to their better efficiency in the electrospray ionization (ESI) system, based on their faster evaporation and lower surface tension[147].
2. **Pump**: This apparatus provides a stable and controlled flow rate to the separation system and the interface[145,146].
3. **Injector:** This device introduces the liquid sample into the mobile phase. The injector is a crucial device to ensure precision and accuracy. Air bubbles must not be present in the sample, and an internal standard can reduce inaccuracy problems (e.g., matrix effects)[146]. An internal standard is a compound chemically and physically similar to the analytes of interest and added to the

sample with a known concentration. For MS detection, an isotopically labeled form of the analyte is the ideal internal standard because it does not occur naturally, has a different mass-to-charge ratio (*m/z)* and shows very similar chemical behavior.

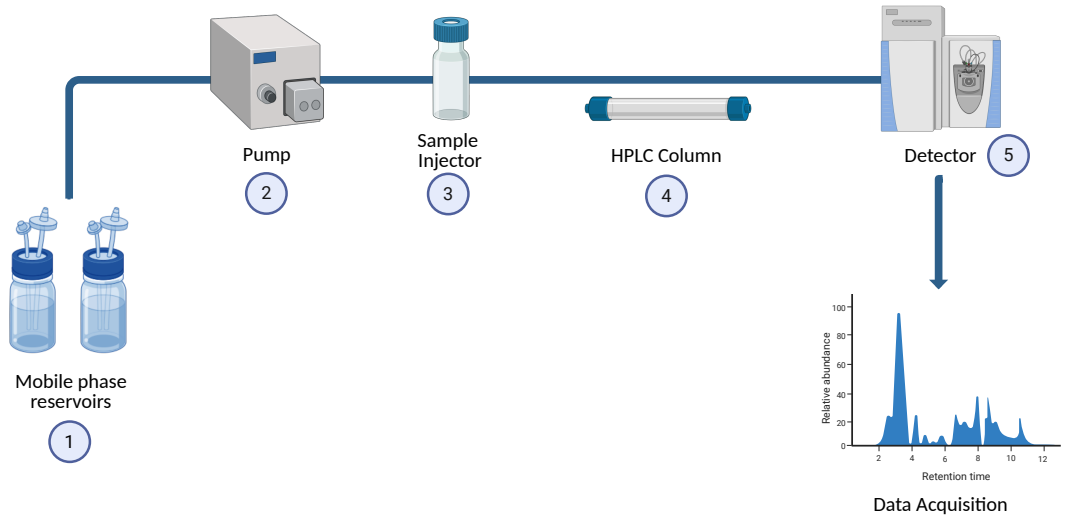

Fig. 1.13 | Schematic illustration of high-performance liquid chromatography (HPLC) system.
The illustration was modified after a template (Eunice Huang) with Biorender.com.

4. **Stationary phase:** Reverse-phase chromatography is the most used elution procedure in HPLC. Here, the mobile phase is more polar than the stationary phase[145]. The most popular stationary phase is the C18 column, characterized by octadecyl alkyl groups bonded to the silica material. In normal-phase chromatography, the stationary phase is more polar than the mobile phase.
5. **Detector:** This apparatus measures the change in the eluent composition based on the physical (e.g., absorption wavelength of the analyte in an ultraviolet detector) or chemical (e.g., *m/z* of analyte in an MS detector) characteristics[145].

For LC-MS analysis, LC is used prior to MS detection because this technique allows the separation of molecules based on their polarity, reducing the mixture's complexity (e.g. reducing matrix effect) and contributing to the identification of analytes with the same molecular weight based on different retention times.

1.5.2 Electrospray ionization

As previously mentioned, LC and MS are linked through an interface. ESI is a soft ionization technique that transforms analytes into gas-phase ions to allow their detection with the mass spectrometer[148]. In contrast to other interfaces (e.g. electron ionization, EI), ESI can ionize thermally labile molecules, avoiding degradation and fragmentation. This passage occurs at atmospheric pressure[146,149].

Mechanistically, the eluent is introduced in the ionization chamber by a metal capillary with a high voltage (e.g. + 3-4 kV for positive ionization, **Fig. 1.14**). The electric field induces the generation of aerosol composed of highly charged droplets. The positive or negative charges are generated from the oxidation (positive ion mode) or reduction (negative ion mode) of solvent molecules by redox reactions[150]. The nebulization is improved by the coaxial sheath nitrogen (N_2) gas[150]. Moreover, N_2 supports the decrease of charged droplet size by solvent evaporation[150]. Solvent evaporation causes the increase of the charge density of the droplets up to the Rayleigh limit when the Coulomb repulsion is greater than the droplet surface tension. Thus, Coulomb fission (or explosion) occurs, leading to smaller droplets. Solvent evaporation and Coulomb fission occur several times until analytes are ejected from the droplets as gas-phase ions before entering the mass spectrometer[150].

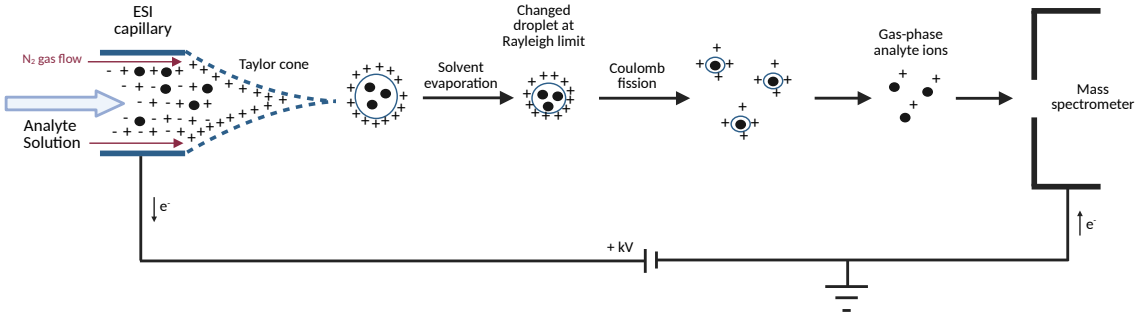

Fig. 1.14 | Schematic illustration of the electrospray ionization (ESI) mechanism in positive mode.

The illustration was modified after a template (Sabitri Lamichhane) with Biorender.com and adapted after Banerjee, S., and Mazumdar, S., 2012[150]; and Konermann, L., *et al.*, 2013[148]. N_2 = molecular nitrogen.

1.5.3 Mass spectrometry

After ionization, molecules are detected by the mass spectrometer. Analytes are characterized based on their mass to charge ratio (*m/z*) and physical-chemical proprieties[151]. In particular, MS^2 provides additional identification confidence based on the fragmentation of the analyte of interest.

The resolution (R) is the parameter related to the ability to differentiate between ions with very similar *m/z*[146].

$$R = \frac{\text{observed } m/z}{\Delta\, m/z}$$

In this study, we detected derivatized α-dicarbonyls and glycated amino acids with a Thermo Scientific™ TSQ Endura™ triple quadrupole mass spectrometer or Thermo Scientific™ Q-Exactive™ quadrupole-orbitrap™ hybrid high-resolution mass spectrometer. The TSQ Endura ensures high

sensitivity and robustness, whereas the high resolution of Q-Exactive allows the identification of ^{13}C-labeled α-dicarbonyls.

- The TSQ Endura triple quadrupole mass spectrometer is a tandem mass spectrometer based on three quadrupoles in series (**Fig. 1.15**). The first (Q1) and third (Q3) quadrupoles are mass analyzers and detect the precursor and product mass, respectively. The second quadrupole (Q2) is used as collision cell, where the precursor ion is fragmented based on the collision with an inert gas (collision-induced dissociation, CID). Multiple reaction monitoring (MRM) is used to detect specific product ions originating from a specific precursor ion. This Q1 to Q3 mass selection is called a mass transition[151]. Lastly, product ions collide with the detector, generating an electric current detected by a voltmeter[152].

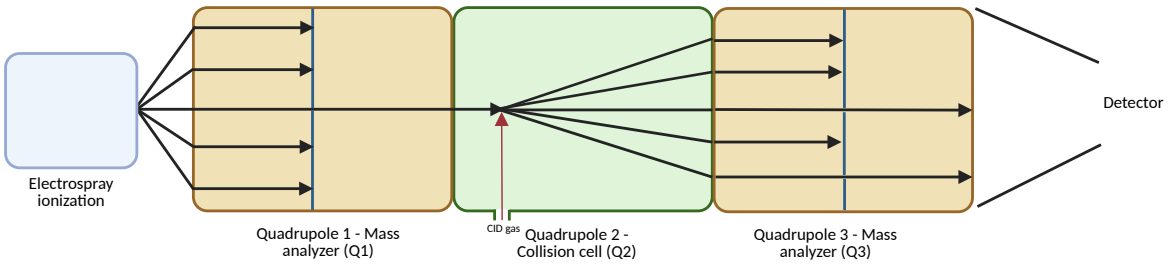

Fig. 1.15| Schematic illustration of the scan on a triple quadrupole mass spectrometer (MS).
The illustration was modified with Biorender.com after Ardrey, 2003[146]; and Yost, 2022[153]. CID = collision-induced dissociation.

- The Q-Exactive™ quadrupole-orbitrap™ hybrid high-resolution mass spectrometer is a tandem mass spectrometer based on combining a quadrupole mass filter and the ion trap Orbitrap mass analyzer (**Fig. 1.16**)[154]. Ions are transported from the ESI source into the instrument by a stacked ring ion guide (S-Lens)[155]. The S-Lens guarantees high ion current with a low sample amount and low injecting times, due to the reduction of ion losses and larger entrance orifice diameters[155,156]. Depending on the experimental settings, the quadrupole mass filter allows only the passage of ions of interest prior to their fragmentation in the high-energy collisional dissociation (HCD) collision cell[154]. The HCD collision cell and the Orbitrap mass analyzer are separated by the C-trap, which traps the fragments and releases the fragmented ions to Orbitrap mass analyzer, when a certain ion count is achieved[157]. Then, a strong electric field attracts the ions to the Orbitrap central electrode. Here, ions are trapped around the central electrode and axially oscillate with a frequency related to their specific *m/z*. Then, two outer electrodes detect the image current based on the ion axial oscillation[158]. The image current

from the ions is subsequently processed and converted to frequency and *m/z* by Fourier Transformation (FT)[154]. A full scan with a specific *m/z* range allows the identification of all molecule ions without fragmentation. Parallel Reaction Monitoring (PRM) is the targeted method used to analyze the product ion spectra from preselected precursor ions with high specificity in a high-resolution mass spectrometer[159].

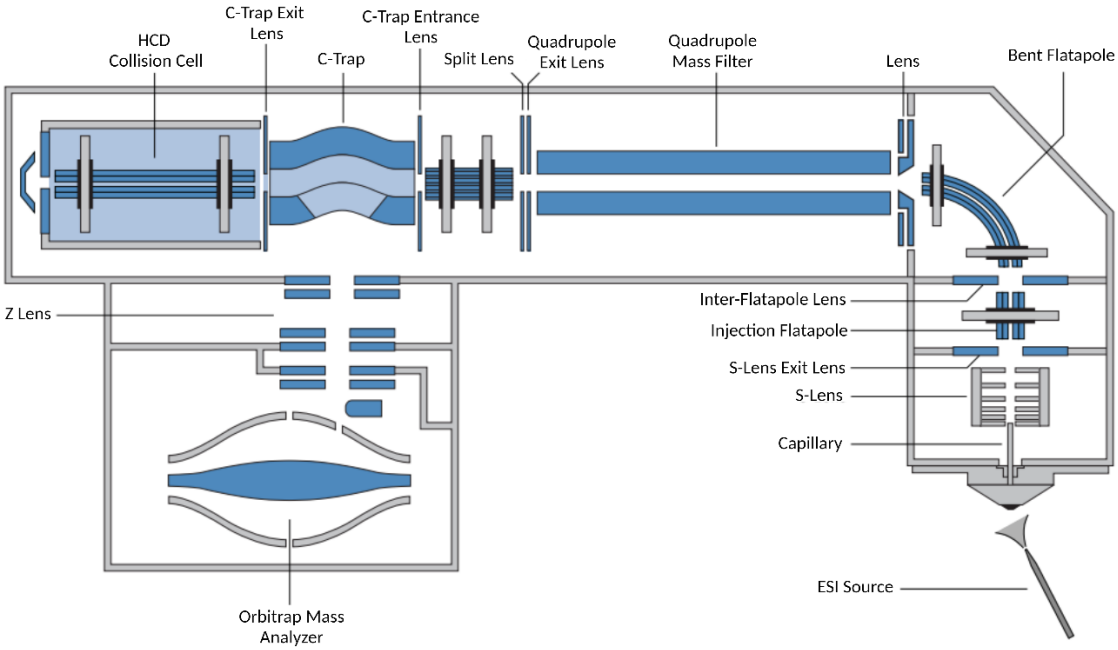

Fig. 1.16 | Schematic and detailed illustration of Q-Exactive mass spectrometer.

The illustration was modified after Michalski, A., *et al.*, 2011[154] with Biorender.com. HCD = high-energy collisional dissociation, S-Lens = stacked ring ion guide, ESI = electrospray ionization.

1.6. Objectives

Diabetes complications are attributed to AGEs, which are generated by the interaction of the α-dicarbonyls with proteins. They induce neuroinflammation, tissue damage and oxidative stress. So far, only 3-DG, Gx and MG have been recognized as reactive glucose metabolites and associated with diabetic complications through protein glycation. Recently, DMG has been classified as a product of cellular pyruvate metabolism and higher concentrations of this compound were found in the serum of patients with diabetes and plasma of type-1 diabetic mice[54,55].

The first aim of my doctoral research is a significant characterization of DMG concentrations in several mouse models under pathological conditions. Thus, concentrations of DMG are investigated in plasma, serum, and tissue homogenate of type-1 diabetic, type-2 diabetic, diet-induced obesity and experimental models of hyperglycemic and ischemic stroke.

Introduction

In bacteria, yeast and plants, DMG is generated from pyruvate by ALS[48]. Thus, this doctoral thesis aims to improve the knowledge of metabolic pathways involved in the generation of DMG in mammals. In particular, the role of the mammal orthologue gene *Ilvbl* is tested in DMG generation using a *Ilvbl* knockout mouse model under different pathological conditions. This doctoral thesis also focuses on other characteristics of the reactive glucose metabolite DMG, such as its capacity to glycate amino acids, its ability to cross intestinal and blood-brain barriers and its effect on neuroinflammation and oxidative stress *in vitro*.

In summary, I mainly address the following points in this study:

- Investigation of the α-dicarbonyl DMG in several mouse models (type-1 diabetes, type-2 diabetes, diet-induced obesity and ischemic stroke).
- Evaluation of the role of *Ilvbl* in the generation of DMG using *Ilvbl* deficient mice.

2. Materials

2.1 Chemicals, reagents and enzymes

Compound	Manufacturer
[$^{12}C_3$]-Pyruvate (≥ 99 %)	Sigma Aldrich, St. Louis (USA)
[$^{13}C_3$]-Pyruvate (99 %)	Cambridge Isotope Laboratories, Inc., Andover (USA)
[$^{13}C_4$]-Dimethylglyoxal	Eptes, Vevey (Switzerland)
2-Methyl-2-butanol	Sigma Aldrich, St. Louis (USA)
2,2,2—Tribromoethanol (Avertin®)	Sigma-Aldrich, St. Louis (USA)
3-Deoxyglucosone (≥ 75 %)	Sigma Aldrich, St. Louis (USA)
Accutase® solution	Sigma Aldrich, St. Louis (USA)
Acetic 5-(chloromethyl)-2-(3,6-diacetoxy-2,7-dichloro-9H-xanthen-9-yl) benzoic anhydride (CM-H_2DCFDA)	Thermo Fisher Scientific, Waltham (USA)
Acetonitrile (LC-MS grade, ≥ 99.9 %)	Merck, Darmstadt (Germany)
Argon (99.999 %)	Airliquid, Düsseldorf (Germany)
Bovine serum albumin	Sigma Aldrich, St. Louis (USA)
Bradford reagent	Sigma Aldrich, St. Louis (USA)
D-(+)-Glucose (≥ 99.5 %)	Merck, Darmstadt (Germany)
D-(+)-Saccharose (or Sucrose)	Carl Roth, Karlsruhe (Germany)
D-[$^{13}C_6$]-Glucose (≥ 99 %)	Sigma Aldrich, St. Louis (USA)
D4-Methylglyoxal	University Hospital Heidelberg, Heidelberg (Germany)
D8-o-Phenylendiamine (98 %)	CDN Isotopes, Pointe-Claire (Canada)
Deuterated N_ε-(1-carboxyethyl)-L-lysine	PolyPeptide Laboratories, San Diego (USA)
DharmaFECT 4 transfection reagent	Horizon Discovery Group, Cambridge (UK)
Diethylenetriaminepentaacetic acid (DETAPAC)	Sigma Aldrich, St. Louis (USA)
Diethylpyrocarbonate	Sigma-Aldrich, St. Louis (USA)
Dimethyl sulfoxide (DMSO)	Sigma Aldrich, St. Louis (USA)
Dimethylglyoxal (97 %)	Sigma Aldrich, St. Louis (USA)
Formic acid (ULC-MS grade, 99 %)	Biosolve Chimie, Dieuze (France)
Glyoxal (40 % in water)	Sigma Aldrich, St. Louis (USA)
Heparin	Ratiopharm, Ulm (Germany)
Hydrogen chloride (Hydrochloric acid fuming 37 %)	Merck, Darmstadt (Germany)
Hydrogen peroxide solution (30 %)	Merck, Darmstadt (Germany)
Isoflurane	Baxter, Deerfield (USA)
Ketamine 100 mg/ml	Dr. E. Graeub AG, Bern (Switzerland)
M-MLV reverse transcriptase (200 u/µl)	Promega, Madison (USA)
Methanol (LC-MS grade, ≥ 99.9 %, LiChrosolv®)	Merck, Darmstadt (Germany)
Methylglyoxal (40 % in water)	Sigma Aldrich, St. Louis (USA)
Nucleoside triphosphate (dNTP)	Thermo Fisher Scientific, Waltham (USA)
N_ε-(1-Carboxyethyl)-L-lysine	PolyPeptide Laboratories, San Diego (USA)
ON-TARGETplus Mouse *Ilvbl* (216136) siRNA – SMARTpool	Horizon Discovery Group, Cambridge (UK)
ON-TARGETplus Non-targeting pool	Horizon Discovery Group, Cambridge (UK)

Penicillin-streptomycin	Sigma Aldrich, St. Louis (USA)
Pentobarbital sodium	Boehringer Ingelheim, Ingelheim am Rhein (Germany)
Pierce LTQ ESI negative ion calibration solution	Thermo Fisher Scientific, Waltham (USA)
Pierce LTQ Velos ESI positive ion Calibration solution	Thermo Fisher Scientific, Waltham (USA)
Platinum SYBR Green qPCR SuperMix, Invitrogen	Thermo Fisher Scientific, Waltham (USA)
Poly-D-lysine solution (1.0 mg/ml)	Sigma Aldrich, St. Louis (USA)
Random primers	Promega, Madison (USA)
Ringer´s solution	Berlin-Chemie, Berlin (Germany)
RNasin® ribonuclease inhibitor (40 U/µl)	Promega, Madison (USA)
Saline solution	Fresenius Kabi, Bad Homburg vor der Höhe (Germany)
Streptozotocin (≥ 98 %)	Sigma Aldrich, St. Louis (USA)
Tri-sodium citrate dihydrate	Fisher Scientific International, Inc., Pittsburgh (USA)
Trichloroacetic acid (≥ 99 %)	Sigma Aldrich, St. Louis (USA)
Trypsin / EDTA (0.05 % / 0.02 % in DPBS)	PAN-Biotech GmbH, Aidenbach (Germany)
Water (LC-MS grade)	Merck, Darmstadt (Germany)
Xylazine (Rompun®) 2 %	Bayer Vital GmbH, Leverkusen (Germany)

2.2 Buffers and media

Buffer or medium	Manufacturer
Dulbecco´s Modified Eagle's Medium (DMEM)	PAN-Biotech GmbH, Aidenbach (Germany)
Dulbecco´s Phosphate-buffered saline (DPBS)	Biowest, Nuaillé (France)
Fetal Calf Serum (FCS)	Sigma Aldrich, St. Louis (USA)
Gibco™ DMEM, no glucose	Fisher Scientific International, Inc., Pittsburgh (USA)
Gibco™ Opti-MEM™	Fisher Scientific International, Inc., Pittsburgh (USA)
Mouse Moloney murine leukemia virus (M-MLV) buffer	Promega, Madison (USA)
Roswell Park Memorial Institute (RPMI) 1640	Fisher Scientific International, Inc., Pittsburgh (USA)

2.3 Instruments

Instrument	Specification	Manufacturer
Blender	Bullet Blender®, Storm 24	Next Advance, Inc., Troy (USA)
Blood glucose meters	Ascensia Elite XL ACCU-CHECK®, Guide me	Roche Diagnostic, Basel (Switzerland) Roche Diagnostic, Basel (Switzerland)
Cell culture incubators	New Brunswick™ Galaxy® 170 S MIDI 40 10-16679	Eppendorf, Hamburg (Germany) Thermo Fisher Scientific, Waltham (USA) BINDER GmbH, Tuttlingen (Germany)

Materials

Centrifuges	5430 R MIKRO 220R	Eppendorf, Hamburg (Germany) Hettich, Tuttlingen (Germany)
Cryotome	CM3050 S	Leica Biosystems, Wetzlar (Germany)
Electro-coagulator	ICC 50	Erbe Elektromedizin GmbH, Tübingen (Germany)
Freezers	Mediline (- 20 °C) Comfort NoFrost (- 20 °C) HFU T SERIES (- 80 °C)	Liebherr, Bulle (Switzerland) Liebherr, Bulle (Switzerland) Thermo Fisher Scientific, Waltham (USA)
Fridges	Mediline (+ 4 °C) Electronic (+ 4 °C)	Liebherr, Bulle (Switzerland) Bosch, Gerlingen (Germany)
Fume extraction plant	SAFE 2020	Thermo Fisher Scientific, Waltham (USA)
Heat sterilizer	2712	Köttermann®, Ütze (Germany)
High performance liquid chromatography	Dionex Ultimate 3000	Thermo Fisher Scientific, Waltham (USA)
Hot-air sterilizer	Köttermann® 2712	Köttermann GmbH, Uetze (Germany)
Ion source	Heated-electrospray ionization (HESI-II) probe	Thermo Fisher Scientific, Waltham (USA)
Mass spectrometers	TSQ Endura™ Q-Exactive™ Hybrid Quadrupole-Orbitrap™	Thermo Fisher Scientific, Waltham (USA) Thermo Fisher Scientific, Waltham (USA)
Microscope	CK2	Olympus, Tokyo (Japan)
Mini centrifuge	Sprout®	Heathrow Scientific, Vernon Hills (USA)
MS syringe	1750RNR 500 µl	Hamilton Company, Reno (USA)
Multipette®	E3X	Eppendorf, Hamburg (Germany)
Physiological cell culture workstation	InvivoO_2	Baker HQ, Sanford (USA)
Pipette pump	Pipetus®	Hirschmann® Laborgeräte GmbH & Co. KG, Eberstadt (Germany)
Pipettes	Research® plus (10 µl, 100 µl, 200 µl, 1000 µl, 5 ml)	Eppendorf, Hamburg (Germany)
Plate reader	CLARIOstar	BMG Labtech, Ortenberg (Germany)
qPCR cycler	LightCycler® 96	Roche, Basel (Switzerland)
Rotator	Intelli-Mixer RM-2L	LTF – Labortechnik, Wasserburg am Bodensee (Germany)
Scales	ENTRIS® precision balance (323I-1S) ENTRIS® analytical balance (124I-1S)	Sartorius AG, Göttingen (Germany) Sartorius AG, Göttingen (Germany)
Sonicator	SONOREX DIGIPLUS DL 514 BH	BANDELIN electronic GmbH & Co. KG, Berlin (Germany)
Spectrophotometer	NanoDrop 2000®	Thermo Fisher Scientific, Waltham (USA)
Stereomicroscope	SM33	Helmut Hund GmbH, Wetzlar (Germany)
Temperature control module	TKM-0904	FMI (Föhr Medical Instruments GmbH), Seeheim-Jugenheim (Germany)
Thermomixers	C Compact 5436	Eppendorf, Hamburg (Germany) Eppendorf, Hamburg (Germany) Eppendorf, Hamburg (Germany)
Vortex mixers	REAX 2000	Heidolph, Schwabach (Germany)

	REAX top Reamix 2789 Vortex-Genie® 2	Heidolph, Schwabach (Germany) Glaswarenfabrik Karl Hecht GmbH & Co. KG, Sondheim vor der Rhön (Germany) Scientific Industries, Inc., Bohemia (USA)
Water bath	VWB2	VWR International, Radnor (USA)
Water purification system	Milli-Q® Integral	MilliporeSigma, Burlington (USA)

2.4 Software

Name	Version	Manufacturer
Adobe Acrobat Pro	2024.005.20320	Adobe Inc., San Jose (USA)
Adobe Illustrator	29.2	Adobe Inc., San Jose (USA)
Adobe Photoshop	2024	Adobe Inc., San Jose (USA)
BioRender	-	BioRender, Toronto (Canada)
CLARIOstar data analysis	3.20 R2	BMG Labtech, Ortenberg (Germany)
CLARIOstar software	5.21 R2	BMG Labtech, Ortenberg (Germany)
FreeStyle	1.6	Thermo Fisher Scientific, Waltham (USA)
GraphPad Prism	8.0	GraphPad Software, Boston (USA)
LightCycler® 96	1.1	Roche, Basel (Switzerland)
NanoDrop 2000/2000c	1.5	Thermo Fisher Scientific, Waltham (USA)
Office365	-	Microsoft, Redmond (USA)
Thermo Xcalibur™	4.3	Thermo Fisher Scientific, Waltham (USA)

2.5 Consumables

Name	Specification	Manufacturer
Aluminum foil	LABSOLUTE®	TH. Geyer GmbH & Co. KG, Renningen (Germany)
Butterfly cannula	Safety-Multifly 21 G	Sarstedt, Nümbrecht (Germany)
Cell culture flasks	CELLSTAR® (25 cm^2, 75 cm^2)	Greiner Bio-One GmbH, Kremsmünster (Austria)
Cell culture plates	CELLSTAR® (24-well plate, 96-well plate)	Greiner Bio-One GmbH, Kremsmünster (Austria)
Conical tubes	FALCON® (15 ml, 50 ml)	Corning, Glendale (USA)

Materials

Diets	Teklad Global, 2018, 18 % Protein Rodent Diet, 2918	Inotiv Inc., Lafayette (USA)
	D12492, 60 kcal % Fat 1314	Research Diets Inc., New Brunswick (USA) Altromin Spezialfutter GmbH & Co. KG, Lage (Germany)
EDTA Tubes	Microvette®, CB300	Sarstedt, Nümbrecht (Germany)
Glass bottles	Fischerbrand®	Fisher Scientific International, Inc., Pittsburgh (USA)
	DURAN®	Hirschmann® Laborgeräte GmbH & Co. KG, Eberstadt (Germany)
	LABSOLUTE®	TH. Geyer GmbH & Co. KG, Renningen (Germany)
Glass vials	MRQ30™ 1.2 ml	Sigma Aldrich, St. Louis (USA)
Graduated cylinders	DURAN® (500 ml,	Hirschmann® Laborgeräte GmbH & Co. KG, Eberstadt (Germany)
Laboratory film	Parafilm®	Amcor plc, Zürich (Switzerland)
Liquid chromatography columns	CORTECS® T3 (2.7 µm, 100 mm x 2.1 mm)	Waters Corporations, Milford (USA)
	XBridge BEH Amide (2.5 µm, 100 mm x 2.1 mm)	Waters Corporations, Milford (USA)
Needles	MicrolanceTM 3, 27G x ½", 0.4 x 13 mm	Becton, Dickinson and Company, Franklin Lakes (USA)
	Reusable Feeding Needle 24	Fine Science Tools, Vancouver (Canada)
Nitrile gloves	Peha-soft® Nitrile	Hartmann, Heidenheim an der Brenz (Germany)
Pasteur pipette	LABSOLUTE®	TH. Geyer GmbH & Co. KG, Renningen (Germany)
PCR 96-well-plate	LightCycler® 480 Multiwell Plate 96, white	Roche, Basel (Switzerland)
Pipette tips	epT.I.P.S.® Standard; 2-200 µl, 50-1000 µl; 0.1-5 ml	Eppendorf, Hamburg (Germany)
Reaction tubes	1.5 ml/2 ml Safe-Lock Tubes 1.5 ml/2 ml	Sarstedt, Nümbrecht (Germany) Eppendorf, Hamburg (Germany)
RNA purification kit	NucleoSpin® 96 RNA purification kit	Macherey-Nagel GmbH & Co. KG, Düren (Germany)
Scalpels	Feather disposable scalpel (No. 10, 11 and 22)	Feather, Osaka (Japan)
Sealing foil	LightCycler®, 480	Roche, Basel (Switzerland)
Serological pipettes	CELLSTAR® (5 ml, 10 ml and 25 ml)	Greiner Bio-One GmbH, Kremsmünster (Austria)

Materials

Syringes	1 ml/50 ml	Becton, Dickinson and Company, Franklin Lakes (USA)
Tissue	Precision Wipes™ ABENA®, cosmetic wipes	Kimberly-Clark Corporation, Irving (USA) ABENA A/S, Aabenraa (Denmark)
Vinyl gloves	Vinyl 2000 PF	Meditrade® GmbH, Kiefersfelden (Germany)
Zirconium oxide beads	ZrOB05 (0.5 mm)	Next Advance, Troy (USA)

3. Methods

3.1. Liquid chromatography – tandem mass spectrometry analysis

3.1.1 α-Dicarbonyls

3.1.1.1 α-Dicarbonyl extraction

α-Dicarbonyls were extracted and derivatized as previously described with some modifications[160,161]. First, the internal standards deuterated MG (d4-MG; 200 nM; 0.2 µl per µl plasma or serum and 0.1 µl per µl tissue homogenate or cell culture supernatant) and/or [$^{13}C_3$]-pyruvate (200 µM; 0.2 µl per µl plasma and 0.1 µl per µl tissue homogenate or cell culture supernatant) were added to 60 µl plasma, 60 µl serum, 120 µl tissue homogenate or 60 µl cell culture supernatant. Proteins were precipitated by adding ice-cold trichloroacetic acid (TCAA; 25 % w/v, 0.4 µl per µl sample). Plasma or serum samples were diluted with 48 µl LC-MS grade water, whereas tissue homogenate and cell culture supernatant samples were extracted without dilution. Samples were mixed with Vortex-Genie® 2 (Scientific Industries, Inc., 10 s) and a thermomixer (4 °C, 10 min, 1,000 rpm), followed by centrifugation (4 °C, 10 min, 14,000 rpm). Afterwards, the supernatant was transferred to a new Eppendorf tube, and the derivatizing agent deuterated o-phenylenediamine (d8-DB; 1 mM, 0.11 µl per µl plasma or serum and 0.08 µl tissue homogenate or cell culture supernatant), freshly dissolved in hydrogen chloride (HCl)/diethylenetriaminepentaacetic acid (DETAPAC; 0.5 mM in 200 mM HCl) was added to the supernatant. Samples were incubated for 4 hours at room temperature in the dark, in order to generate quinoxalines from the interaction between the α-dicarbonyls and derivatizing agent (**Fig. 3.1**).

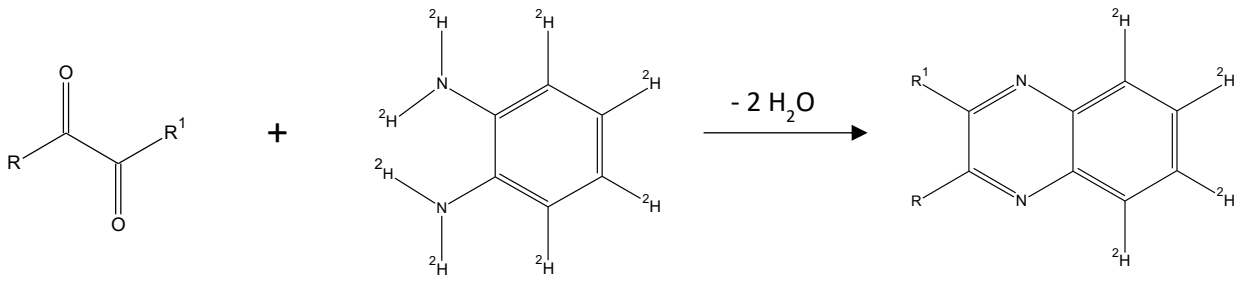

α-Dicarbonyl D8-o-phenylenediamine Quinoxaline

Fig. 3.1 | Illustration of the reaction between α-dicarbonyls and d8-o-phenylenediamine and relative product quinoxaline.

After derivatization, samples were centrifugated (4 °C, 10 min, 14,000 rpm), and the supernatant was transferred to glass vials for LC-MS analysis. Standard solutions were prepared as described below in **Tables 3.1**, **3.2** and **3.3** and derivatized as the extracted samples.

Table 3.1 |Standard solutions for calibration line – Plasma and serum.

DMG = dimethylglyoxal, MG = methylglyoxal, Gx = glyoxal, 3-DG = 3-deoxyglucosone, TCAA = trichloroacetic acid, d8-DB = deuterated o-phenylenediamine.

Calibration point	C0	C1	C2	C3	C4	C5	C6
Stock Solution (µl)	0	3	15	30	60	90	120
Water (LC-MS grade, µl)	120	117	105	90	60	30	0
Internal standard mix (µl)	24	24	24	24	24	24	24
TCAA (µl)	48	48	48	48	48	48	48
Water (LC-MS grade, µl)	96	96	96	96	96	96	96
1 mM d8-DB (µl)	24	24	24	24	24	24	24
Concentrations							
DMG, $^{13}C_4$-DMG and MG (nM)	0	1.5	7.5	15	30	45	60
Gx and 3-DG (nM)	0	15	75	150	300	450	600
Pyruvate (µM)	0	15	75	150	300	450	600

Table 3.2 | Standard solutions for calibration line – Tissue homogenate.

DMG = dimethylglyoxal, MG = methylglyoxal, Gx = glyoxal, 3-DG = 3-deoxyglucosone, TCAA = trichloroacetic acid, d8-DB = deuterated o-phenylenediamine.

Calibration point	C0	C1	C2	C3	C4	C5
Stock Solution (µl)	0	3	18	45	90	180
Water (LC-MS grade, µl)	180	177	162	135	90	0
Internal standard mix (µl)	18	18	18	18	18	18
TCAA (µl)	72	72	72	72	72	72
1 mM d8-DB (µl)	18	18	18	18	18	18
Concentrations						
DMG, $^{13}C_4$-DMG and MG (nM)	0	1	6	15	30	60
Gx and 3-DG (nM)	0	10	60	150	300	600
Pyruvate (µM)	0	10	60	150	300	600

Table 3.3 | Standard solutions for calibration line – Cell culture supernatant.

DMG = dimethylglyoxal, MG = methylglyoxal, Gx = glyoxal, 3-DG = 3-deoxyglucosone, TCAA = trichloroacetic acid, d8-DB = deuterated o-phenylenediamine.

Calibration point	C0	C1	C2	C3	C4	C5
Stock Solution (µl)	0	2	9	22.5	45	90
Water (LC-MS grade, µl)	90	88	81	67.5	45	0
Internal standard mix (µl)	9	9	9	9	9	9
TCAA (µl)	36	36	36	36	36	36
1 mM d8-DB (µl)	9	9	9	9	9	9
Concentrations						
DMG and MG (nM)	0	1.33	6	15	30	60
Gx and 3-DG (nM)	0	13.33	60	150	300	600

3.1.1.2 α-Dicarbonyl detection

The TSQ Endura triple quadrupole mass spectrometer was used to detect the native quinoxalines, while for experiments where ^{13}C-labeled quinoxalines are expected, the Q-Exactive quadrupole-orbitrap hybrid high-resolution mass spectrometer was used. Both mass spectrometers were coupled to a Dionex Ultimate 3000 HPLC system by heated-electrospray ionization (HESI-II). Derivatized α-dicarbonyls were separated using the reverse phase C18 column Cortecs® T3 (100 mm x 2.1 mm x 2.7 µm) at 35 °C. For gradient elution, 0.1 % formic acid in LC-MS grade water as mobile phase A and 0.1 % formic acid in LC-MS grade acetonitrile as mobile phase B were used. An isocratic step of 5 % B with a flow rate of 0.2 ml/min was applied for 2 min. Subsequently, B was increased to 50 % in 5 min and raised to 100 % between 7 and 11 min. The column was washed in these conditions for 1 min, followed by an augmentation of the flow rate to 0.3 ml/min for 3 min. Then, B was reduced to 50 % between 15 and 17.5 min. Lastly, the re-equilibration occurred between 17.5 and 21 min back with 5 % B and 0.2 ml/min flow rate. Ion source settings are listed in **Tables 3.4**, **3.5** and **3.6**. Detailed information for detecting quinoxalines is provided in **Tables 3.7** and **3.8**. MRM (TSQ-Endura) or full MS data-dependent MS^2 acquisition (Top 10) in combination with PRM (Q-Exactive) was applied to detect and identify the molecules in the positive ionization mode. Absolute quantification was performed with an external calibration line based on the ratio of the areas under the peaks to the internal standard. Relative quantification was based only on the ratio to the internal standard.

Table 3.4 | Ion source parameters for derivatized α-dicarbonyl method.

Ion source	
Spray voltage (kV)	4.6 (Positive mode)
Sheath gas (Arb)	30
Auxiliary gas (Arb)	10
Capillary temperature (°C)	300
Vaporized temperature (°C)	100

Table 3.5 | Further instrument setting – TSQ Endura.

Q1 = First quadrupole, Q3 = third quadrupole, CID = collision-induced dissociation.

MRM properties	
Q1 resolution (FWHM)	0.7
Q3 resolution (FWHM)	0.4
CID gas (mTorr)	2.5
Chromatographic peak width (s)	20

Table 3.6 | Further instrument setting – Q-Exactive.

IT = injection time, AGC = Automatic gain control, NCE = Normalized collision energy.

Full MS	
Resolution	70,000

AGC target	$3e^6$
Maximum IT (ms)	200
Scan range	50 – 750 *m/z*
dd-MS²	
Resolution	17,500
AGC target	$1e^5$
Maximum IT (ms)	100
Loop count	10 (= Top 10)
Isolation window	0.4 *m/z*
Stepped NCE (eV)	10, 50, 100
dd-Settings	
Minimum IT (ms)	$5e^3$
Exclude isotopes	-
Dynamic exclusion (s)	20
PRM – MS²	
Resolution	17,500
AGC target	$5e^5$
Maximum IT (ms)	100
Isolation window	0.6 *m/z*
Stepped NCE (eV)	10, 50, 100

Table 3.7 | α-Dicarbonyls specifications (TSQ Endura; *m/z* of α-dicarbonyls refers to the respective d4-quinoxaline derivate).

MG = methylglyoxal, 3-DG = 3-deoxyglucosone, Gx = glyoxal, DMG = dimethylglyoxal.

Compound	Retention time (min)	Precursor ion (*m/z*)	Product ion (*m/z*)	Collision energy (V)
d4-MG	7.35	153.13	83.05	35
			99.07	35
			125.1	35
[$^{13}C_3$]-Pyruvate	6.58	168.11	96.07	35
			139.11	35
3-DG	5.84	239.13	149.10	35
			161.10	35
			175.12	35
			203.11	35
Gx	6.84	135.09	81.06	35
			99.07	35
			108.07	35
MG	7.38	149.10	81.06	35
			99.07	35
			122.09	35
DMG	7.76	163.12	81.06	35
			99.07	35
			122.09	35
Pyruvate	6.58	165.09	96.07	35
			137.10	35

Table 3.8 | α-Dicarbonyls specifications (Q-Exactive; *m/z* of α-dicarbonyls refers to the respective d4-quinoxaline derivate).

3-DG = 3-deoxyglucosone, Gx = glyoxal, MG = methylglyoxal, DMG = dimethylglyoxal.

Compound	^{12}C- or ^{13}C-labeled Ion (m/z)
3-DG	239.13283
3-DG (M+6)	245.15295
Gx	135.08548
Gx (M+2)	137.09220
MG	149.10113
MG (M+2)	151.10784
MG (M+3)	152.11120
DMG	163.11678
DMG (M+2)	165.12349
DMG (M+4)	167.13020
Pyruvate	165.09615
Pyruvate (M+3)	168.10616

3.1.2 Glycated amino acids

3.1.2.1 Glycated amino acid extraction

Glycated amino acids were extracted by adding 5 µl the internal standard deuterated N_ε-(1-carboxyethyl)-L-lysine (d4-CEL, 800 nM) to 50 µl brain homogenate sample. Then, 180 µl 0.1 % formic acid in LC-MS grade acetonitrile was added to the sample for protein precipitation. The sample was mixed with Vortex-Genie® 2 (Scientific Industries, Inc., 10 s), followed by incubation for 60 min at -20 °C and centrifugation (4 °C, 30 min, 14,000 rpm). 120 µl supernatant was removed and placed into a new Eppendorf tube prior to a second centrifugation (4 °C, 30 min, 14,000 rpm). Lastly, the supernatant was transferred into a glass vial for LC-MS measurements. The CEL standard solutions were prepared as described below in **Table 3.9**.

Table 3.9 | CEL standard solutions for calibration line.

CEL = N_ε-(1-carboxyethyl)-L-lysine

Calibration point	C0	C1	C2	C3	C4	C5	C6
800 µM CEL solution (µl)	0	7.5	22.5	30	37.5	52.5	60
Water (LC-MS grade, µl)	60	52.5	37.5	30	22.5	7.5	0
Internal standard (µl)	6	6	6	6	6	6	6
0.1 % formic acid in acetonitrile (LC-MS grade, µl)	216	216	216	216	216	216	216

3.1.2.2 Glycated amino acid detection

Glycated amino acids were detected using the Q-Exactive quadrupole-orbitrap hybrid mass spectrometer coupled to a Dionex Ultimate 3000 HPLC system by HESI-II. Glycated amino acids were

separated using the XBridge BEH Amide column (100 mm x 2.1 cm x 2.5 µm) at 40 °C. For gradient elution, 0.1 % formic acid in LC-MS grade water as mobile phase A and 0.1 % formic acid in LC-MS grade acetonitrile as mobile phase B were used. Initially, an isocratic step of 95 % B was applied for 3 min with a flow rate of 0.4 ml/min. Then, B was decreased to 60 % in 3 min, followed by a further decrease of B to 30 % in 6 min. During a subsequent washing step, the mobile phase was kept stable for 5 min. Lastly, B was increased to starting conditions in 2 min and held constant for 6 min. Ion source settings are listed in **Table 3.10**. Detailed information for detecting glycated amino acids is provided in **Table 3.11**. Full MS data-dependent MS^2 acquisition (Top 10) was applied to detect and identify the molecules in the positive ionization mode. Relative quantification of N_ε-3-hydroxy-2-butanonelysine (HBL) was based only on the ratio of the absolute area to the internal standard.

Table 3.10 | Ion source parameter for glycated amino acid method.

Ion source	
Spray voltage (kV)	3.5 (Positive mode)
Sheath gas (Arb)	35
Auxiliary gas (Arb)	10
Capillary temperature (°C)	300
Vaporized temperature (°C)	200
Full MS	
Resolution	70,000
AGC target	$3e^6$
Maximum IT (ms)	200
Scan range	200 – 600 *m/z*
dd-MS^2	
Resolution	17,500
AGC target	$1e^6$
Maximum IT (ms)	50
Loop count	10 (= Top 10)
Isolation window	0.4 *m/z*
Stepped NCE (eV)	30
dd-Settings	
Minimum IT (ms)	$5e^3$
Exclude isotopes	-
Dynamic exclusion (s)	10

Table 3.11| Glycated amino acid specifications (Q-Exactive).

CEL = N_ε-(1-carboxyethyl)-L-lysine, HBL = N_ε-3-hydroxy-2-butanonelysine.

Compound	**^{12}C- or ^{13}C-labeled Ion (m/z)**
d4-CEL	223.15959
CEL	219.13448
HBL	233.14958

3.1.3 Tissue sample preparation and protein determination

Frozen brain tissue (prefrontal cortex: 20-80 mg; hemispheres: 40-130 mg) and frozen liver tissue (50-150 mg) were dissected in the cryotome (-20 °C). The tissue piece was immediately transferred to an Eppendorf tube containing a similar volume of zirconium oxide beads and cold LC-MS grade water (300 µl, 750 µl, or 500 µl, respectively). The tissue was homogenized in a blender (Bullet Blender, 4 °C, 3 min, speed 8) and centrifuged (4 °C, 5 min, 2,000 g). The supernatant was collected in a new Eppendorf tube and diluted with LC-MS grade water to reach a protein concentration between 0.20 and 1.25 mg/ml. Protein concentration of diluted homogenate samples was determined using the Bradford assay. 5 µl standard solutions (from 10 mg/ml bovine serum album, BSA, **Table 3.12**) and samples were added to separated wells of a 96-well plate.

Table 3.12| Standard solution for Bradford assay calibration line.

BSA = bovine serum album.

Protein content (mg/ml)	10 mg/ml BSA (µl)	LC-MS water (µl)
1.25	50	350
1	50	450

Protein content (mg/ml)	1 mg/ml BSA (µl)	LC-MS water (µl)
0.8	80	20
0.6	60	40
0.4	40	60
0.2	20	80

Then, 250 µl Bradford reagent was added to each well and incubated in the dark for 10 min. The absorbance was measured at 595 nm with a plate reader (CLARIOstar), and the protein concentration was obtained using the external calibration line.

3.2 Animal experiments

Animals were housed in groups of three to five in cages under a 12-h light/dark cycle at 23 °C. They had *ad libitum* access to food (#1314, Altromin, except high-fat diet, HFD) and water. C57BL/6 N wild-type mice were ordered from Charles River Europe. *Ilvbl*$^{-/-}$ mice (Ilvbl$^{em1(IMPC)Bay}$ null allele (C57BL/6 N), MGI:1351911) were kindly provided by the Knockout Mouse Phenotyping Project (KOMP2), while *Ilvbl*$^{+/+}$ mice were obtained by heterozygous breeding. Male leptin receptor-deficient (*db/db*) mice were used as model of type 2 diabetes. *db/+* or *db/db* (BKS(D)-*Lepr*^{db}/JOrlRj) mice were ordered from Janvier Labs (France). Ines Stölting, Dr. Zaib Ali Shaheryar, Teresa Christina Faupel, and Ümit Özorhan, all members of the Institute of Experimental and Clinical Pharmacology and Toxicology at the University of Lübeck, conducted the following animal experiments.

3.2.1 Type-1 diabetes mouse model

Under anesthetic conditions induced by isoflurane, male C57BL/6J, *Ilvbl*$^{+/+}$ or *Ilvbl*$^{-/-}$ mice were treated with 50 mg/kg streptozotocin (STZ, 12 mg/ml in 50 mM tri-sodium citrate dihydrate buffer, pH = 4.5) via intraperitoneal (i.p.) injection for 5 consecutive days. During these days, sucrose water (10 % w/v) was provided to the animals to prevent hypoglycemia. Glucose levels were evaluated on tail blood (10 µl) using glucose test stripes (Ascensia Elite XL, Roche Diagnostics). Glucose levels were measured 2, 12 or 15 weeks after STZ injections. Mice were excluded from further analysis if blood glucose did not rise to >11.1 mM 6 weeks after STZ administration. Twelve or 15 weeks after STZ injections, mice were deeply anesthetized with Xylazine/Ketamine (24 mg/kg in 0.9 % saline solution; 200 mg/kg) or Avertin® (2,2,2—tribromoethanol) dissolved in 2-methyl-2-butanol (15-20 µl/g body weight; 2.5 % v/v in saline solution), followed by an intracardial collection of whole blood in ethylenediaminetetraacetic acid (EDTA) containing tubes. After centrifugation (4 °C, 5 min, 14,000 rpm), plasma was collected and snap frozen in liquid nitrogen. Perfusion using 15-20 ml Ringer´s solution containing heparin (10 IU/ml) was performed by entering a butterfly cannula into the left ventricle, while the right atrium was incised using scissors. All organ samples, including the brain, were snap frozen in liquid nitrogen and stored at -80 °C.

3.2.2 High-fat diet (HFD)

Male C57BL/6J mice were fed with a standard diet (Teklad Global, 2018, 18 % Protein Rodent Diet, irradiated, 2918, Inotiv) or HFD (D12492, 60 kcal % Fat, Research Diets, Inc.) for 12 weeks. Under fasting conditions, glucose levels were measured using glucose test stripes (ACCU-CHECK®, Guide me, Roche Diagnostics). Mice were euthanized by decapitation, followed by a collection of whole blood from the mouse trunk in Eppendorf tubes. After centrifugation (4 °C, 15 min, 6,000 rpm), serum was collected and stored at -80 °C. Serum samples were shipped from the Department of Physiology of the University of Santiago de Compostela-Instituto de Investigación Sanitaria in Santiago de Compostela (Spain).

3.2.3 Germ-free mice

Female specific-pathogen-free (SPF) and germ-free mice were housed in gnotocages and shipped from the Zentrale Tierhaltung of the Universitätsklinikum Schleswig-Holstein in Kiel (Germany). All mouse sterility tests were negative and measured by 16S Polymerase Chain Reaction (PCR) and microbial cultures. Twelve-15-week-old mice were euthanized by cervical dislocation under anesthesia with isoflurane. Whole blood was intracardially collected in EDTA containing tubes and EDTA plasma was obtained as described before.

3.2.4 Permanent middle cerebral artery occlusion (pMCAO)

Hyperglycemic ischemic stroke was induced by [$^{13}C_6$] glucose injection and permanent occlusion of the distal middle cerebral artery (MCAO) in female and male *Ilvbl*$^{+/+}$ and *Ilvbl*$^{-/-}$ mice at the age of 8-16 weeks. The mice were deeply anesthetized with an i.p. injection of pentobarbital (10 µl/g body weight). Subsequently, saline solution (NaCl, 0.9 % w/v, 0.2 ml per mouse) or [$^{13}C_6$]-glucose solution (50 mg dissolved in 0.2 ml saline solution per mouse) was injected i.p. before sham or pMCAO surgery. Under anesthetic conditions, the mice were placed under the microscope (Helmut Hund) in right lateral recumbency. To maintain the temperature at 37 °C, the mice were placed on a heating pad. The temperature was continuously monitored using a rectal thermometer. Then, a skin incision of 2 cm was performed between the left ear and the left eye. Drops of saline solution were added to the tissue in order to keep it moist. After removing the temporal muscle and drilling a burr hole, the middle cerebral artery was occluded with a microbipolar electro-coagulator (Model ICC 50, Erbe Elektromedizin GmbH). Then, the mice were kept in the cage under the infrared lamp. For sham surgery, mice were anesthetized, and a skin incision was made, followed by skin closure with a suture. The mice were re-anesthetized 25 min after pMCAO or 50 min after sham or pMCAO using Avertin® (2,2,2—tribromoethanol) dissolved in 2-methyl-2-butanol (15-20 µl/g body weight; 2.5 % v/v in saline solution), followed by an intracardial collection of whole blood. EDTA plasma was obtained as described before. Then, the mice were transcardially perfused with Ringer´s solution containing heparin (10 IU/ml). Afterwards, the ipsilateral and contralateral sides of the brain were snap-frozen in liquid nitrogen, and samples were stored at -80 °C. Glucose levels were measured before the surgery, 25 min after glucose administration, and before the perfusion using glucose test stripes (Ascensia Elite XL, Roche Diagnostics). The mice were excluded from further analysis if blood glucose levels did not rise to >11.1 mM.

3.2.5 Acute and chronic dimethylglyoxal treatment of mice

To assess the intestinal absorption of DMG, a dose of 5 mg/kg [$^{13}C_4$] DMG was administrated to three male C57BL/6J mice via oral gavage (250 µl), whereas control mice were treated with saline solution. Mice were sacrificed 20 min after the treatment under deeply anesthetic conditions using Xylazine/Ketamine (24 mg/kg in 0.9 % saline solution; 200 mg/kg), by an intracardial collection of blood. EDTA plasma was obtained as described before. The brain and liver were frozen in liquid nitrogen after the perfusion using 15-20 ml Ringer´s solution containing heparin (10 IU/ml). Samples were stored at -80 °C. For chronic experiments, the drinking water of mice was supplemented with 500 mg/l native DMG, resulting in a dosage of approximately 100 mg/kg/day. The water was changed every two days, and the water consumption was tracked. After 15 weeks, mice were deeply anesthetized with Xylazine/Ketamine (24 mg/kg in 0.9 % saline solution; 200 mg/kg), followed by an intracardial

collection of blood. EDTA plasma was obtained as described before. The brain was frozen in liquid nitrogen after the perfusion using 15-20 ml Ringer´s solution containing heparin (10 IU/ml). Samples were stored at -80 °C.

3.3. *In vitro* experiments

In vitro experiments were performed on bEnd.3 mouse brain endothelial cells, HT-22 mouse hippocampal neuronal cells, and Hep G2 human liver cancer cells. bEnd.3 cells (ATCC, CRL-2299) are derived from BALB/c mice and immortalized via polyoma middle T antigen, whereas HT-22 cells are derived from the HT-4 cell line. Hep G2 cells are immortalized cells from an Argentinian 15-year-old Caucasic male[162]. The composition of used media is listed in **Table 3.13**.

Table 3.13| Medium composition for each cell line.

Cell line	Medium composition
bEnd.3 Mouse brain endothelial cells	Dulbecco´s Modified Eagle's Medium (DMEM) + 10 % Fetal Calf Serum (FCS) + 1 % penicillin-streptomycin (100 U/ml; 0.1 mg/ml)
Hep G2 Human liver cancer cells	Roswell Park Memorial Institute (RPMI) 1640 + 10 % Fetal Calf Serum (FCS) + 1 % penicillin-streptomycin (100 U/ml; 0.1 mg/ml)
HT-22 Mouse hippocampal neuronal cells	Dulbecco´s Modified Eagle's Medium (DMEM) + 10 % Fetal Calf Serum (FCS) + 1 % penicillin-streptomycin (100 U/ml; 0.1 mg/ml)

The cells were split when they reached a confluence of approximately 90 %. After washing cells with 10 ml Dulbecco´s phosphate buffered saline (DPBS), cells were treated with 3 ml accutase (bEnd.3 and HT-22 cells) or 2 ml trypsin (Hep G2 cells) to facilitate the cell detachment at 37 °C for 5-10 min. Then, 8 ml medium was added to the old 75 cm^2 flask and the subculture was transferred to a new 75 cm^2 flask with a dilution of 1:20, 1:10 or 1:5. During the experiments, cells were seeded with a concentration of 1 x 10^5 cells/ml or 2 x 10^5 cells/ml and incubated for two days to reach the proper confluence.

3.3.1 Generation of ^{13}C-labeled α-dicarbonyls

bEnd.3 cells were treated with 25 mM [$^{12}C_6$] glucose, [$^{13}C_6$] glucose or 4 mM [$^{13}C_3$] pyruvate in the cell culture medium for 6 hours under normoxic or hypoxic (0.1-0.6 % O_2) conditions at 37 °C. For that, native glucose, labeled glucose or labeled pyruvate were freshly dissolved in glucose-free Dulbecco´s Modified Eagle's Medium (DMEM) with 10 % fetal calf serum (FCS) and penicillin-streptomycin (100 U/ml; 0.1 mg/ml). After 6 hours, medium (300 µl) was frozen in liquid nitrogen. Cells were washed with DPBS, and collected by adding TCAA (7.14 % w/v, 300 µl) and detaching the cells with a cell scraper, or lysed by adding buffer RA1 as described in chapter 3.3.5. Medium and cells were stored at -80 °C.

3.3.2 Detection of reactive oxygen species (ROS) after dimethylglyoxal treatment

Oxidative stress in bEnd.3, HT-22 and Hep G2 cells was determined using the ROS-sensitive fluorescent dye CM-H_2DCFDA. Fifty µl dye was dissolved in 21.6 µl sterile dimethyl sulfoxide (DMSO, 4 mM), followed by dilution of the 4 mM dye solution (20 µL) in 20 ml DPBS (dilution 1:1000). Cells were washed with DPBS before the treatment with 4 µM dye solution (200 µl per well) for 30-40 min in the dark at 37 °C and 5 % CO_2. Subsequently, the dye solution was discarded, and the cells were washed with DPBS and treated with different concentrations of DMG (in DPBS containing 5 mM glucose, **Table 3.14**) for 10 min in the dark at 37 °C and 5 % CO_2.

Table 3.14| Dilutions of DMG in 5 mM glucose in DPBS.

DMG = dimethylglyoxal, DPBS = Dulbecco´s phosphate buffered saline.

DMG concentration (µM)	*500 mM DMG solution (µl)*	*5 mM glucose in DPBS (µl)*
500	4	3996

DMG concentration (µM)	*500 µM DMG solution (µl)*	*5 mM glucose in DPBS (µl)*
200	1200	1800
50	200	1800

DMG concentration (µM)	*200 µM DMG solution (µl)*	*5 mM glucose in DPBS (µl)*
100	500	500
20	100	900

DMG concentration (µM)	*50 µM DMG solution (µl)*	*5 mM glucose in DPBS (µl)*
5	100	900

The fluorescent signal was detected at 492-495 nm excitation with a 517-527 nm emission wavelength. As positive control, 10 µM hydrogen peroxide was added simultaneously. Cell-free wells served as negative controls. HT-22 and Hep G2 cells were seeded on poly-D-lysine-coated wells for these experiments. A stock solution of poly-D-lysine (1 mg/ml) was diluted with sterile DPBS to 0.1 mg/ml (1:10). The wells were coated with 200 µl of the diluted poly-D-lysine solution overnight at room temperature. Subsequently, the wells were washed twice with sterile DPBS and seeded with HT-22 or Hep G2 cells.

3.3.3 *Ilvbl* knockdown in bEnd.3 cells

To reduce the expression of *Ilvbl*, bEnd.3 cells were transfected with ON-TARGETplus Mouse SMARTpool of four small interfering ribonucleic acids (siRNAs, **Table 3.15**) against *Ilvbl* or with relative control (ON-TARGETplus Non-Targeting pool). The siRNA pellet (5 nmol) was resuspended in RNAse-free water (diethylpyrocarbonate in milli-Q water, 1 g/l) reaching a solution concentration of 20 µM. The solution was placed on a rotator for 30 min at room temperature, followed by a further dilution with RNAse-free water to 5 µM. To increase the efficiency of the transfection, an antibiotic-free medium (DMEM + 10 % FCS, 400 µl) was added to the well at least 4 hours before the transfection. siRNA (5 µM, 2.5 µl per well) was diluted in a reduced-serum medium (Opti-MEM®; 47.5 µl per well). The DharmaFECT 4 transfection reagent (2.5 µl per well) was diluted in a reduced-serum medium (47.5 µl per well). Both solutions were incubated for 5 min at room temperature. Then, the solutions were mixed, followed by 20 min of incubation at room temperature. Finally, 100 µl transfection solution was added to each well containing 400 µl of the antibiotic-free medium. Cells were incubated for 40 hours at 37 °C (5 % CO_2). After the transfection, cells were treated with 25 mM [$^{13}C_6$] glucose or 4 mM [$^{13}C_3$] pyruvate as described above. The supernatant was frozen in liquid nitrogen and stored at -80 °C.

Table 3.15| *Ilvbl* siRNA sequences.

Ilvbl = IlvB acetolactate synthase like; siRNA = small interfering ribonucleic acid.

siRNA number	Sequence
1	GCUUAGAGCUGCCGUGGAG
2	GGUCAAGGUACUUCGUGAA
3	GGGCUGAGGAGCUUCGGAA
4	GGACCCAGAUUUCUCGAGA

3.3.4 Dimethylglyoxal treatment of HT-22 cells

Confluent HT-22 cells were treated with 0 µM, 20 µM, 100 µM, 200 µM or 500 µM DMG (**Table 3.16**) in DMEM containing 25 mM glucose, 10 % FCS, and 1 % penicillin-streptomycin for 24 hours at 37 °C and 5 % CO_2. To avoid DMG contaminations due to its high volatility, cells were seeded in three different 24-well plates based on the DMG concentrations (First 24-well plate: 0 µM; Second 24-well plate: 20 µM and 100 µM; Third 24-well plate: 200 µM and 500 µM) and the three 24-well plates were placed in three individual conventional incubators.

Table 3.16| Concentrations of DMG in medium.

DMG = dimethylglyoxal.

DMG concentration (µM)	*500 mM DMG solution (µl)*	*Medium (µl)*
500	10	9990

DMG concentration (µM)	*500 µM DMG solution (µl)*	*Medium (µl)*
200	2000	3000
100	1000	4000

DMG concentration (µM)	*200 µM DMG solution (µl)*	*Medium (µl)*
20	300	2700

3.3.5 Real-time PCR after *Ilvbl* knockdown or dimethylglyoxal treatment

RNA from bEnd.3 or HT-22 cells was extracted by NucleoSpin® 96 RNA purification kit (Macherey-Nagel) at room temperature according to manufacturer's instructions. Initially, cells were washed with DPBS and lysed by adding 350 µl buffer RA1. Afterwards, the lysate was filtrated through the NucleoSpin® Filter to reduce viscosity and centrifuged for 1 min at 11,000 x *g*. After adding 350 µl ethanol (70 %) to the lysate, the cell homogenate was loaded to the NucleoSpin® Column and centrifuged for 30 s at 11,000 x *g*. Then, the salt was removed from the membrane by adding 350 µl membrane desalting buffer for a more efficient DNase digestion (15 min, room temperature). Later, the membrane was washed with 200 µl Buffer RA2 to stop the previous reaction and twice with Buffer RA3. The membrane was centrifuged for 2 min at 11,000 x *g* to let it dry, followed by the elution of RNA in 40 µl RNase-free water through centrifuging for 1 min at 11,000 x *g*. To evaluate the RNA concentration, 2 µl sample was measured by UV-VIS spectrophotometer at 260 nm. Based on the RNA concentration, samples were diluted with RNase-free water to reach a concentration of 20 ng/µl. Subsequently, RNA was converted to complementary DNA (cDNA) by reverse transcription. Master mix solution (15 µl, **Table 3.17**) containing reverse transcriptase was added to 35 µl RNA solution (700 ng), and the solution was incubated for 10 min at room temperature, followed by consecutive incubation for 90 min at 37 °C.

Table 3.17| Composition of the reverse transcription master mix solution.

Compound	Volume per 35 µl sample (µl)
Mouse Moloney murine leukemia virus (M-MLV) buffer	10
Nucleoside triphosphate (dNTP, 25 mM)	2
Random primers	1
RNasin (40 U/µl)	1
M-MLV-transcriptase	1

Then, 23 µl SuperMix solution was added to a PCR-96-well plate. Detailed information on the composition of the SuperMix solution is provided in **Table 3.18**.

Table 3.18|Composition of SuperMix solution.

Compound	Volume (µl)
Platinum SYBR Green qPCR SuperMix	12.5
RNase-free water	9
Forward primer (10 pmol/µl)	0.75
Reverse primer (10 pmol/µl)	0.75

Lastly, 2 µl cDNA sample was mixed with 23 µl SuperMix, while 2 µl RNase-free water was added to a well as negative control. The PCR-96-well plate was sealed with an adhesive PCR sealing foil, and after centrifugation, the PCR-96-well plate was placed in the Light Cycler. After the preincubation cycle for 10 min at 95 °C, the target cDNAs were amplified with 38 cycles (30 s at 95 °C, 30 s at 60 °C and 30 s at 72 °C), followed by a melting cycle (10 s at 95 °C, 60 s at 65 °C and 1 s at 97°C). Primers for real-time PCR are listed in **Table 3.19**. β-*actin* or Cyclophilin A (*Ppia)* were used as housekeeping genes for data normalization according to the ΔΔthreshold cycle (ΔΔCt) method.

$$\Delta Ct = Ct\,(gene) - Ct\,(Housekeeping\ gene)$$

$$\Delta\Delta Ct = \Delta Ct - Average\ \Delta Ct\,(Control)$$

$$Relative\ Gene\ mRNA\ Expression = \frac{2^{-\Delta\Delta Ct}}{Average\ 2^{-\Delta\Delta Ct}(Control)}$$

Table 3.19| Primers for real-time PCR.

Ppia = Cyclophilin A, *Ilvbl* = IlvB acetolactate synthase like, *Pla2g4a* = Phospholipase A2 Group IVA, *Ptges* = prostaglandin E synthase, *Ptgs2* = prostaglandin-endoperoxide synthase 2, *Bim* = BCL2 Like 11.

Gene	*Species*	Direction	Sequence
Ppia	Mouse	forward	5'-AGGTCCTGGCATCTTGTCCAT-3'
		reverse	5'-GAACCGTTTGTGTTTGGTCCA-3'
β-*Actin*	Mouse	forward	5'-ATGGAATCCTGTGGCATCCAT-3'
		reverse	5'-TTCTGCATCCTGTCAGCAATG-3'
Ilvbl	Mouse	forward	5'-CCCAGGTCCAGTGTTTGTGG-3'
		reverse	5'-ACGGCAGCTCTAAGCTTGTT-3'
Pla2g4a	Mouse	forward	5'-GAAGGCACAGAGAAGCCTGAG-3'

		reverse	5‘-ATGCTGAACCGTAGGTCTGG-3‘
Ptges	Mouse	forward	5‘-CTTGCGGACTTGGTGTCTCT-3‘
		reverse	5‘-GCACTCAAAGGACGGTGGTA-3‘
Ptgs2	Mouse	forward	5‘-CATCCCCTTCCTGCGAAGTT-3‘
		reverse	5‘-CATGGGAGTTGGGCAGTCAT-3‘
Bim	Mouse	forward	5‘-ACAGAACCGCAAGCTTCCAT-3‘
		reverse	5‘-CAGATCTTCAGGTTCCTCCTGAGA-3‘

3.4. Statistical analysis

Data were analyzed using GraphPad Prism 8 (GraphPad Software) with the suggestion of Dr. Sonja Binder (Rhein, S., Costalunga, R., Inderhees, J. *et al.*, 2024[55]). Significance was considered if p value < 0.05. Detailed statistical information is provided in the statistical table on page 78. Parametric statistics (e.g., t-test, ANOVA) were only applied if variances were homogeneous between groups (tested by Brown-Forsythe, Levene’s or *F*-test, depending on the statistical method used) and if data respected the Gaussian distribution of the residuals by D’Agostino-Pearson test. If the previous assumptions were not met or the sample size was small, non-parametric methods were used as described in the statistical table on page 78. Two-tailed tests were applied if not indicated otherwise. Greenhouse-Geisser correction was used in ANOVA statistics if the sphericity assumption was violated (Mauchly test). Outliers were identified by the ROUT method (Q = 1%). No data points were excluded if not stated otherwise in the statistical table on page 78.

4. Results

Parts of the following results have already been published in the manuscript “The reactive pyruvate metabolite dimethylglyoxal mediates neurological consequences of diabetes” by Rhein, S., Costalunga, R., Inderhees, J. *et al.* in 2024[55].

4.1 Concentrations of the α-dicarbonyl dimethylglyoxal are elevated in diabetic mice

To measure α-dicarbonyls in plasma, serum, tissue homogenate, and cell culture supernatant and lysate, quinoxalines were generated by taking advantage of the reaction between the α-dicarbonyls and the derivatizing reagent d8-DB. As previously described in the method part, quinoxalines were detected using LC-MS^2. First, I measured α-dicarbonyl and pyruvate levels in the plasma of mice treated with STZ (**Fig. 4.1a**). STZ is an alkylating antineoplastic drug that induces the destruction of beta cells of the mammalian pancreas, preventing the generation and the subsequent release of insulin in the bloodstream[163,164]. Consequently, STZ injections induced type-1 diabetes in the treated mice[163,164,165]. For this reason, STZ treatment elevated concentrations of glucose in the blood (**Fig. 4.1b**). As expected, type-1 diabetic mice significantly drank more water compared to the control mice (**Fig. 4.1c**) As already shown in other studies, concentrations of 3-DG (2.30-fold) and MG (1.49-fold) were increased in the mouse plasma 15 weeks after the STZ injections[166,167] (**Fig. 4.1d**). At the same time, concentrations of Gx were not significantly changed, even though there was a trend towards an increase in the STZ-treated mice (1.44-fold, **Fig. 4.1d**). Interestingly, DMG concentrations were also significantly elevated 1.36-fold in the plasma of type-1 diabetic mice compared to the control (**Fig. 4.1d**). Moreover, pyruvate concentrations were decreased 15 weeks after the STZ injections (**Fig. 4.1f**)**.** To investigate the potential association between periphery and central nervous system, α-dicarbonyls were measured in homogenates of the prefrontal cortex. Here, only DMG was significantly elevated in the type-1 diabetic mice (1.52-fold), whereas no differences were observed in the concentrations of Gx or MG between treatments (**Fig. 4.1e**). 3-DG was not detected in the brain, probably due to the low concentrations of this metabolite in the prefrontal cortex homogenate (**Fig. 4.1e**). Further, pyruvate concentrations were unchanged between the two treatments in the brain (**Fig. 4.1g**). Based on these findings, we wanted to measure the levels of α-dicarbonyls and pyruvate in the plasma and tissue homogenates of leptin receptor-deficient *db/db* mice, an established model of type-2 diabetes[168]. First, *db/db* mice significantly gained more weight than the heterozygous littermates *db/+* mice (**Fig. 4.2a, b**). Moreover, *db/db* mice developed hyperglycemia (**Fig. 4.2c**).

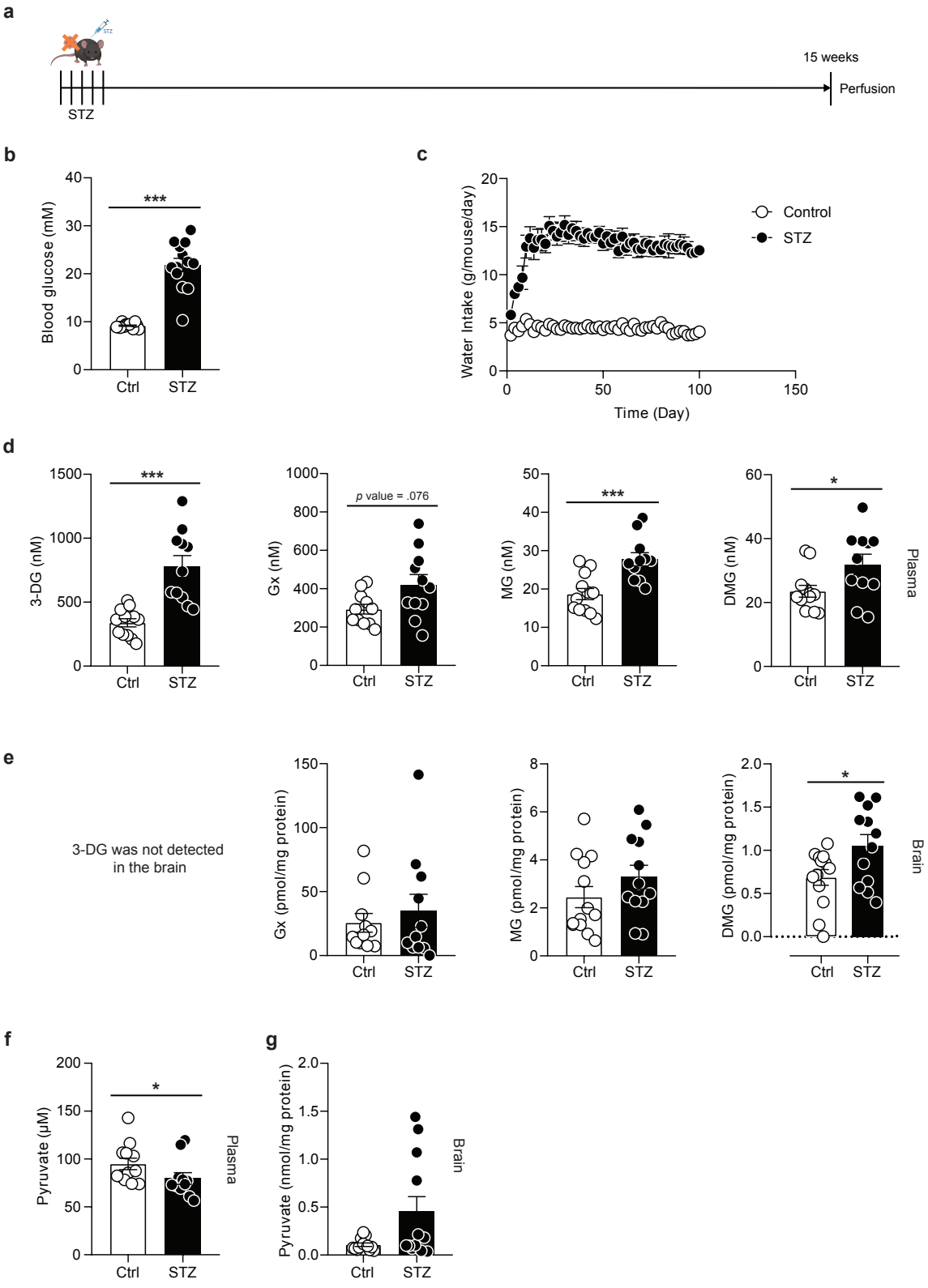

Fig. 4.1| Type-1 diabetes increases dimethylglyoxal concentrations in plasma and brain.

a Timeline of streptozotocin (STZ)-induced diabetes and sample collection in mice. Part of the image was created with BioRender.com. **b** Blood glucose concentrations 15 weeks after vehicle or STZ injections (*n*=13 per group). **c** Tap water intake of control and STZ-treated mice (50 time points per group, 4-6 cages per group). **d** Plasma concentrations of 3-deoxyglucosone (3-DG), glyoxal (Gx), methylglyoxal (MG) and dimethylglyoxal (DMG) in mice

15 weeks after vehicle (*n*=11-12) or STZ (*n*=11) injections. **e** Concentrations of Gx, MG and DMG in mouse brain homogenate 15 weeks after vehicle (*n*=11-13) or STZ (*n*=11-12) injections. **f** Concentrations of pyruvate in mouse plasma 15 weeks after vehicle (*n*=12) or STZ (*n*=11) injections. **g** Concentrations of pyruvate in mouse brain homogenate 15 weeks after vehicle or STZ injections (*n*=12 per group). For normalization, deuterated methylglyoxal (d4-MG) and [$^{13}C_3$] sodium pyruvate were used as internal standards (**d-g**). Values are means ± SEM. Statistical comparisons by two-tailed Mann-Whitney U test (**b**; **d**, 3-DG and Gx; **e**, Gx; **f**; **g**) or two-tailed unpaired *t* test (**d**, MG and DMG; **e**, MG and DMG). *$p < 0.05$; ***$p < 0.001$. Detailed information on the test statistics is provided in the Statistical table.

Importantly, DMG concentrations were significantly increased 1.88-fold in the plasma of *db/db* mice, similar to 3-DG (1.76-fold) and MG (1.92-fold, **Fig. 4.2d**). In contrast, Gx and pyruvate levels were not changed between the two genotypes (**Fig. 4.2d, e**). In addition, Gx, MG, DMG and pyruvate concentrations were unaltered in the prefrontal cortex homogenate between the genotypes (**Fig. 4.2f, g**). Following the results in the type-1 diabetic mouse model, 3-DG was not detected in the brain of *db/+* or *db/db* mice (**Fig. 4.2f**). Furthermore, concentrations of MG and pyruvate were significantly elevated in the liver homogenate of type-2 diabetic mice, while 3-DG and DMG levels were not changed between the groups (**Fig. 4.2h, i**). In contrast, Gx levels were downregulated in the liver of *db/db* mice compared to the *db/+* mice (**Fig. 4.2h**)**.** The obese phenotype of the *db/db* mice suggests that obesity could be involved in the upregulation of the levels of DMG and the other α-dicarbonyls. Therefore, levels of α-dicarbonyls were measured in the serum of mice fed with HFD for 12 weeks, an established model of diet-induced obesity[169]. As expected, the body weight of HFD-fed mice was significantly higher than the body weight of mice fed with standard diet (**Fig. 4.3a**). Even though the HFD led to hyperglycemic conditions (**Fig. 4.3b**), concentrations of 3-DG, MG or DMG were not influenced by the diet (**Fig. 4.3c**). Interestingly, Gx concentrations were significantly higher in mice fed with HFD than in controls (**Fig. 4.3c**). These results suggest that diabetes, but not obesity itself, elevates the levels of DMG.

Results

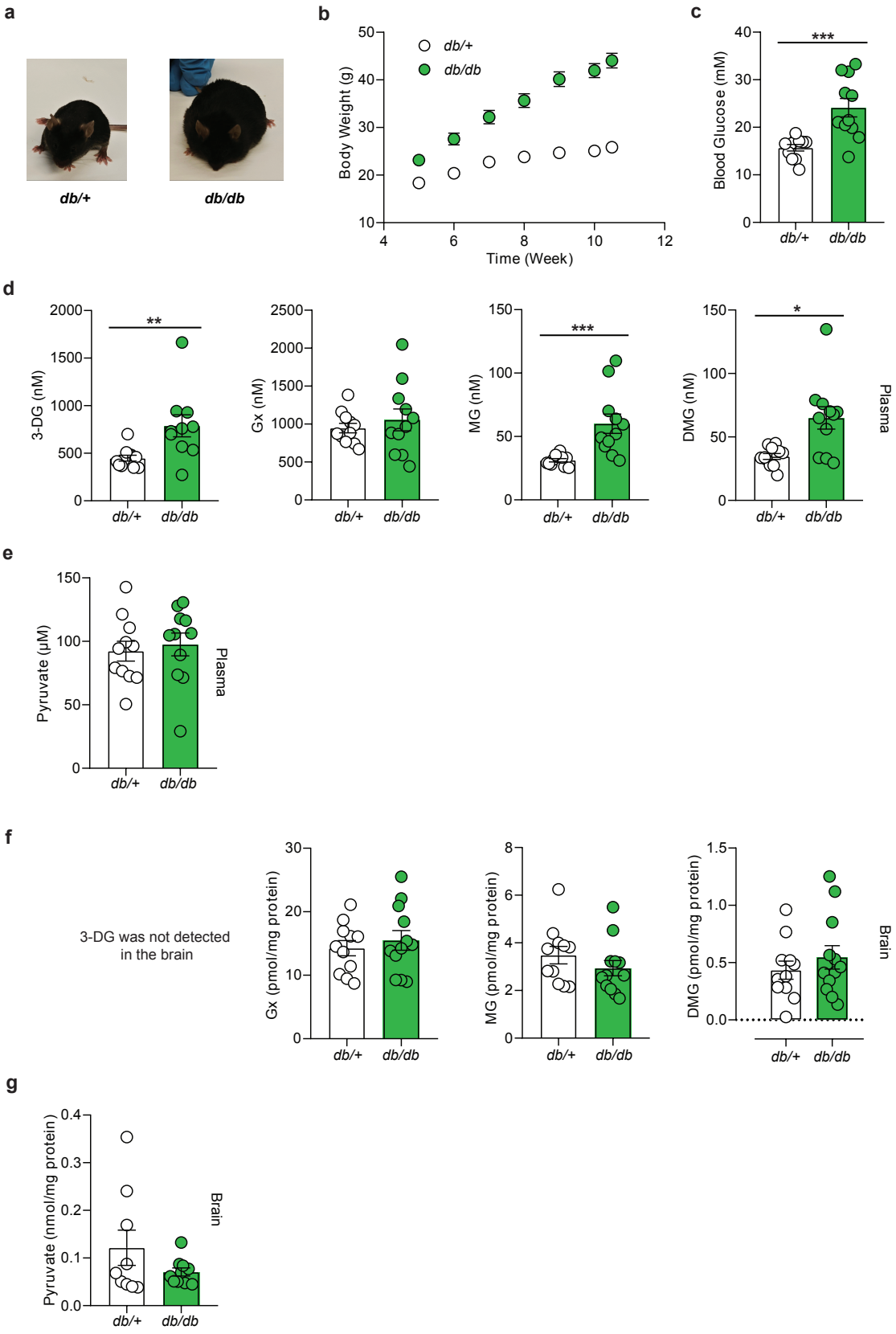
a
db/+
db/db
b
db/+
db/db
Body Weight (g)
Time (Week)
c
Blood Glucose (mM)
***
d
3-DG (nM)
**
Gx (nM)
MG (nM)
***
DMG (nM)
*
Plasma
e
Pyruvate (μM)
Plasma
f
3-DG was not detected
in the brain
Gx (pmol/mg protein)
MG (pmol/mg protein)
DMG (pmol/mg protein)
Brain
g
Pyruvate (nmol/mg protein)
Brain

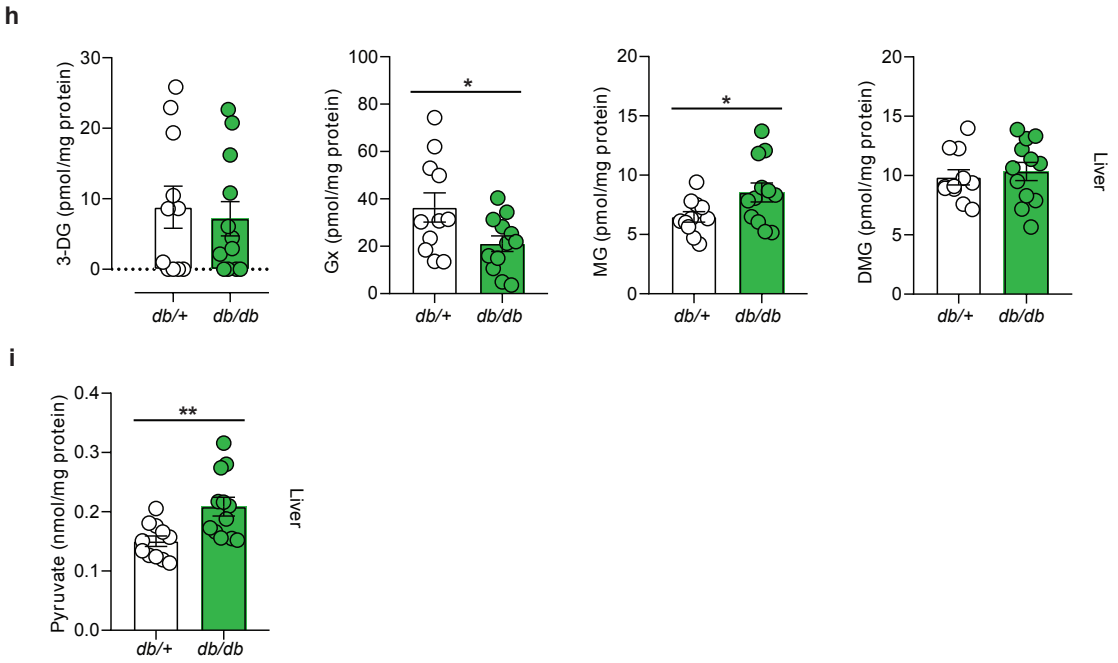

Fig. 4.2 | Type-2 diabetes increases dimethylglyoxal concentrations in plasma.

a Pictures of leptin receptor-deficient *db/db* mouse and heterozygous *db/+* littermate. **b** Body weight over time (*n*=12 per group) in 10-11-week-old *db/+* and *db/db* mice. **c** Blood glucose concentrations (*n*=11 per group) in 10-11-week-old *db/+* and *db/db* mice. **d** Plasma concentrations of 3-deoxyglucosone (3-DG), glyoxal (Gx), methylglyoxal (MG) and dimethylglyoxal (DMG) in *db/+* (*n*=11) and *db/db (n*=10-11*)* mice. **e** Concentrations of pyruvate in plasma of *db/+* and *db/db* mice (*n*=11 per group). **f** Concentrations of Gx, MG and DMG in brain homogenate of *db/+* (*n*=11) and *db/db* (*n*=12) mice. **g** Brain homogenate concentrations of pyruvate in *db/+* (*n*=9) and *db/db* (*n*=10) mice. **h** Liver homogenate concentrations of 3-DG, Gx, MG and DMG in *db/+* (*n*=11) and *db/db* (*n*=12) mice. **i** Pyruvate concentrations in liver homogenate of *db/+* (*n*=11) and *db/db* (*n*=12) mice. For normalization, deuterated methylglyoxal (d4-MG) and [$^{13}C_3$] sodium pyruvate were used as internal standards (**d-i**). Values are means ± SEM. Statistical comparisons by 2-way RM ANOVA (**b**), two-tailed Mann-Whitney U test (**c; d**; **g**) or two-tailed unpaired *t* test (**e**; **f**; **h**; **i**). **p* < 0.05; ***p* < 0.01; ****p* < 0.001. Detailed information on the test statistics is provided in the Statistical table.

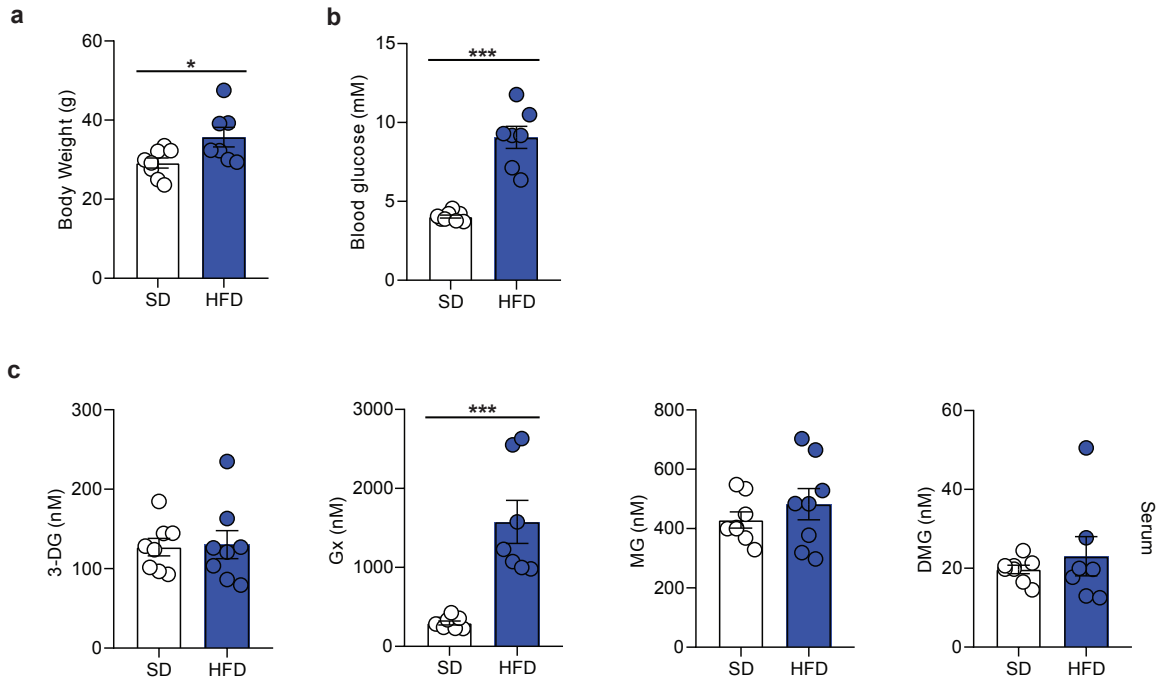

Fig. 4.3 | High-fat diet does not increase serum dimethylglyoxal.

a Body weight of mice fed with standard diet (SD, *n*=8) or high-fat diet (HFD, *n*=7) for 12 weeks. **b** Blood glucose concentrations of mice fed with SD (*n*=8) or HFD (*n*=7) for 12 weeks. **c** Serum concentrations of 3-deoxyglucosone (3-DG), glyoxal (Gx), methylglyoxal (MG) and dimethylglyoxal (DMG) in mice fed with SD (*n*=8) or HFD (*n*=7-8) for 12 weeks. For normalization, deuterated methylglyoxal (d4-MG) was used as internal standard (**c**). Values are means ± SEM. Statistical comparisons by two-tailed unpaired *t* test (**a**; **c**, 3-DG and MG) or two-tailed Mann-Whitney U test (**b**; **c**, Gx and DMG). *$p < 0.05$; ***$p < 0.001$. Detailed information on the test statistics is provided in the Statistical table.

4.2 Hypoxia stimulates the dimethylglyoxal generation from glucose or pyruvate

The previous results show that DMG is raised under diabetic conditions. Former studies of our group showed that DMG is endogenously generated from glucose[54,55]. Moreover, DMG contained two or four glucose-derived carbons, suggesting that DMG is generated from two C-C blocks of glucose[54,55]. Indeed, DMG is generated from two molecules of pyruvate[54,55]. Interestingly, hypoxic conditions promote glycolysis due to the stabilization of HIF-1α[170,171]. Thus, I wanted to evaluate the effect of hypoxia on the generation of DMG and other α-dicarbonyls. Furthermore, in plants, fungi and prokaryotes, ALS is an enzyme involved in the synthesis of DMG from pyruvate[172]. The mammal orthologue gene *Ilvbl* could have maintained the function of a DMG catalyst by α-acetolactate as intermediate compound in mammals.

First, to evaluate if cells hold α-dicarbonyls in the intracellular space, bEnd.3 cells were treated with 25 mM native or [$^{13}C_6$] glucose for 6 hours under hypoxic conditions (0.3 % O_2, **Fig. 4.4a**). Here, α-dicarbonyls were measured in both supernatant and cell lysate. [$^{13}C_6$] 3-DG, [$^{13}C_2$] Gx, [$^{13}C_3$] pyruvate, [$^{13}C_2$] DMG and [$^{13}C_4$] DMG were only detected in the supernatant, suggesting the tendency of the cells to secrete these reactive glucose metabolites to the medium (**Fig. 4.4b, c, e, f**). In contrast, [$^{13}C_2$] MG and [$^{13}C_3$] MG were detected in the cells, probably due to the higher levels of this metabolite compared the other α-dicarbonyls (**Fig. 4.4d**). However, [$^{13}C_2$] MG and [$^{13}C_3$] MG were higher in the medium compared to the cell lysate (**Fig. 4.4d**). Moreover, the treatment with [$^{13}C_6$] glucose elevated the generation of [$^{13}C_2$] DMG, even though this metabolite is also generated from native glucose (**Fig. 4.4f**). Since α-dicarbonyls are mainly secreted in the supernatant, medium was the proper target for the evaluation of α-dicarbonyl levels in the next experiments *in vitro*.

To test the role of HIF-1α and ILVBL in generating DMG, mouse brain endothelial bEnd.3 cells, transfected with *Ilvbl* siRNA for 40 hours, were treated with 25 mM [$^{13}C_6$] glucose for 6 hours under normoxic or hypoxic (0.1-0.5 %) conditions (**Fig. 4.5a**). First, the *Ilvbl* siRNA transfection significantly lowered the expression of *Ilvbl* mRNA to 28 % compared to mRNA expression in the control cells transfected with the scramble siRNA (**Fig. 4.5b**). The expression of *Ilvbl* mRNA was not changed based on oxygen concentration (**Fig. 4.5b**). Interestingly, levels of [$^{13}C_6$] 3-DG and [$^{13}C_2$] Gx in the medium were not influenced by the concentration of oxygen (**Fig. 4.5c, d**). In contrast, [$^{13}C_3$] MG and [$^{13}C_3$] pyruvate levels were increased under hypoxic conditions (**Fig. 4.5e, f**). Importantly, half-labeled and fully-labeled DMG levels were also upregulated under hypoxia (**Fig. 4.5g**), indicating that hypoxia promotes the generation of DMG, similar to pyruvate and MG. Further, *Ilvbl* knockdown did not influence the generation of DMG or the other α-dicarbonyls, neither under atmospheric nor hypoxic conditions (**Fig. 4.5c, d, e, g**)**.** In contrast, *Ilvbl* knockdown significantly reduced fully-labeled pyruvate levels under hypoxic conditions (**Fig. 4.5f**). Lastly, we treated bEnd.3 cells with 4 mM [$^{13}C_3$] pyruvate for 6 hours under atmospheric or hypoxic (0.6 % O_2) conditions, 40 hours after transfection with *Ilvbl* siRNA (**Fig. 4.6a**). Even though no changes were observed in the levels of [$^{13}C_3$] pyruvate (**Fig. 4.6b**), [$^{13}C_2$] DMG and [$^{13}C_4$] DMG levels were significantly increased under hypoxic conditions (**Fig. 4.6c**). Similar to the previous experiment, the generation of labeled DMG from [$^{13}C_3$] pyruvate was not influenced by *Ilvbl* knockdown (**Fig. 4.6c**). On the other hand, the overexpression of *Ilvbl* after transfection of bEnd.3 cells with a plasmid stimulated the formation of [$^{13}C_4$] DMG from [$^{13}C_6$] glucose under hypoxic conditions[55]. Labeled forms of other α-dicarbonyls were not detected (data not shown) after the treatment with [$^{13}C_3$] pyruvate.

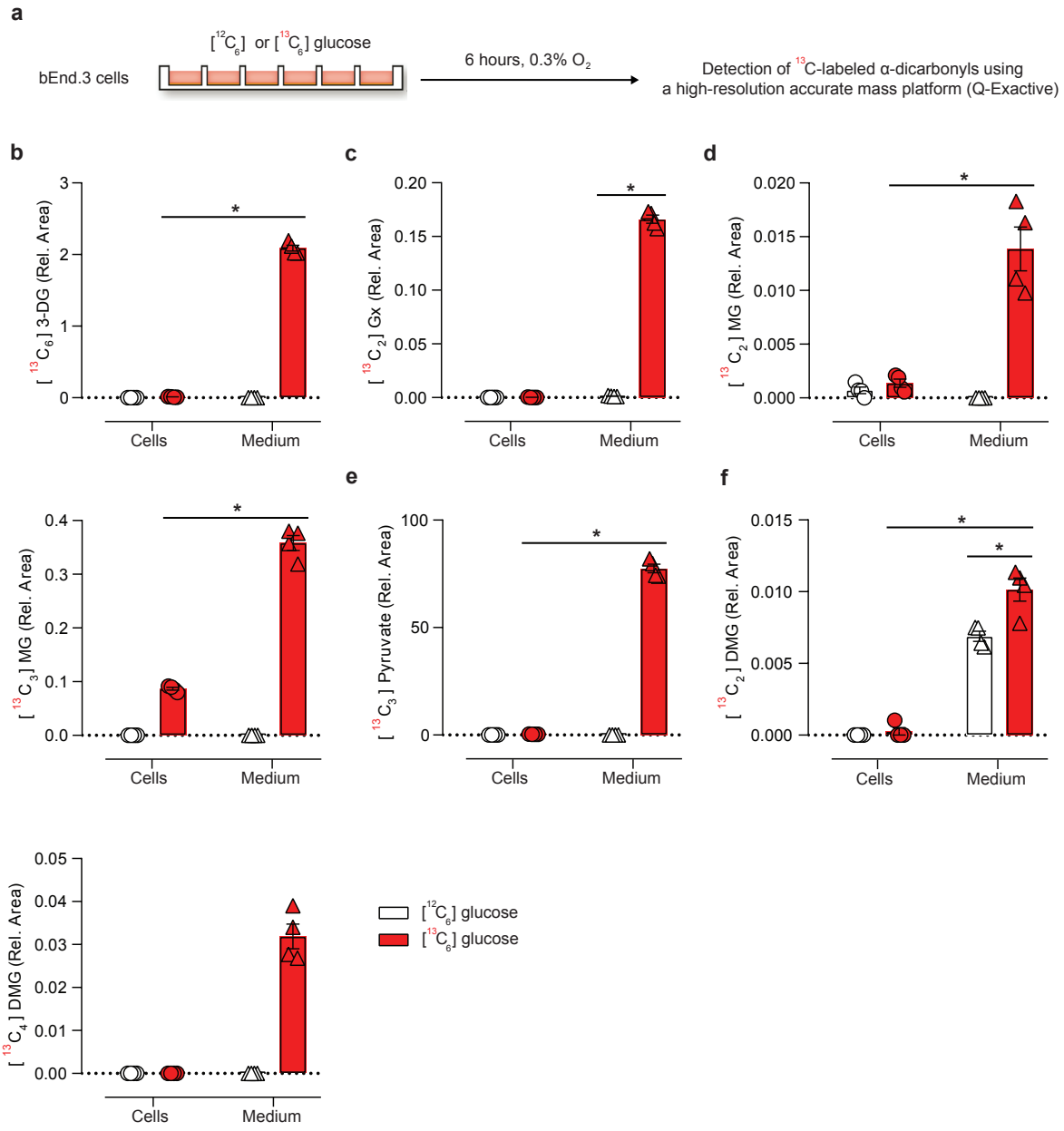

Fig. 4.4 |α-Dicarbonyls are excreted from cells to the medium.

a Treatment of mouse brain endothelial bEnd.3 cells with native or [$^{13}C_6$] glucose for 6 hours under hypoxic (0.3 % O_2) conditions. **b** [$^{13}C_6$] 3-deoxyglucosone ([$^{13}C_6$] 3-DG) in the medium or cell lysate (*n*=4 per group). **c** [$^{13}C_2$] glyoxal ([$^{13}C_2$] Gx) in the medium or cell lysate (*n*=4 per group). **d** [$^{13}C_2$] methylglyoxal ([$^{13}C_2$] MG) and [$^{13}C_3$] MG in the medium or cell lysate (*n*=4 per group). **e** [$^{13}C_3$] pyruvate in the medium or cell lysate (*n*=4 per group). **f** [$^{13}C_2$] dimethylglyoxal ([$^{13}C_2$] DMG) and [$^{13}C_4$] DMG in the medium or cell lysate (*n*=4 per group). For normalization, deuterated methylglyoxal (d4-MG) was used as internal standard (**b-f**). Values are means ± SEM. Statistical comparisons by two-tailed Mann-Whitney U test (**b**; **c**; **d**; **e**) or two-tailed Mann-Whitney U test followed by Bonferroni–Holm correction (**f**). *$p < 0.05$. Detailed information on the test statistics is provided in the Statistical table.

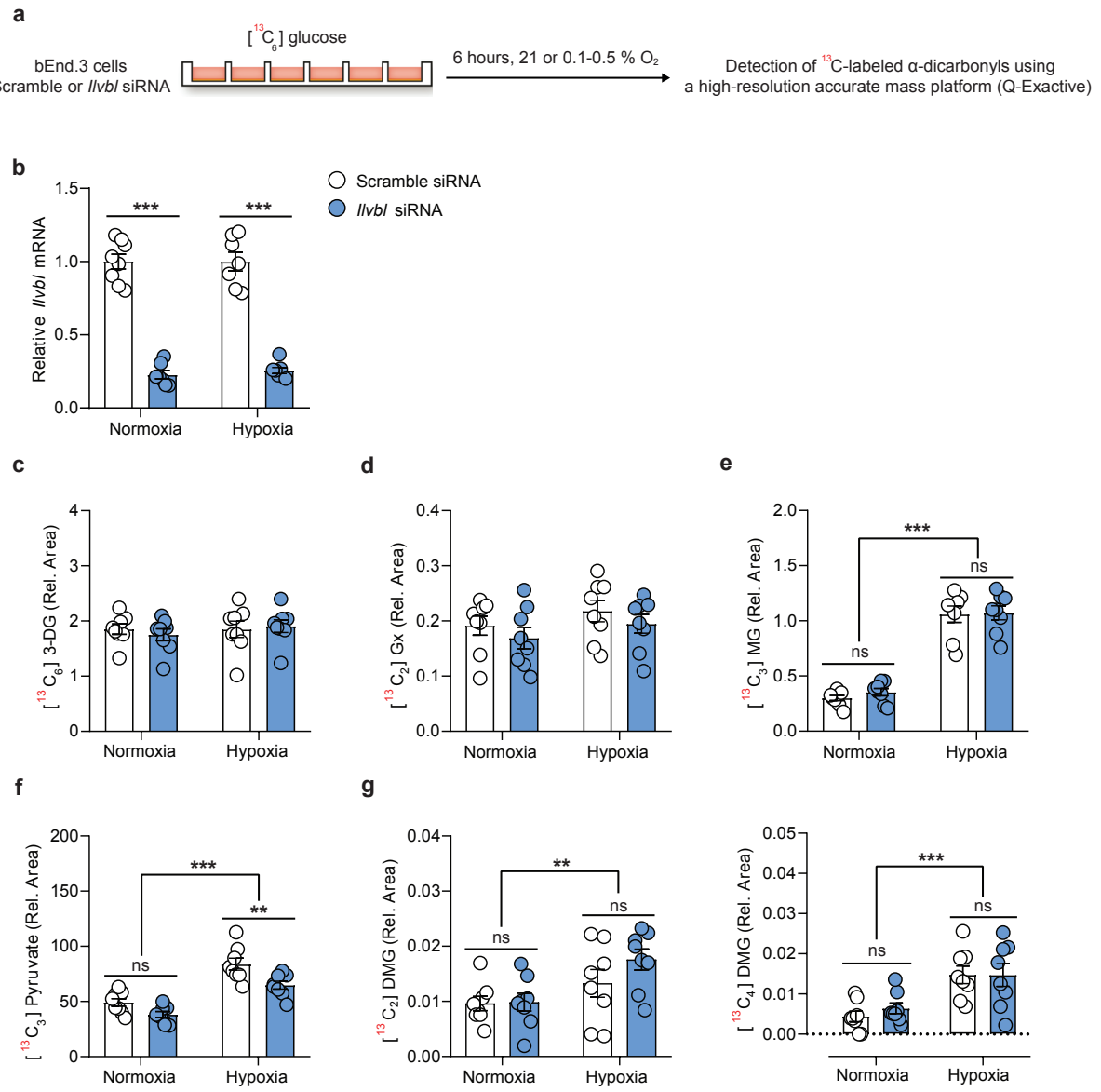

Fig. 4.5 |Hypoxic conditions increase levels of dimethylglyoxal, but *Ilvbl* is not involved in the generation of dimethylglyoxal from glucose *in vitro*.

a Treatment of mouse brain endothelial bEnd.3 cells with [$^{13}C_6$] glucose for 6 hours under normoxic or hypoxic (0.1-0.5 % O_2) conditions. Before the treatment, cells were transfected with scramble or *Ilvbl* siRNA for 40 hours. **b** Relative *Ilvbl* mRNA expression in bEnd.3 cells treated with scramble (*n*=7-8 per group) or *Ilvbl* (*n*=8 per group) siRNA for 40 hours. **c** [$^{13}C_6$] 3-deoxyglucosone ([$^{13}C_6$] 3-DG) in the medium of control or *Ilvbl* knockdown cells (*n*=8 per group). **d** [$^{13}C_2$] glyoxal ([$^{13}C_2$] Gx) in the medium of control or *Ilvbl* knockdown cells (*n*=8 per group). **e** [$^{13}C_3$] methylglyoxal ([$^{13}C_3$] MG) in the medium of control or *Ilvbl* knockdown cells (*n*=8 per group). **f** [$^{13}C_3$] pyruvate in the medium of control or *Ilvbl* knockdown cells (*n*=8 per group). **g** [$^{13}C_2$] dimethylglyoxal ([$^{13}C_2$] DMG) and [$^{13}C_4$] DMG in the medium of control or *Ilvbl* knockdown cells (*n*=8 per group). For normalization, deuterated methylglyoxal (d4-MG) was used as internal standard (**c**-**g**). Values are means ± SEM. Statistical comparisons by Scheirer-Ray-Hare test followed by two-tailed Mann–Whitney U post hoc tests and Bonferroni–Holm correction (**b**), Scheirer-Ray-Hare test (**c**; **e**; **g**, [$^{13}C_4$] DMG), 2-way ANOVA (**d**; **g**, [$^{13}C_2$] DMG) or 2-way ANOVA followed by

Sidak´s post hoc tests (**f**). $^{**}p < 0.01$; $^{***}p < 0.001$. Detailed information on the test statistics is provided in the Statistical table.

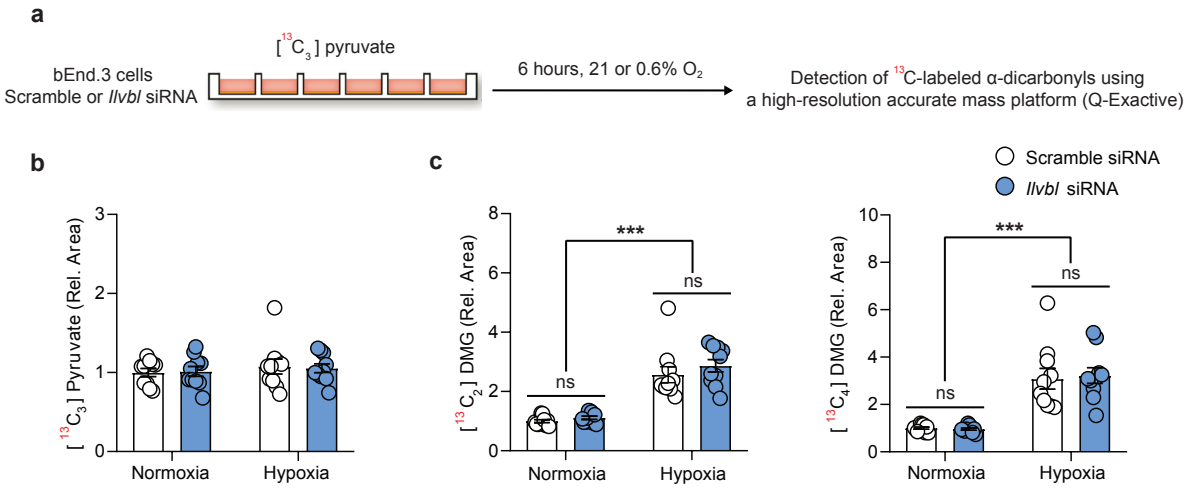

Fig. 4.6 | *Ilvbl* does not influence the generation of dimethylglyoxal from pyruvate *in vitro*.

a Treatment of mouse brain endothelial bEnd.3 cells with [$^{13}C_3$] pyruvate for 6 hours under normoxic or hypoxic (0.6 % O_2) conditions. Before the treatment, cells were transfected with scramble or *Ilvbl* siRNA for 40 hours. **b** [$^{13}C_3$] pyruvate in the medium of control or *Ilvbl* knockdown cells (n=10 per group). **c** [$^{13}C_2$] dimethylglyoxal ([$^{13}C_2$] DMG) and [$^{13}C_4$] DMG in the medium of control or *Ilvbl* knockdown cells (n=10 per group). For normalization, deuterated methylglyoxal (d4-MG) was used as internal standard (**b**; **c**). Values are means ± SEM. Statistical comparisons by Scheirer-Ray-Hare test. $^{***}p < 0.001$. Detailed information on the test statistics is provided in the Statistical table.

4.3 ILVBL is involved in the generation of dimethylglyoxal in the brain of hyperglycemic and ischemic mice

Previous studies showed that *Ilvbl* overexpression augmented the DMG levels *in vitro*[55]. Thus, I wanted to evaluate the role of ILVBL in the generation of DMG *in vivo*. *Ilvbl*$^{-/-}$ mice (**Fig. 4.7a**) did not show any particular phenotype and were fertile. Under basal conditions, levels of DMG were not changed in plasma, brain and peripheral organs between *Ilvbl*$^{+/+}$ and *Ilvbl*$^{-/-}$ mice (**Fig. 4.7b-f**). Since hypoxic conditions increased the generation of DMG *in vitro*, we wanted to evaluate ischemic conditions and DMG formation *in vivo*. First, to confirm that DMG is generated from glucose in our model and to evaluate whether *Ilvbl* influences the DMG generation, *Ilvbl*$^{+/+}$ and *Ilvbl*$^{-/-}$ mice received an intraperitoneal injection of saline solution or 50 mg/0.2 ml [$^{13}C_6$] glucose prior to inducing ischemic stroke by pMCAO (**Fig. 4.8a**). Here, half-labeled and fully-labeled DMG were detected in the plasma and whole-brain homogenate of mice treated with [$^{13}C_6$] glucose 25 min after pMCAO (**Fig. 4.8b, d**), whereas labeled forms of DMG were not generated in mice treated with saline solution (**Fig. 4.8b** and data not shown). This analysis showed that DMG is a product of glucose metabolism *in vivo*.

Moreover, levels of native DMG were higher in the plasma of mice treated with [$^{13}C_6$] glucose compared to the control (**Fig. 4.8b**). In contrast, native DMG levels were lower in the whole-brain homogenate of [$^{13}C_6$] glucose-treated mice compared to the control (**Fig. 4.8c**). Moreover, no differences were observed in the generation of labeled forms of DMG between the ischemic ipsilateral and the contralateral hemispheres of the brain (**Fig. 4.8d**). Lastly, the presence of *Ilvbl* did not influence the concentration of DMG either in the plasma or in both sides of the brain, 25 min after pMCAO (**Fig. 4.8b – d**).

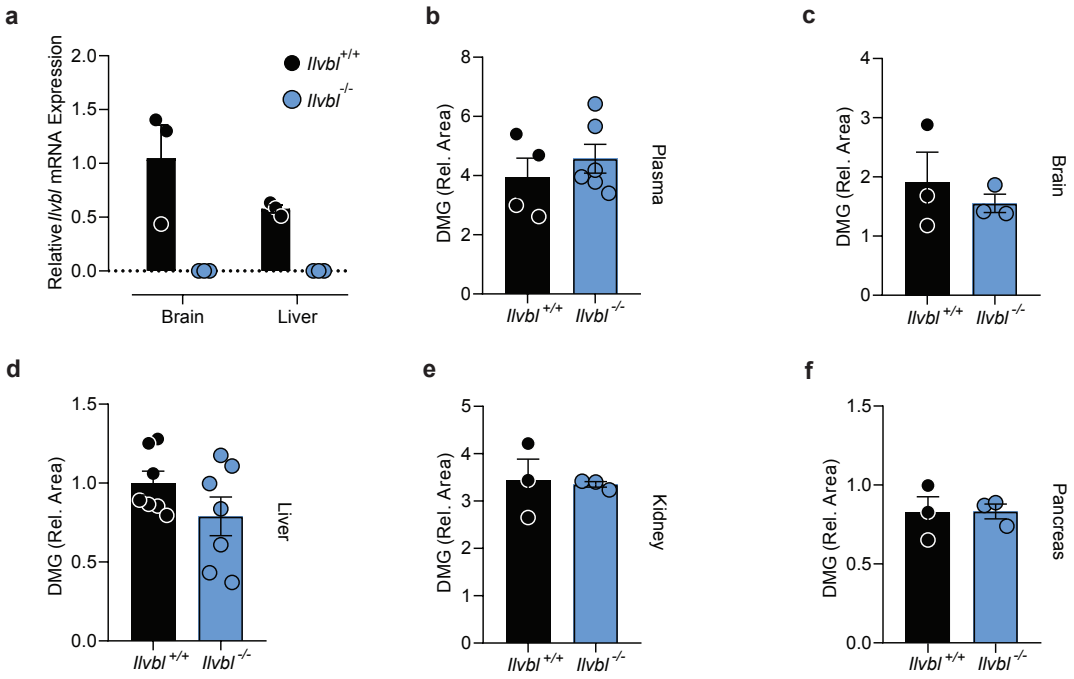

Fig. 4.7 | *Ilvbl* deficiency does not influence the levels of dimethylglyoxal under basal conditions.

a Relative *Ilvbl* mRNA expression in brain and liver of *Ilvbl*$^{+/+}$ and *Ilvbl*$^{-/-}$ mice (*n*=3 per group). **b** Dimethylglyoxal (DMG) levels in plasma of *Ilvbl*$^{+/+}$ (*n=4*) and *Ilvbl*$^{-/-}$ (*n*=6) mice under basal conditions. **c** DMG levels in brain homogenate of *Ilvbl*$^{+/+}$ and *Ilvbl*$^{-/-}$ mice (*n*=3 per group) under basal conditions. **d** DMG levels in liver homogenate of *Ilvbl*$^{+/+}$ and *Ilvbl*$^{-/-}$ mice (*n*=7 per group) under basal conditions. **e** DMG levels in kidney homogenate of *Ilvbl*$^{+/+}$ and *Ilvbl*$^{-/-}$ mice (*n*=3 per group) under basal conditions. **f** DMG levels in pancreas homogenate of *Ilvbl*$^{+/+}$ and *Ilvbl*$^{-/-}$ mice (*n*=3 per group) under basal conditions. For normalization, deuterated methylglyoxal (d4-MG) was used as internal standard (**b-f**). Values are means ± SEM. Statistical comparisons by two-tailed unpaired *t* test (**b**; **c**; **d**; **f**) or two-tailed Mann-Whitney U test (**e**). Detailed information on the test statistics is provided in the Statistical table.

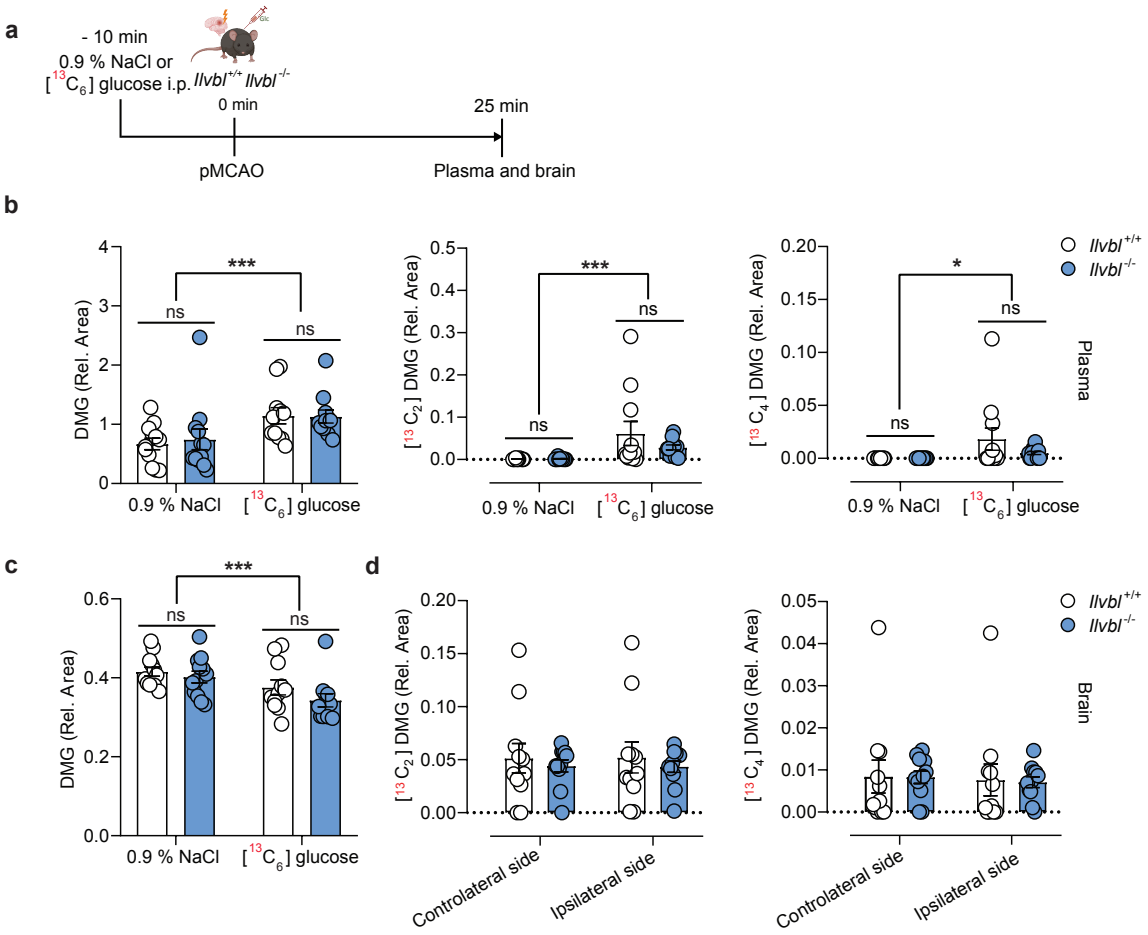

Fig. 4.8 |Dimethylglyoxal is a product of glucose metabolism *in vivo.*

a Timeline of saline or [$^{13}C_6$] glucose injection, occlusion of the distal middle cerebral artery (MCAO), and sample collection. Part of the image was created with BioRender.com. **b** Dimethylglyoxal (DMG), [$^{13}C_2$] DMG and [$^{13}C_4$] DMG in plasma of *Ilvbl*$^{+/+}$ or *Ilvbl*$^{-/-}$ mice treated with saline (*n*=12 per group) or [$^{13}C_6$] glucose (*n*=11 per group) solutions prior to MCAO. **c** DMG in brain homogenate (average of ipsi- and contralateral sides) of *Ilvbl*$^{+/+}$ or *Ilvbl*$^{-/-}$ mice treated with saline (*n*=12 per group) or [$^{13}C_6$] glucose (*n*=11 per group) solutions prior to MCAO. **d** [$^{13}C_2$] DMG and [$^{13}C_4$] DMG in the contralateral and ipsilateral sides of acute hyperglycemic *Ilvbl*$^{+/+}$ or *Ilvbl*$^{-/-}$ MCAO-treated mice treated with [$^{13}C_6$] glucose. For normalization, deuterated methylglyoxal (d4-MG) was used as internal standard (**b-f**). Values are means ± SEM. Statistical comparisons by Scheirer-Ray-Hare test (**b**; **c**) or 2-way RM ANOVA (**d**). *p < 0.05; ***p < 0.001. Detailed information on the test statistics is provided in the Statistical table.

Further, to evaluate if hypoxia/ischemia indeed stimulate the generation of DMG from glucose *in vivo*, we performed sham or pMCAO treatment in acute hyperglycemic mice by injecting 50 mg/0.2 ml [$^{13}C_6$] glucose. In this experiment, *Ilvbl*$^{+/+}$ and *Ilvbl*$^{-/-}$ mice were sacrificed 50 min after the sham or pMCAO treatment (**Fig. 4.9a**). First, levels of labeled forms of DMG, but not native DMG, were significantly higher in the plasma of ischemic mice compared to the sham control (**Fig. 4.9b**), suggesting the ischemic conditions stimulate the production of DMG from glucose. However, DMG levels were not influenced by the presence of *Ilvbl* in the plasma (**Fig. 4.9b**). Furthermore, native MG levels were significantly higher in the plasma of ischemic mice compared to the sham (**Fig. 4.9c**), whereas levels of native 3-DG, Gx and pyruvate and fully-labeled 3-DG, Gx and MG were not changed depending on surgeries (**Fig. 4.9c – f**). Interestingly, fully-labeled pyruvate levels were lower in the plasma of hyperglycemic and ischemic mice compared to the control (**Fig. 4.9f**). Lastly, as expected, *Ilvbl* knockout did not influence the levels of the other α-dicarbonyls or pyruvate (**Fig. 4.9c – f**). Subsequently, we measured levels of α-dicarbonyls and pyruvate in the homogenates of the whole contralateral or ipsilateral side of the brain. Interestingly, ischemic stroke significantly augmented levels of native and labeled forms of DMG in both contralateral and ipsilateral sides of the brain compared to the sham treatment (**Fig. 4.9g**), indicating that hypoxia/ischemia enhances the generation of DMG in the brain *in vivo*. Moreover, native, half-labeled and fully-labeled DMG levels were significantly higher in the ipsilateral compared to the contralateral hemisphere of the brain of the acute hyperglycemic and ischemic mice, while levels of native and labeled forms of DMG were not changed between the brain sides of sham-treated mice (**Fig. 4.9g**). Importantly, *Ilvbl* knockout lowered levels of native and half-labeled DMG in the ischemic side of the brain (**Fig. 4.9g**). Native DMG levels were reduced even in the contralateral side of MCAO-treated *Ilvbl* knockout mice (**Fig. 4.9g**). In contrast, levels of DMG were not influenced by *Ilvbl* deficiency in the sham-treated mice (**Fig. 4.9g**). Levels of native Gx, Mg, pyruvate and fully-labeled MG and pyruvate were not affected by *Ilvbl* deficiency in the brain (**Fig. 4.9h – j**). However, ischemic stroke induced the generation of native MG, Gx and pyruvate in the ipsilateral side of the brain (**Fig. 4.9h – j**). In contrast, pMCAO reduced the levels of fully-labeled MG, even though the reduction was attenuated in the ipsilateral hemisphere (**Fig. 4.9h**). Lastly, native 3-DG and fully-labeled forms of 3-DG and Gx were not detected in the brain homogenate (data not shown). Taken together, these findings suggest that DMG is generated at least partially by *Ilvbl* in the brain of acute hyperglycemic and ischemic mice, 50 min after pMCAO. In contrast, *Ilvbl* does not influence the plasma or brain DMG levels in mice 25 min after pMCAO, probably due to a shorter latency time for glucose to be metabolized to dimethylglyoxal.

Results

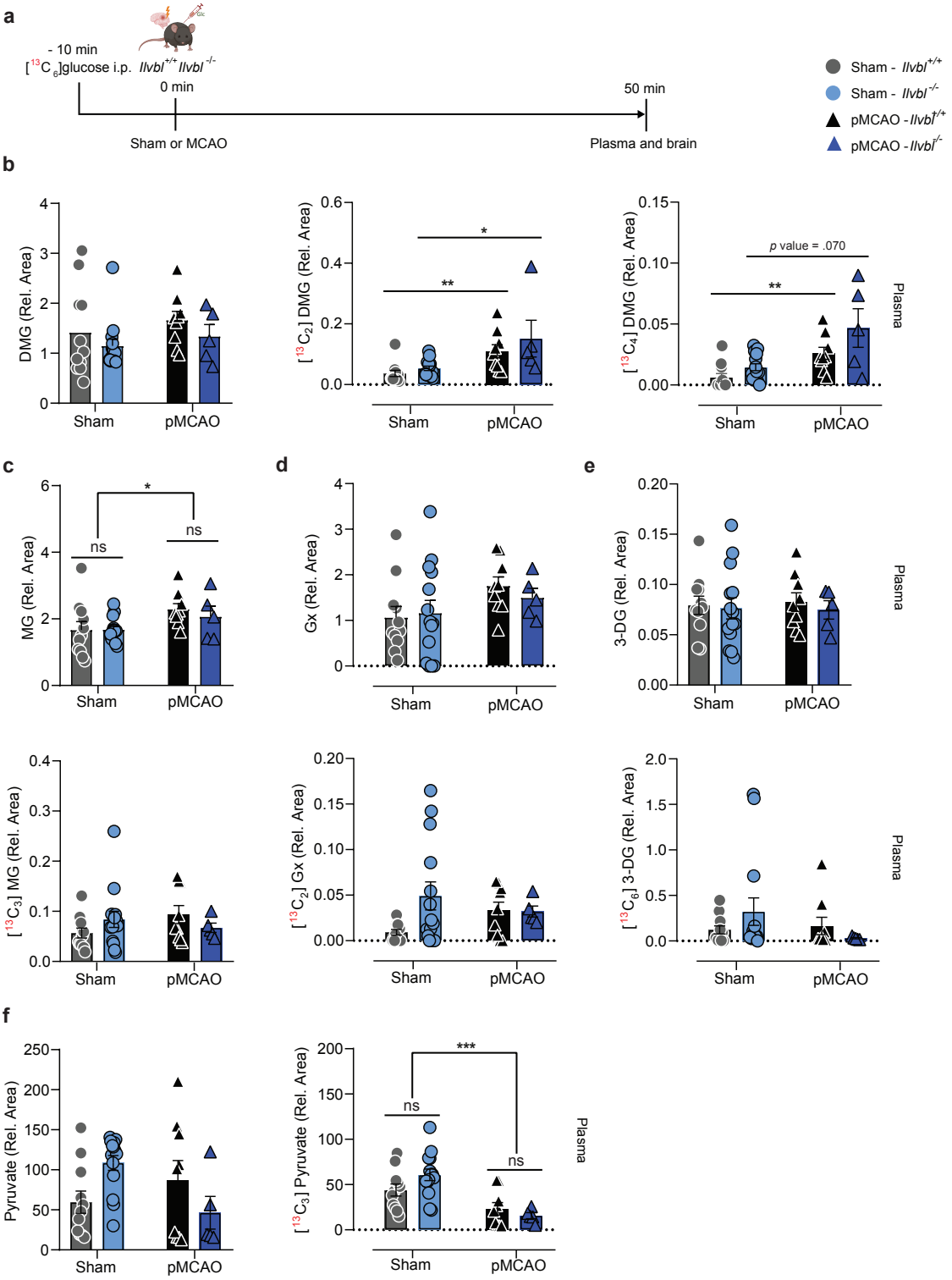
a
- 10 min
[13C6]glucose i.p.
Ilvbl+/+ Ilvbl-/-
0 min
Sham or MCAO
50 min
Plasma and brain
Sham - Ilvbl+/+
Sham - Ilvbl-/-
pMCAO - Ilvbl+/+
pMCAO - Ilvbl-/-
b
DMG (Rel. Area)
[13C2] DMG (Rel. Area)
[13C4] DMG (Rel. Area)
p value = .070
Plasma
c
MG (Rel. Area)
ns
[13C3] MG (Rel. Area)
d
Gx (Rel. Area)
[13C2] Gx (Rel. Area)
e
3-DG (Rel. Area)
[13C6] 3-DG (Rel. Area)
f
Pyruvate (Rel. Area)
[13C3] Pyruvate (Rel. Area)
Sham
pMCAO

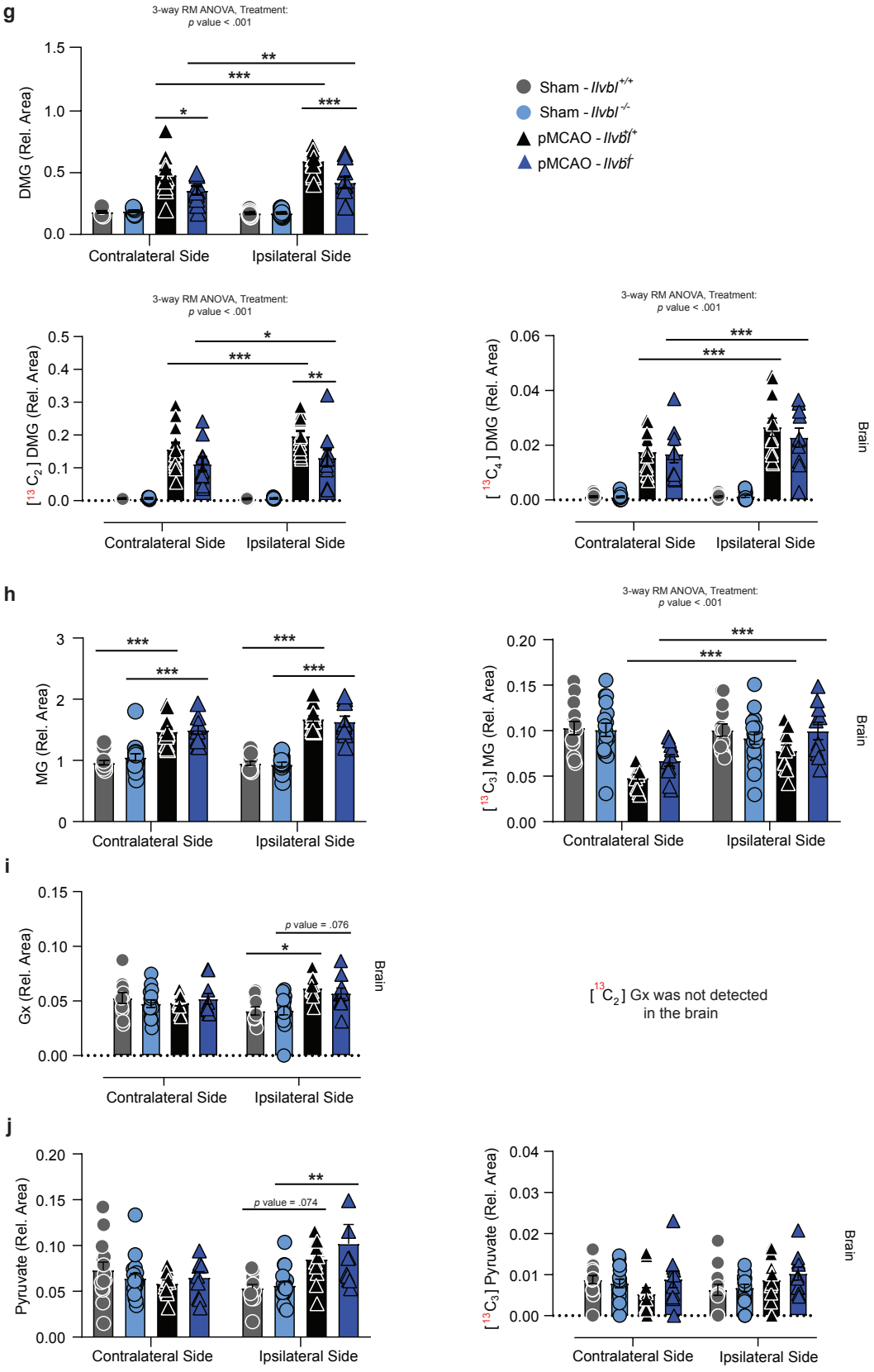

Fig. 4.9 | *Ilvbl* is involved in the generation of dimethylglyoxal in the brain of acute hyperglycemic and ischemic mice.

a Timeline of [$^{13}C_6$] glucose injection, sham surgery or occlusion of the distal middle cerebral artery (MCAO), and sample collection. Part of the image was created with BioRender.com. **b** Dimethylglyoxal (DMG), [$^{13}C_2$] DMG and [$^{13}C_4$] DMG in plasma of *Ilvbl*$^{+/+}$ or *Ilvbl*$^{-/-}$ mice after sham surgery (*n*=11, *Ilvbl*$^{+/+}$; *n*=14, *Ilvbl*$^{-/-}$) or pMCAO (*n*=9, *Ilvbl*$^{+/+}$; *n*=5, *Ilvbl*$^{-/-}$). **c** Methylglyoxal (MG) and [$^{13}C_3$] MG in plasma of *Ilvbl*$^{+/+}$ or *Ilvbl*$^{-/-}$ mice after sham surgery (*n*=11, *Ilvbl*$^{+/+}$; *n*=14, *Ilvbl*$^{-/-}$) or pMCAO (*n*=9, *Ilvbl*$^{+/+}$; *n*=5, *Ilvbl*$^{-/-}$). **d** Glyoxal (Gx) and [$^{13}C_2$] Gx in plasma of *Ilvbl*$^{+/+}$ or *Ilvbl*$^{-/-}$ mice after sham surgery (*n*=11, *Ilvbl*$^{+/+}$; *n*=14, *Ilvbl*$^{-/-}$) or pMCAO (*n*=9, *Ilvbl*$^{+/+}$; *n*=5, *Ilvbl*$^{-/-}$). **e** 3-Deoxyglucosone (3-DG) and [$^{13}C_6$] 3-DG in plasma of *Ilvbl*$^{+/+}$ or *Ilvbl*$^{-/-}$ mice after sham surgery (*n*=11, *Ilvbl*$^{+/+}$; *n*=14, *Ilvbl*$^{-/-}$) or pMCAO (*n*=9, *Ilvbl*$^{+/+}$; *n*=5, *Ilvbl*$^{-/-}$). **f** Pyruvate and [$^{13}C_3$] pyruvate in plasma of *Ilvbl*$^{+/+}$ or *Ilvbl*$^{-/-}$ mice after sham surgery (*n*=11, *Ilvbl*$^{+/+}$; *n*=14, *Ilvbl*$^{-/-}$) or pMCAO (*n*=9, *Ilvbl*$^{+/+}$; *n*=5, *Ilvbl*$^{-/-}$). **g** DMG, [$^{13}C_2$] DMG and [$^{13}C_4$] DMG in the contralateral and ipsilateral sides of *Ilvbl*$^{+/+}$ or *Ilvbl*$^{-/-}$ mice after sham surgery (*n*=14, *Ilvbl*$^{+/+}$; *n*=17, *Ilvbl*$^{-/-}$) or pMCAO (*n*=12, *Ilvbl*$^{+/+}$; *n*=10, *Ilvbl*$^{-/-}$). **h** MG and [$^{13}C_3$] MG in the contralateral and ipsilateral sides of *Ilvbl*$^{+/+}$ or *Ilvbl*$^{-/-}$ mice after sham surgery (*n*=14, *Ilvbl*$^{+/+}$; *n*=17, *Ilvbl*$^{-/-}$) or pMCAO (*n*=12, *Ilvbl*$^{+/+}$; *n*=10, *Ilvbl*$^{-/-}$). **i** Gx in the contralateral and ipsilateral sides of *Ilvbl*$^{+/+}$ or *Ilvbl*$^{-/-}$ mice after sham surgery (*n*=11, *Ilvbl*$^{+/+}$; *n*=15, *Ilvbl*$^{-/-}$) or pMCAO (*n*=9, *Ilvbl*$^{+/+}$; *n*=10, *Ilvbl*$^{-/-}$). **j** Pyruvate and [$^{13}C_3$] pyruvate in the contralateral and ipsilateral sides of *Ilvbl*$^{+/+}$ or *Ilvbl*$^{-/-}$ mice after sham surgery (*n*=14, *Ilvbl*$^{+/+}$; *n*=17, *Ilvbl*$^{-/-}$) or pMCAO (*n*=12, *Ilvbl*$^{+/+}$; *n*=10, *Ilvbl*$^{-/-}$). For normalization, deuterated methylglyoxal (d4-MG) was used as internal standard (**b-j**). Values are means ± SEM. Statistical comparisons by Scheirer-Ray-Hare test followed by two-tailed Mann–Whitney U post hoc tests and Bonferroni–Holm correction (**b**), Scheirer-Ray-Hare test (**c**; **d**, [$^{13}C_2$] Gx; **e**, [$^{13}C_6$] 3-DG), 2-way ANOVA (**d**, Gx; **e**, 3-DG; **f**), 3-way RM ANOVA followed by Sidak´s post hoc tests (**g**; **h**; **i**; **j**) *$p < 0.05$; **$p < 0.01$; ***$p < 0.001$. Detailed information on the test statistics is provided in the Statistical table.

4.4 ILVBL is involved in the generation of dimethylglyoxal in the brain of type-1 diabetic mice

Thereafter, I wanted to explore the role of ILVBL in generating DMG in a type-1 diabetic mouse model. Here, plasma was collected before and 12 weeks after the STZ injections (**Fig. 4.10a**). As expected, blood glucose concentrations were significantly higher 12 weeks after STZ injections compared to the same mice before the STZ injections (**Fig. 4.10b**). Notably, *Ilvbl*$^{-/-}$ mice developed hyperglycemia like their *Ilvbl*$^{+/+}$ littermates (**Fig. 4.10b**). Levels of 3-DG and Gx were higher in plasma of *Ilvbl*$^{+/+}$ and *Ilvbl*$^{-/-}$ mice 12 weeks after the STZ injections (**Fig. 4.10c**). In contrast, MG levels were unchanged after the latency time (**Fig. 4.10c**). At the same time, levels of DMG were upregulated in plasma compared to the baseline (**Fig. 4.10c**). Neither the generation of DMG nor of the other α-dicarbonyls in plasma were influenced by *Ilvbl* (**Fig. 4.10c**). Likewise, *Ilvbl* did not influence levels of α-dicarbonyls in the liver homogenate (**Fig. 4.10d**). Then, we measured the levels of α-dicarbonyls in the prefrontal cortex homogenate of the STZ-treated mice. Importantly, DMG levels were reduced in the brain of *Ilvbl*$^{-/-}$ compared to *Ilvbl*$^{+/+}$ mice (**Fig. 4.10e**), indicating that *Ilvbl* stimulates the local generation of DMG in the brain of type-1 diabetic mice. In contrast, as negative control, levels of brain Gx and MG were similar between the genotypes (**Fig. 4.10e**). Like in the previous analyses, 3-DG was not detected in

the brain homogenate (**Fig. 4.10e**). Therefore, ILVBL increases the production of DMG in the brain of type-1 diabetic mice.

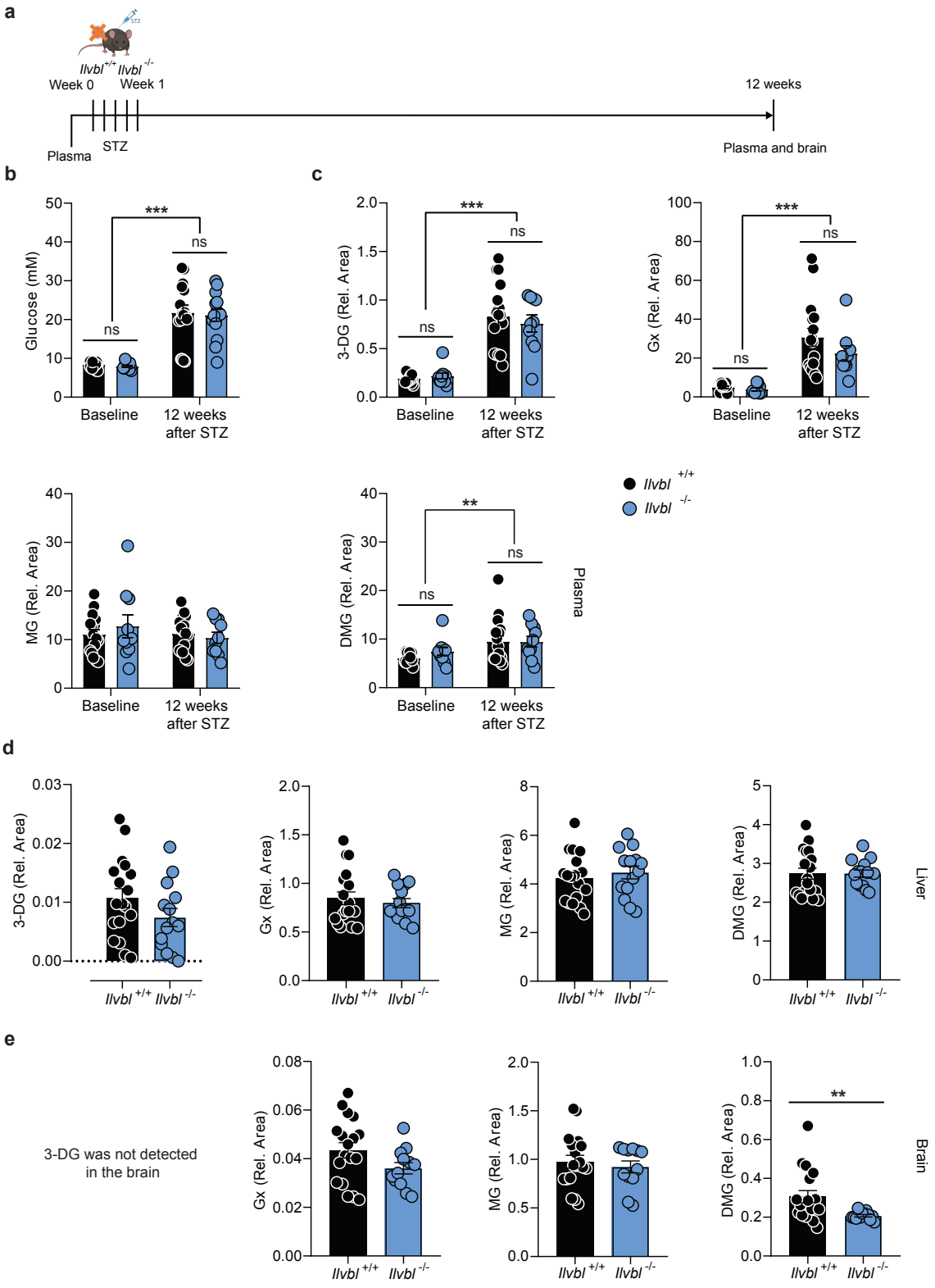

Fig. 4.10 | *Ilvbl* is involved in the generation of dimethylglyoxal in the brain of mice with type-1 diabetes.

a Timeline of plasma collection before the treatment, streptozotocin (STZ)-induced diabetes, and sample collection 12 weeks after STZ injections. **b** Blood glucose concentrations of *Ilvbl*$^{+/+}$ (*n*=18) and *Ilvbl*$^{-/-}$ (*n*=14) mice at baseline and 12 weeks after STZ treatment. **c** 3-deoxyglucosone (3-DG), glyoxal (Gx), methylglyoxal (MG) and dimethylglyoxal (DMG) in plasma of *Ilvbl*$^{+/+}$ (*n*=16) and *Ilvbl*$^{-/-}$ (*n*=9-10) mice at baseline and 12 weeks after STZ treatment. **d** 3-DG, Gx, MG and DMG in the liver homogenate of *Ilvbl*$^{+/+}$ (*n*=18) and *Ilvbl*$^{-/-}$ (*n*=14) mice 12 weeks after STZ treatment. **e** Gx, MG and DMG in the brain homogenate of *Ilvbl*$^{+/+}$ (*n*=18) and *Ilvbl*$^{-/-}$ (*n*=12) mice 12 weeks after STZ treatment. For normalization, deuterated methylglyoxal (d4-MG) was used as internal standard (**c**-**e**). Values are means ± SEM. Statistical comparisons by 2-way RM ANOVA (**b**; **c**), two-tailed unpaired *t* test (**d**, 3-DG, Gx and MG; **e**, Gx and MG) or two-tailed Mann-Whitney U test (**d**, DMG; **e**, DMG). $^{**}p < 0.01$; $^{***}p < 0.001$. Detailed information on the test statistics is provided in the Statistical table.

4.5 The gut microbiota does not influence plasma dimethylglyoxal concentrations

As previously mentioned, DMG is generated from glucose in the mammal metabolism and is a product of pyruvate metabolism via ALS in bacteria, yeast and prokaryotes. Bacteria and yeasts are microorganisms that are part of the mammal gut microbiota.

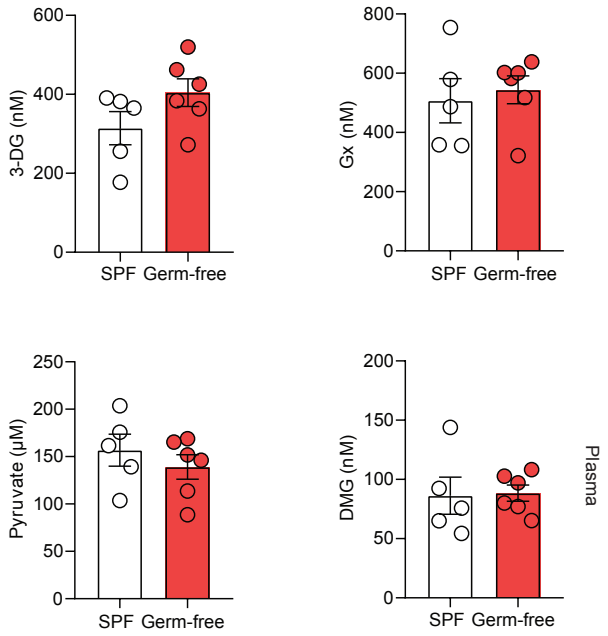

Fig. 4.11 | The gut microbiota does not influence plasma dimethylglyoxal concentrations.

3-Deoxyglucosone, glyoxal, methylglyoxal, pyruvate and dimethylglyoxal in plasma of specific-pathogen-free (SPF, *n*=5) or germ-free mice (*n*=6). For normalization, deuterated methylglyoxal (d4-MG) and [$^{13}C_3$] sodium pyruvate were used as internal standards. Values are means ± SEM. Statistical comparisons by two-tailed unpaired *t* test. Detailed information on the test statistics is provided in the Statistical table.

To evaluate the influence of gut microbiota on plasma levels of DMG in mammals, LC-MS^2 analysis was performed to detect α-dicarbonyls in the plasma of SPF and germ-free mice. SPF mice are a suitable control model for germ-free mice since they have gut microbiota but are pathogen-free. Interestingly, we did not find any differences in the levels of 3-DG, Gx, MG, pyruvate and DMG between the two groups (**Fig. 4.11**). These results show that the microbiome of SPF mice does not significantly contribute to the DMG levels in the mouse bloodstream.

4.6 Dimethylglyoxal is the precursor of N_ε-3-hydroxy-2-butanonelysine (HBL) in hyperglycemic mice

Reactive glucose metabolites are involved in the pathophysiology of diabetes by the formation of AGEs. AGEs are non-enzymatically generated by the interaction between α-dicarbonyls and proteins[173].

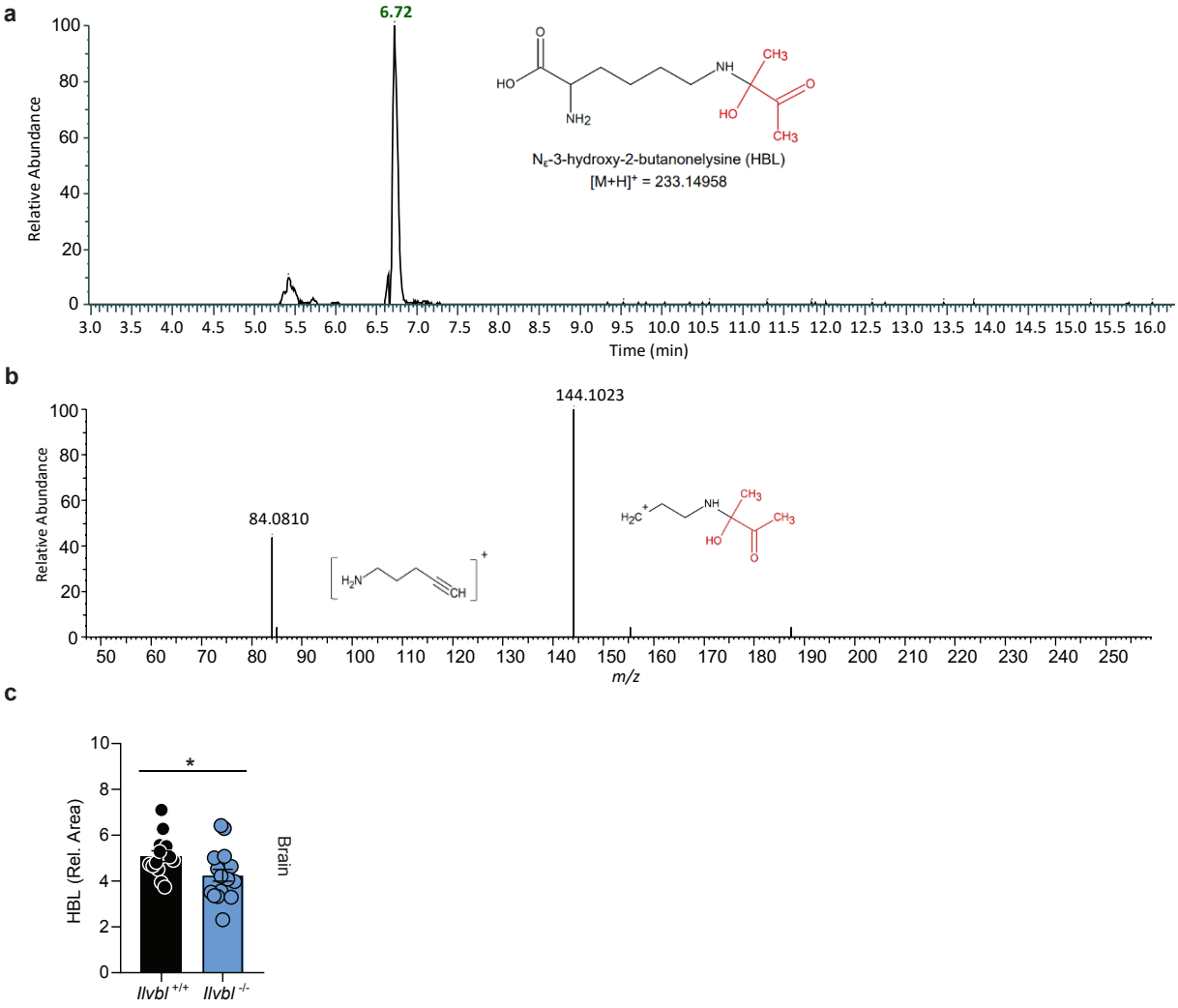

Fig. 4.12| Dimethylglyoxal reacts with lysine to the glycated amino acid Nε-3-hydroxy-2-butanonelysine *in vivo*.

a Representative chromatogram of Nε-3-hydroxy-2-butanonelysine (HBL, retention time = 6.72 min; *m/z* = 233.14958) in an acute hyperglycemic mouse brain. **b** Representative fragmentation spectrum of HBL (fragment *m/z* = 84.0810, and 144.1023) in an acute hyperglycemic mouse brain. **c** Levels of HBL in the brain homogenate of *Ilvbl*$^{+/+}$ (*n*=14) or *Ilvbl*$^{-/-}$ (*n*=17) mice with acute hyperglycemia. For normalization, labeled standard d4-Nε-carboxyethyllysine (d4-CEL) was used as internal standard. The molecules were created by ChemSketch and published in Rhein, S., Costalunga, R., Inderhees, J., *et al.*, 2024[55]**.** Values are means ± SEM. Statistical comparisons by two-tailed unpaired *t* test (**c**). *$p < 0.05$. Detailed information on the test statistics is provided in the Statistical table.

As well established in the literature, α-dicarbonyls react mainly with basic amino acids[173,174].Therefore, we wanted to evaluate the presence of dimethylglyoxal-glycated amino acids in the brain of acute hyperglycemic mice. Notably, HBL - a compound generated by the interaction between dimethylglyoxal and lysine - was identified based on the precursor mass (*m/z* = 233.14958), retention time and fragmentation spectrum. The retention time of HBL was 6.72 min (**Fig. 4.12a**), passing the stationary phase just slightly faster than the internal standard d4-CEL (6.88 min), a structurally similar compound. Moreover, two fragments were of a respective *m/z* of 84.0810 and 144.1023, fitting the predicted structure of HBL (**Fig. 4.12b**). Interestingly, HBL levels were lowered in the brain of *Ilvbl*$^{-/-}$ mice compared to the *Ilvbl*$^{+/+}$ littermates (**Fig. 4.12c**). These results confirm the role of *Ilvbl* in the generation of DMG and the ability of DMG to interact with amino acids *in vivo*, as described for other α-dicarbonyls.

4.7 Dimethylglyoxal crosses the intestinal and blood-brain barriers

Once established that DMG is a product of glucose metabolism in mammals and could generate glycated amino acids, I wondered if ingested DMG can pass the intestine and be distributed from the bloodstream to the organs. To evaluate the intestinal absorption of dimethylglyoxal, [$^{13}C_4$] DMG (5 mg/kg) was administrated to three mice via oral gavage (**Fig. 4.13a**). This way, I was able to track the route of [$^{13}C_4$] DMG due to the ability of high-resolution mass spectrometry to distinguish native or labeled compounds based on the exact mass.

Notably, [$^{13}C_4$] DMG was detected in the plasma of mice treated with [$^{13}C_4$] DMG 20 min after the gavage (**Fig. 4.13b**), demonstrating that DMG can cross the intestinal barrier. Interestingly, [$^{13}C_4$] DMG was also detected in the brain homogenate, suggesting that DMG is able to cross the BBB (**Fig. 4.13c**). Moreover, we detected [$^{13}C_4$] DMG in the liver homogenate (**Fig. 4.13d**), proving that DMG can also be distributed to peripherical organs. Lastly, labeled forms of 3-DG, Gx, MG or pyruvate were not detected in the plasma or tissue homogenates (data not shown), suggesting that DMG is not catabolized to pyruvate or the other α-dicarbonyls.

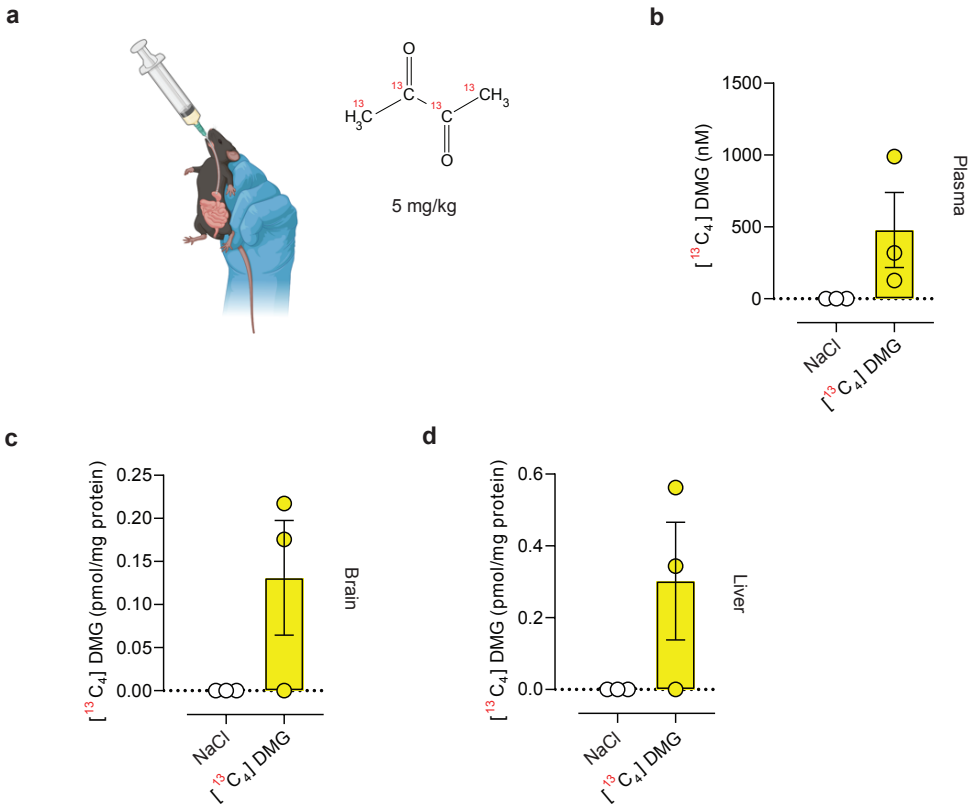

Fig. 4.13 | Dimethylglyoxal crosses the intestinal and blood-brain barriers.

a Treatment of wild-type mice with saline solution or 5 mg/kg [$^{13}C_4$] dimethylglyoxal ([$^{13}C_4$] DMG) solution via oral gavage. The molecule was created using ChemSketch. **b** [$^{13}C_4$] DMG concentrations in plasma 20 min after gavage of mice with NaCl or [$^{13}C_4$] DMG (*n* = 3 per group). **c** Concentrations of [$^{13}C_4$] DMG in brain homogenate 20 min after gavage of mice with NaCl or [$^{13}C_4$] DMG (*n* = 3 per group). **d** Concentrations of [$^{13}C_4$] DMG in liver homogenate 20 min after gavage of mice with NaCl or [$^{13}C_4$] DMG (*n* = 3 per group). For normalization, deuterated methylglyoxal (d4-MG) was used as internal standard. Values are means ± SEM. Detailed information on the test statistics is provided in the Statistical table.

4.8 Long-term dimethylglyoxal treatment increases plasma dimethylglyoxal concentrations

Based on the ability of DMG to cross the intestinal barrier, investigating the long-term consequences of DMG exposure in mice was possible by administrating the compound via water. Wild-type mice were treated with native DMG (100 mg/kg/day) dissolved in drinking water for 15 weeks (**Fig. 4.14a**). Mice treated with DMG were normoglycemic like control mice (**Fig. 4.14b**).

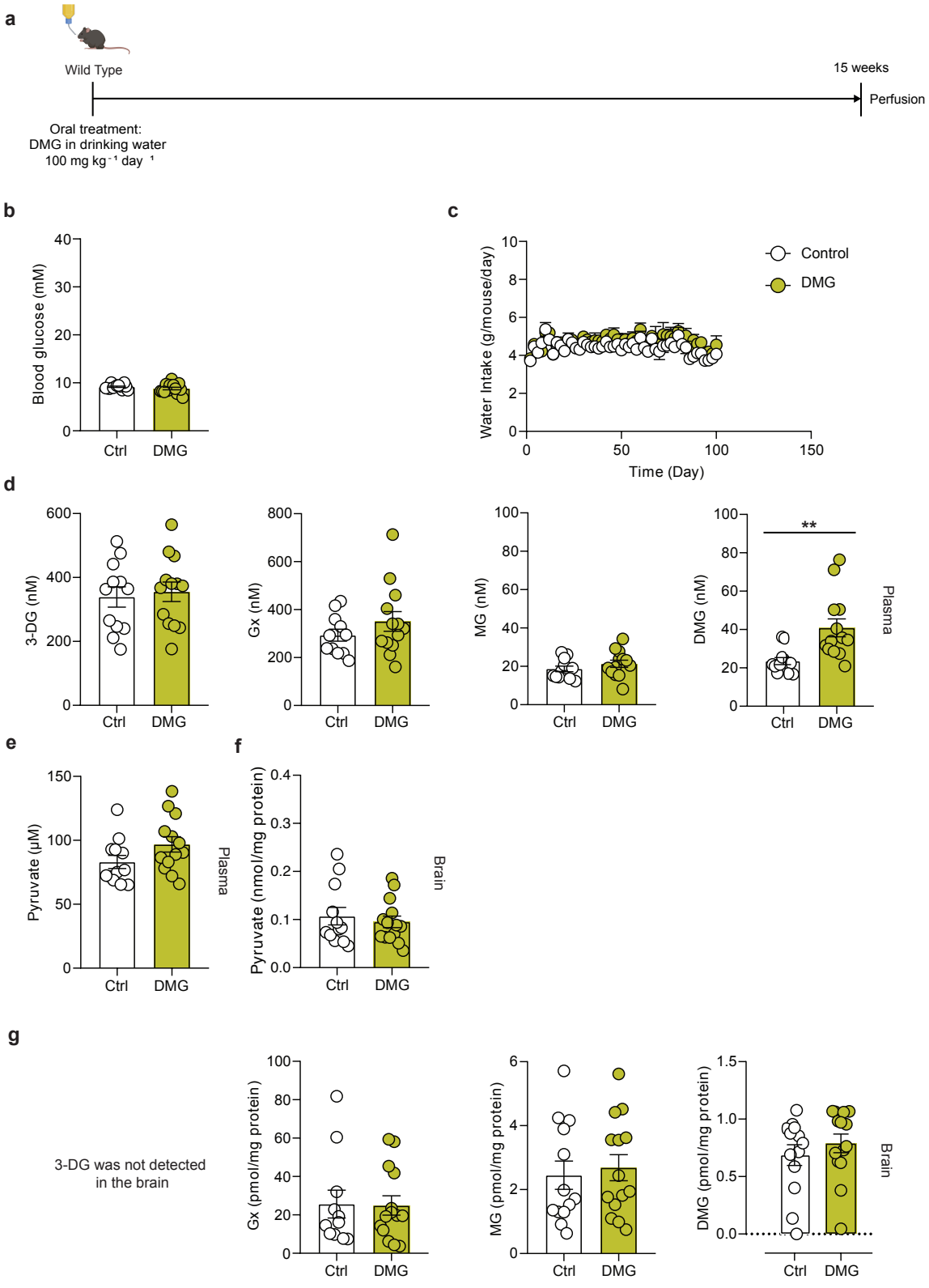

Fig. 4.14 |Long-term treatment with dimethylglyoxal increases concentrations of dimethylglyoxal in the plasma.

a Timeline of treatment with dimethylglyoxal (DMG) in drinking water and sample collection after 15 weeks. Part of the image was created with BioRender.com. **b** Blood glucose concentrations after 15 weeks of DMG oral treatment (Control, *n*=13; DMG, *n*=14). **c** Water intake of control and STZ-treated mice with tap water and water

intake of mice with DMG in tap water (50 time points per group, 4-6 cages per group). **d** 3-Deoxyglucosone (3-DG), glyoxal (Gx), methylglyoxal (MG) and DMG concentrations in plasma after 15 weeks of DMG oral treatment (Control, *n*=11-12; DMG, *n*=13). **e** Plasma pyruvate concentrations after 15 weeks of DMG oral treatment (Control, *n*=12; DMG, *n*=13). **f** Pyruvate concentrations in brain homogenate after 15 weeks of DMG oral treatment (Control, *n*=12; DMG, *n*=14). **g** Gx, MG and DMG concentrations in brain homogenate after 15 weeks of DMG oral treatment (Control, *n*=11-13; DMG, *n*=14). For normalization, deuterated methylglyoxal (d4-MG) and [$^{13}C_3$] sodium pyruvate were used as internal standards (**d-g**). Values are means ± SEM. Statistical comparisons by two-tailed Mann-Whitney U test (**b**; **d**, Gx and DMG; **g**, Gx and DMG), Kruskal-Wallis followed by Dunn´s post hoc tests (**c**), two-tailed unpaired *t* test (**d**, 3-DG and MG; **e**; **f**; **g**, MG). *$p < 0.05$; **$p < 0.01$; ***$p < 0.001$. Detailed information on the test statistics is provided in the Statistical table.

Even though this drug has a very intense smell and taste, DMG presence did not influence the water intake between control and DMG-treated mice (**Fig. 4.14c**)[175,176]. As expected, the long-term treatment with DMG increased the plasma concentrations of DMG compared to the control group (**Fig. 4.14d**), to a similar level than in the STZ-treated mice (**Fig. 4.1d**). Moreover, 3-DG, Gx, MG or pyruvate levels were not changed between the two treatments, confirming that DMG is not a precursor of other α-dicarbonyls (**Fig. 4.14d, e**). The same results were observed regarding Gx, MG and pyruvate concentrations in the brain homogenate (**Fig. 4.14f, g**). As in previous analyses, 3-DG was not detected in the brain (**Fig. 4.14g**). Importantly, even though we proved that DMG can cross the BBB (**Fig. 4.13c**), the concentration of DMG was not changed in the brain by the chronic treatment with oral DMG (**Fig. 4.14g**), in contrast to the DMG upregulation in the type-1 diabetic mouse model (**Fig. 4.1e**).

4.9 Dimethylglyoxal induces oxidative stress and neuroinflammation *in vitro*

Previous studies showed that MG augments oxidative stress[38,177], thus I wondered if DMG has similar effects *in vitro*. I detected ROS production with the fluorescent dye CM-H_2DCFDA in bEnd.3 cells, Hep G2 cells and HT-22 cells. In bEnd.3 cells and in Hep G2 cells, oxidative stress is proportionally augmented by DMG in a concentration-dependent manner (**Fig. 4.15a, b**). In accordance, the highest concentration (500 µM) of DMG also increased the generation of ROS in the HT-22 cells (**Fig. 4.15c**). These findings show that DMG induces oxidative stress in cells. Lastly, to evaluate the neuroinflammatory effects of DMG, I treated HT-22 cells with DMG for 24 hours in a conventional incubator (37 °C, 5 % CO_2). Interestingly, DMG induced the expression of the pro-inflammatory genes phospholipase A2 Group IVA (*Pla2g4a*), prostaglandin E synthase (*Ptges)* and prostaglandin-endoperoxide synthase *2* (*Ptgs2*) and the expression of the pro-apoptotic gene BCL2 Like 11 (*Bim*) (**Fig. 4.15d**).

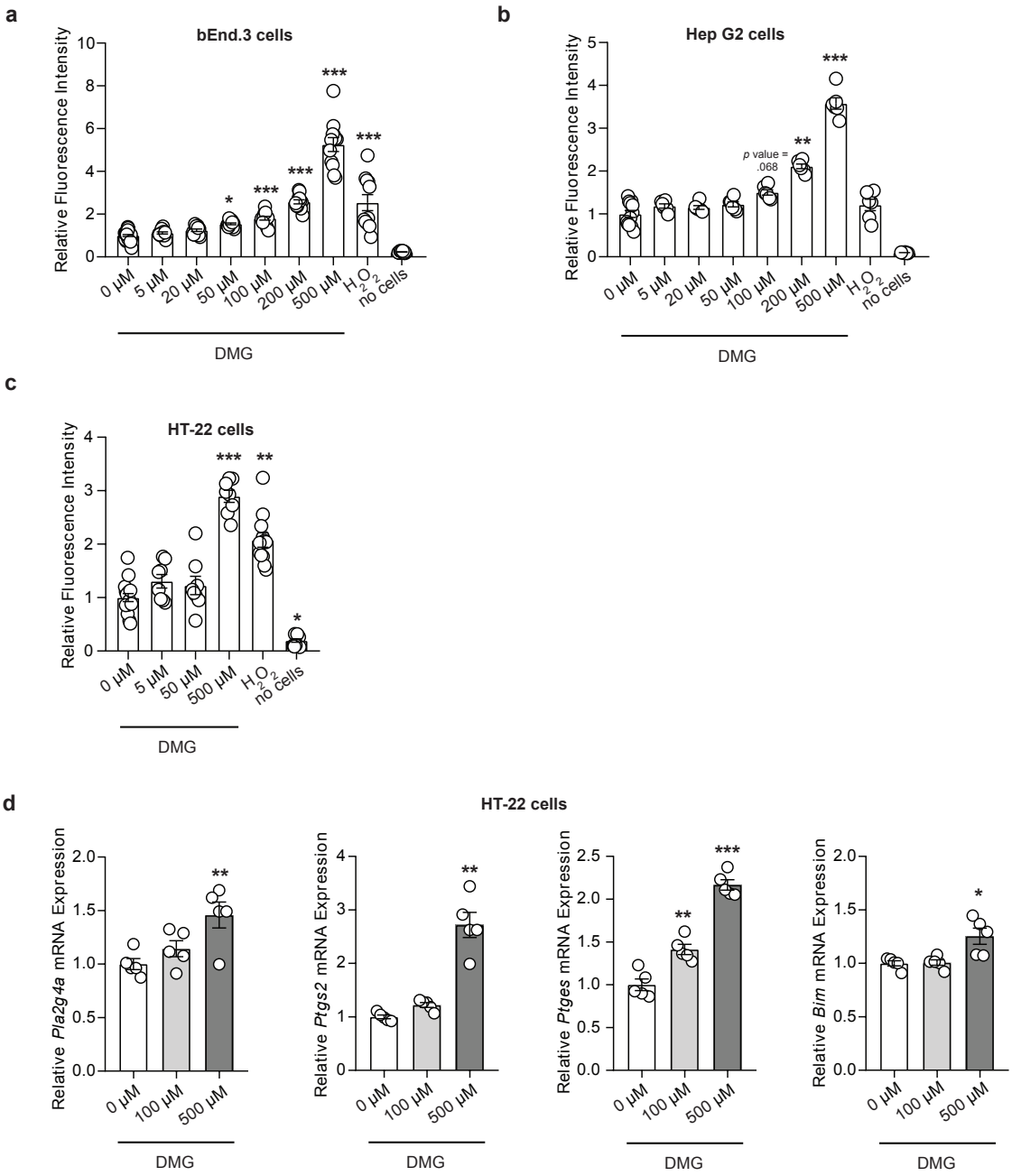

Fig. 4.15 | Dimethylglyoxal induces oxidative stress and neuroinflammation *in vitro*.

a Induction of reactive oxygen species (ROS) in mouse brain endothelial bEnd.3 cells (*n*=11-12 per group, *n*=24 for 0 µM DMG). **b** Induction of ROS in human liver cancer Hep G2 cells (*n*=6 per group, *n*=12 for 0 µM DMG). **c** Induction of ROS in mouse hippocampal neuronal HT-22 cells (*n*=8 per group, *n*=16 for 0 µM DMG). **d** mRNA expression of pro-inflammatory or pro-apoptotic genes in HT-22 cells (*n*=5 per group) treated with DMG for 24 hours. Values are means ± SEM. Statistical comparisons by Kruskal-Wallis followed by Dunn´s post hoc tests (**a**; **b**; **c**; **d**, *Ptgs2* and *Bim*) or one-way ANOVA followed by Dunnett´s post hoc tests (**d**, *Pla2g4a* and *Ptges*). **p* < 0.05; ***p* < 0.01; ****p* < 0.001. Detailed information on the test statistics is provided in the Statistical table.

5. Discussion

5.1 Dimethylglyoxal upregulation under diabetic conditions

Reactive glucose metabolites are involved in diabetic complications through the generation of AGEs[178]. So far, only α-dicarbonyls 3-DG, Gx and MG have been in-depth investigated and associated with diabetic complications[9,27,36]. 3-DG and Gx are non-enzymatically generated from glucose by Maillard reaction, whereas MG is also a glycolytic metabolite[6,7,29]. As described in the introduction, diabetic and hyperglycemic conditions increase concentrations of 3-DG, Gx and MG, leading to higher concentrations of AGEs[14,16,24,96]. Thus, AGEs upregulation and their interaction with RAGE have been associated with diabetic neuropathy, retinopathy and nephropathy[101,179].

First, the current study shows that type-1 diabetic conditions increase 3-DG concentrations in mouse plasma, suggesting that the STZ-treated mouse model may be suitable for studying the dicarbonyl stress in diabetes[16,166]. Since 3-DG is a non-enzymatic glucose metabolite and the Maillard reaction occurs *in vivo*, its plasma concentrations are positively and directly associated with blood glucose concentration in the bloodstream. Moreover, to the best of my knowledge, the current study shows the first measurements of 3-DG concentration in a mouse model of type-2 diabetes. As expected, hyperglycemic conditions increased 3-DG concentrations in *db/db* mice. In line with the experimental diabetes models, 3-DG upregulation was also observed in the serum of patients with type-1 and type-2 diabetes[14,55]. To my knowledge, Rhein *et al.* and I first reported Gx analyses in type-1 diabetic mice, while this current study shows the first Gx concentration measurements in a mouse model of type-2 diabetes[54]. Gx levels were not upregulated in type-1 or type-2 diabetes mice, whereas Gx concentrations were higher in patients with type-2 diabetes[55]. Thus, Gx is not a suitable α-dicarbonyl for evaluating dicarbonyl stress in experimental diabetes models. On the other hand, previous studies and the current research have shown that plasma or serum MG concentrations are upregulated in both type-1 and type-2 diabetic animals[167,180]. In contrast, another previous study showed that type-1 diabetic conditions do not change MG concentrations[54]. Even though lack of insulin prevents glucose uptake if it depends on insulin, hyperglycemic conditions lead to higher glucose uptake in non-insulin-dependent cells[71]. Moreover, glycogenesis is reduced by insulin deficiency, leading to higher glucose concentration in the extracellular space and probably to a higher generation of MG by non-insulin-dependent cells[181]. Thus, glycolytic metabolites are also generated and released in the bloodstream independently of insulin sensitivity. Furthermore, since hyperglycemic conditions reduce glyoxalase I activity, MG degradation is inhibited and levels are probably higher under diabetic conditions[182]. The upregulation of MG has also been observed in patients with type-2 diabetes, showing that the *db/db* mouse model is also a proper experimental model for investigating the role of MG in diabetic complications[55,183]. Pyruvate was also investigated during the current study, as it is the endpoint of the

glycolytic pathway. Generally, researchers measure lactate levels rather than pyruvate because lactate can easily be detected and is associated with metabolic dysfunction[184,185]. However, the current results showed that plasma pyruvate concentrations are lowered in the type-1 diabetic mice probably because it is metabolized to lactate. This research also shows that MG and pyruvate are upregulated in the liver of *db/db* mice. Since they are both glycolytic products, their upregulation could be caused by the overexpression of glycolytic genes in *db/db* mouse liver[186].

Only recently, α-dicarbonyl DMG has been recognized as a reactive glucose metabolite, since it is a product of glucose and pyruvate metabolism in mammal cells[54]. As mentioned in the introductive part of this thesis, DMG was previously not associated with hyperglycemia or glucose metabolism in mammals. In 2013, a research reported that DMG was detected in the breath of patients with diabetes only after oral glucose administration, but researchers associated this finding with glucose metabolism in mouth bacteria[187]. Recently, Rhein *et al.* found that plasma and brain DMG concentrations are higher in type-1 diabetic mice[54]. In my thesis, the upregulation of DMG in the plasma and brain of type-1 diabetic mice was evident, confirming the previous results. Thus, our studies reported that type-1 diabetes causes DMG increase in mouse plasma, like 3-DG and MG. Furthermore, DMG was the only α-dicarbonyl upregulated in the brain of STZ-injected animals. Then, this thesis shows the measurement of DMG concentrations for the first time in type-2 diabetic mouse plasma, brain and liver. As found in type-1 diabetic mice, plasma DMG concentrations were upregulated in *db/db* mice, coherently with the higher levels of other α-dicarbonyls in this mouse model. Similar to MG, hyperglycemic conditions may increase DMG by the higher metabolization rate of glucose after non-insulin-dependent uptake. As a confirmation of the upregulation of DMG under diabetic conditions, a clinical study showed that serum DMG concentrations are augmented in patients with type-1 and type-2 diabetes[55]. Even though DMG concentrations are slightly lower in humans, mouse experimental models of type-1 and type-2 diabetes used during the current thesis are suitable for the evaluation of DMG-mediated dicarbonyl stress in diabetes. Since obesity is an established phenotype and risk factor of type-2 diabetes, α-dicarbonyls were analyzed in diet-induced obese mice. My analyses showed that serum DMG levels are not increased in mice fed with HFD, like 3-DG and MG. In contrast, HFD increased the concentration of Gx. Even though HFD caused an increase in blood glucose concentration, not even the close glucose metabolite 3-DG was affected. Recently, a Dutch study showed that fasting levels of 3-DG, Gx and MG are not changed between non-diabetic lean and obese men, whereas only postprandial levels of 3-DG and MG are upregulated in obese men[188]. Importantly, they fed men using a mixed meal containing 44 % of energy from carbohydrates and 46.6 % of energy from fat[188]. Since the HFD mouse model has been considered a model of early type-2 diabetes, glucose introduced by diet is not properly converted to glycogen in the liver, probably leading to higher glucose conversion to reactive glucose metabolites in non-insulin-dependent cells[189]. In the current study, obese mice

were fed with an HFD containing 60 % kcal from fat and only 20 % kcal from carbohydrates, whereas control mice were fed with a standard diet containing 18 % kcal from fat and 58 % kcal from carbohydrates. Thus, the low carbohydrate consumption could explain why 3-DG, MG and DMG were not changed in diet-induced obese mice. For further investigation of DMG with a diet-induced obesity model, I recommend developing the diet-induced obesity model using HFD and subsequently feeding the mice with a higher content of carbohydrates, identical to control mice. This way, DMG concentrations will be investigated in obese and control mice on the same high-carbohydrate diet. Moreover, almost one-third of HFD consists of lard (31.66 % w/w), which comprises 9.5 % w/w linoleic acid and 0.8 % w/w linolenic acid[190]. My analyses showed that Gx concentrations are dramatically increased in mice fed with HFD compared to the control group. Likely, lipid peroxidation of linoleic and linolenic acids causes the upregulation of Gx due to the significant presence of lard in the HFD formula[18,191]. As mentioned in the introduction, high Gx concentrations can cause calcium oxalate stone accumulation in the urinary tract by its metabolization to glyoxylate and then oxalate[22,23]. Nephrolithiasis can be prevented by diuretic treatment or diet modifications such as reduction of sodium intake, enhancement of fluid intake and reduction of oxalate intake[192]. Thus, the current research suggests that lard could play a potential role in generating oxalate stones. Further research could investigate the association between lard intake and nephrolithiasis in experimental models and/or clinical studies.

In summary, diabetic conditions elevate plasma DMG concentration, theoretically leading to DMG-mediated dicarbonyl stress. Dicarbonyl stress is a metabolic condition that comprises upregulation and accumulation of α-dicarbonyls. As mentioned at the beginning of this chapter, dicarbonyl stress and diabetic complications have been attributed only to 3-DG, Gx and MG so far. Rhein *et al.* and my findings suggest that DMG could be a meaningful α-dicarbonyl involved in developing diabetic complications[54].

5.2 Generation of the pyruvate metabolite dimethylglyoxal by ILVBL in mammals under pathological conditions

In plants, bacteria and yeast, DMG is generated from pyruvate, a metabolite produced from glucose via glycolysis, or from the TCA metabolite citrate by malolactic fermentation[53,193]. Indeed, malolactic fermentation increases the DMG concentration in wine, increasing the buttery aroma[194]. Rhein *et al.* found that bEnd.3 cells generate DMG from glucose by pyruvate as an intermediate product[55]. After the C-1 decarboxylation of pyruvate, the C-2 and C-3 of two pyruvate molecules interact, generating a DMG molecule[55]. In prokaryotes and yeasts, DMG is produced from pyruvate by α-acetolactate formation. Here, the enzyme ALS is involved in the formation of α-acetolactate from pyruvate[195]. Subsequently, DMG is generated from α-acetolactate by oxidative decarboxylation. The current study

has investigated the role of *Ilvbl*, the mammal orthologue of ALS, in the generation of DMG in mammals. To investigate the role of *Ilvbl in vitro*, bEnd.3 cells were transfected with *Ilvbl* siRNA. Beforehand, this research shows that DMG is secreted from the cells to the media, like all other α-dicarbonyls. For this reason, all following *in vitro* experiment outcomes were obtained by measuring α-dicarbonyls in the media. bEnd.3 cells were chosen because they are vulnerable to MG-mediated dicarbonyl stress, and they metabolize both glucose and lactate[196-198]. In the first experiment using *Ilvbl* siRNA, transfected bEnd.3 cells were treated with [$^{13}C_6$] glucose under normoxic or hypoxic conditions. The use of the labeled form of glucose allows the isotopic tracking of the catabolism of glucose and the generation of labeled forms of α-dicarbonyls, avoiding the ambiguity caused by the inevitable presence of native α-dicarbonyls. First, my experiment confirmed that glucose is a precursor of DMG in mammal cells. Here, hypoxia increased MG, pyruvate and DMG levels, whereas 3-DG and Gx levels were not influenced by oxygen concentration. As already quoted in the introduction, hypoxic conditions increase the stability of the protein HIF-1α, and its activation inhibits the enzyme PDH through its inhibitor PDK1[125]. Since PDH is downregulated, the metabolism shifts the ATP generation from the mitochondrial TCA cycle to the cytosolic glycolysis. Thus, HIF-1α increases the expression of glycolytic genes and glucose transporters, besides the upregulation of LDH and the consequent lactate increase[125]. The upregulation of glycolysis induces the glycolytic products MG and pyruvate and the post-glycolytic product DMG. In these experiments, [$^{13}C_2$] DMG was increased under hypoxic conditions, suggesting that it is a product of the interaction between a [$^{13}C_3$] pyruvate and a native [$^{12}C_3$] pyruvate. However, [$^{13}C_2$] DMG was also detected in cells treated with native glucose, indicating that this isotopic metabolite could be naturally generated from native [$^{13}C_1$] pyruvates with a carbon-13 in position 2 or 3. Here, the relative area of [$^{13}C_2$] DMG was about one hundredth of the relative area of native DMG, consistent with the ratio of 1/100 for $^{13}C/^{12}C$ (data not shown). Since [$^{13}C_2$] DMG levels were higher in cell media after treatment with [$^{13}C_6$] glucose compared with native glucose, [$^{13}C_2$] DMG seems to be generated both from the condensation of a [$^{13}C_3$] pyruvate and a native [$^{12}C_3$] pyruvate and the interaction between two native [$^{13}C_1$] pyruvates. Lastly, 3-DG and Gx are non-enzymatic products of glucose, thus HIF-1α stabilization does not influence the levels of these reactive glucose metabolites. [$^{13}C_4$] DMG was also generated in bEnd.3 cells treated with [$^{13}C_3$] pyruvate, and its levels were higher under hypoxic conditions. These results confirm that DMG is a post-glycolytic metabolite in mammals, and its generation is enhanced by the downregulation of PDH activity and the consequent shift of pyruvate catabolism. [$^{13}C_4$] DMG was the only α-dicarbonyl generated from [$^{13}C_3$] pyruvate, confirming that 3-DG, Gx and MG are only generated during the first part of glucose metabolism. In her doctoral thesis, Rhein showed that [$^{13}C_4$] DMG is downregulated in the media of bEnd.3 cells transfected with *Ilvbl* siRNA, under hypoxic conditions[54]. In contrast, my results show that *Ilvbl* knockdown does not influence the formation of [$^{13}C_4$] DMG from [$^{13}C_6$] glucose or [$^{13}C_3$] pyruvate

in vitro, neither in normoxia nor hypoxia. However, overexpression of *Ilvbl* leads to increased DMG levels in bEnd.3 cell media under hypoxic conditions[55]. Thus, the role of *Ilvbl* in the DMG generation *in vivo* is investigated and discussed in the current thesis. First, *Ilvbl* knockout mice were fertile and showed no particular phenotype. Moreover, *Ilvbl* deficiency did not influence the generation of DMG in plasma, brain or peripheral organs of healthy mice. As mentioned above, hypoxia induces the generation of DMG, as well as the glycolytic products MG and pyruvate. To stimulate DMG formation, hyperglycemic ischemic stroke was induced by the administration of [$^{13}C_6$] glucose prior to pMCAO. Hypoxic conditions occur during ischemic stroke due to the lower blood supply and the lack of oxygen distribution in the brain. Thus, ischemic conditions can stimulate the upregulation of glycolysis, and the lower chemical energy generation caused by the downregulation of the TCA cycle contributes to cell membrane damage by enhancing oxidative stress[128]. Acute hyperglycemic conditions were induced, representing the fact that ischemic stroke can induce hyperglycemia even in patients without diabetes[117,118]. Moreover, a previous study showed that plasma DMG levels are increased in acute hyperglycemic and ischemic mice[55]. Therefore, the current experimental model of ischemic and hyperglycemic stroke is a suitable model for the evaluation of DMG-mediated dicarbonyl stress.

In the first model, normoglycemic and hyperglycemic *Ilvbl*$^{+/+}$ and *Ilvbl*$^{-/-}$ mice were sacrificed 25 min after pMCAO. The current study confirms that hyperglycemic conditions increase plasma DMG levels in ischemic mice. As partially mentioned above, Rhein *et al.* previously found a significant plasma upregulation of DMG in stroke-induced mice 50 min after pMCAO, whereas an insignificant positive trend was observed in mice sacrificed 30 min after pMCAO[55]. In contrast, my data showed lower DMG levels in the brain of hyperglycemic mice, whereas Rhein´s study showed no differences between the two groups[55]. Thus, future studies should be performed to investigate DMG catabolism in the brain. It would be interesting to evaluate if DMG downregulation is caused by its interaction with amino acids or its catabolism to hydrophilic metabolites. This experiment also showed that plasma and brain [$^{13}C_2$] and [$^{13}C_4$] DMG are generated from [$^{13}C_6$] glucose, confirming that DMG is a glucose metabolite *in vivo*. Lastly, *Ilvbl* deficiency did not influence the plasma or brain DMG levels in normoglycemic or hyperglycemic ischemic mice 25 min after pMCAO. In the following experiment, hyperglycemic mice were sacrificed 50 min after pMCAO. Here, normoglycemic mice were not studied since I confirmed that plasma DMG levels are higher in hyperglycemic mice, and labeled forms of DMG are generated from [$^{13}C_6$] glucose *in vivo*. Instead, mice with sham surgery were included in this study to evaluate the effect of ischemia – and not only hyperglycemia – in the DMG generation. First, plasma [$^{13}C_2$] and [$^{13}C_4$] DMG concentrations were upregulated in ischemic mice, probably due to the higher glycolytic gene expression caused by hypoxia. In support of this hypothesis, native MG levels were also upregulated in hyperglycemic and stroke-induced ischemic mice, whereas ischemic stroke did not influence the non-glycolytic glucose metabolites 3-DG and Gx levels. In contrast, plasma [$^{13}C_3$] pyruvate levels were

downregulated in ischemic mice, probably because hypoxia also enhances the conversion of pyruvate to lactate[125,199]. Lactate upregulation in stroke play have a positive role in protecting against neuronal damage[200]. As mentioned in the introduction, ischemic stroke induces the upregulation of glutamate, causing excitotoxicity due to increased Ca^{2+} concentration in cells[122,130]. A Swiss group found that lactate plays a neuroprotective role against excitotoxicity through increased and released chemical energy[201]. On the contrary, ischemic stroke increased native pyruvate in the ipsilateral side of the brain, probably by glycolytic upregulation under hypoxic/ischemic conditions. However, this result cannot exclude the enhanced shift from pyruvate to lactate in the brain. In support of this hypothesis, two Chinese studies showed that lactate is upregulated in the ipsilateral side of the brain of ischemic rats compared to the sham group, 60 min after surgeries[202,203]. Moreover, native MG and Gx levels were also higher in the ipsilateral hemisphere of the ischemic mice. In addition, ischemic stroke increases MG levels in the contralateral side of the brain. Several studies showed that the contralateral side – and not only the ipsilateral side – of the brain is metabolically affected by ischemic stroke in animal models[202,203].

In the current study, brain DMG levels were markedly increased in stroke-induced ischemic mice. Interestingly, [$^{13}C_2$] and [$^{13}C_4$] DMG generation occurred from [$^{13}C_6$] glucose in both ipsilateral and contralateral hemispheres of the brain after ischemic stroke, whereas they were absent in the brain of sham-treated mice. Therefore, the current thesis proposes that hyperglycemic and ischemic stroke may cause DMG-mediated dicarbonyl stress, suggesting that DMG may play an important role in ischemic stroke complications. Recently, Rhein, Inderhees *et al.* found that Gx, MG and their glycated amino acids are positively correlated with poor outcomes in patients with acute ischemic stroke[118]. Furthermore, during the current study, DMG levels were higher in the ipsilateral compared to the contralateral hemisphere of the brain of ischemic mice. Since the ischemic hemisphere is affected by higher anaerobic glycolysis and lower ATP generation, the brain's contralateral hemisphere could compensate for the lack of chemical energy caused by ischemic stroke, increasing glucose uptake and metabolism. Therefore, DMG upregulation could be explained by higher glucose uptake in cells of the contralateral hemisphere. Future experimental and clinical studies may focus on the role of the contralateral side in glucose metabolism under hyperglycemic and ischemic stroke. Importantly, my research shows that *Ilvbl* knockout decreased DMG levels in the ipsilateral and contralateral hemispheres of the brain after hyperglycemic and ischemic stroke. Specifically, *Ilvbl* deficiency was more efficient in DMG reduction in the ipsilateral than the contralateral side of the brain. Since type-1 diabetic conditions increase DMG concentrations, STZ-injected *Ilvbl*$^{+/+}$ and *Ilvbl*$^{-/-}$ mice were also investigated in DMG generation. Here, *Ilvbl* deficiency also lowered DMG levels in the brain but did not influence plasma DMG levels. Thus, the current research found that *Ilvbl* plays a significant role in DMG generation in mammals, as well as in procaryotes and yeast. However, the role of *Ilvbl* was only

observed in the brain of diabetic and acute hyperglycemic stroke-induced ischemic mice, whereas *Ilvbl* deficiency did not affect DMG levels in healthy mice.

In summary, my studies have shown that DMG is a glucose metabolite generated by the condensation of two pyruvate molecules in mammals. Under pathological conditions, ILVBL catalyzes the catabolism of two pyruvates to α-acetolactate, an unstable metabolite converted to DMG by oxidative decarboxylation (**Fig. 5.1**)[204].

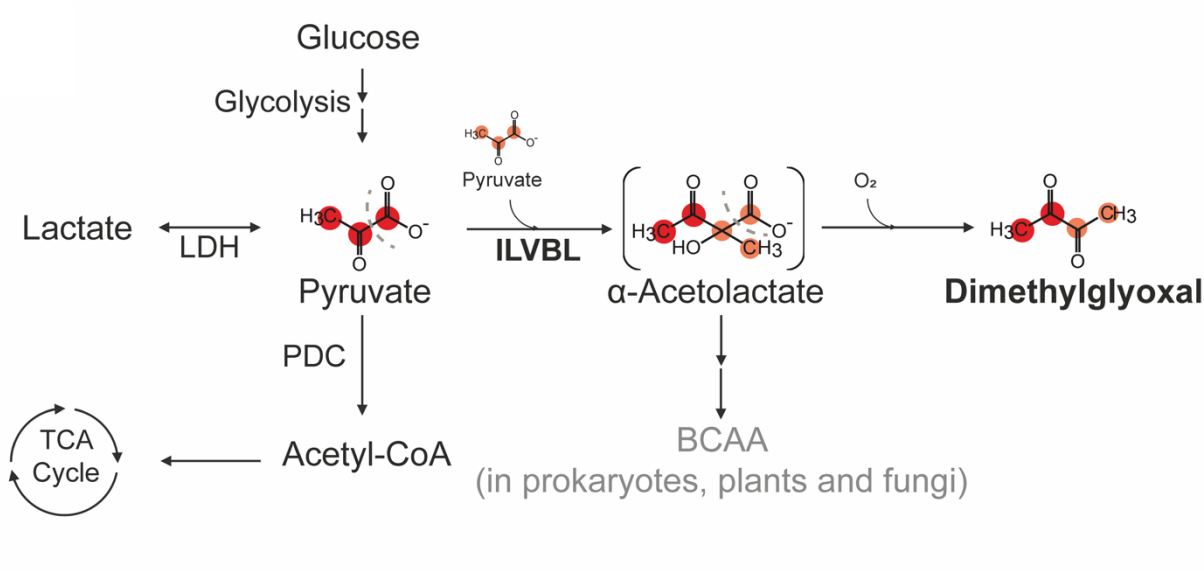

Fig. 5.1| Proposed schematic anabolic pathway to dimethylglyoxal in mammals.

The illustration was created by Biorender.com and published in Rhein, S., Costalunga, R., Inderhees, J., *et al.*, 2024[55]. LDH = lactate dehydrogenase, TCA = tricarboxylic acid, PDC = pyruvate dehydrogenase, BCAA = branched-chain amino acids.

5.3 Gut microbiota does not contribute to plasma dimethylglyoxal concentrations

Once it was established that cellular glucose metabolism generates DMG and ILVBL is only partly involved in its formation in mammals, I wondered if other sources of DMG contribute to its plasma concentrations. Since bacteria and yeasts inhabit the intestine and form the gut microbiota, their contribution in the plasma DMG concentration has been investigated in this thesis. Intestinal microbiota plays a significant role in metabolic disorders and disease development[205]. For example, alteration of the gut microbiota composition can lead to dysbiosis, a condition caused by several risk factors such as a diet rich in animal fat and proteins, a sedentary life, alcohol intake and smoking[205]. Dysbiosis can reduce insulin secretion, causing hyperglycemic conditions, and is associated with type-2 diabetes[205]. Future research may evaluate the consequence of dysbiosis in generating DMG since these conditions increase blood glucose concentration. Dysbiosis conditions can be developed in germ-free mice by human fecal microbiota transplantation, even though the human-microbiota-associated

(HMA) mouse model has significant limitations[206]. However, this current study did not focus on microbiota alterations affecting the mammal cellular DMG generation but on intestinal bacteria and yeasts contribution to DMG concentration in the bloodstream. Specifically, gut microbiota comprises lactobacilli, enterobacteria, and streptococcus, and their ability to generate DMG has been reported in the literature[207-210]. To investigate whether a potential DMG generation in the intestine contributes to plasma DMG concentration in mammals, DMG and other α-dicarbonyl concentrations were measured in the plasma of SPF and germ-free mice. Germ-free mice are animals completely deprived of microorganisms, and they are characterized by memory impairment, increased BBB permeability and dysregulation in metabolism and brain gene expression[211,212]. SPF mice possess microbiota but are free of pathogens and were used as control. The current study showed that plasma DMG concentrations were not influenced by microbiota. These findings do not exclude that DMG is a potential metabolite of microbiota but show that microbiota does not significantly influence the concentration of DMG in mammal plasma. Thus, further studies must be conducted to verify if DMG is a gut microbiota metabolite. For example, mice could be treated with [$^{13}C_6$] glucose via oral gavage or dissolved in drinking water, and [$^{13}C_4$] DMG presence could be investigated in the intestine. Importantly, the current research does not support the idea that any potential intervention in the microbiota would reduce DMG-mediated dicarbonyl stress. Moreover, microbiota did not influence the bacterial product MG and pyruvate concentrations in plasma[213]. Lastly, as expected, 3-DG and Gx levels were not altered by microbiota since they are not cellular metabolites.

In summary, DMG is generated from pyruvate via ILVBL in mammals, whereas gut microbiota does not contribute to its levels in plasma. Therefore, other sources of DMG have to be investigated in further experiments. In bacteria, DMG is a product of alanine and aspartate catabolism by pyruvate as an intermediate[214]. Since the amino acid catabolism cannot explain the partial role of ILVBL in DMG formation, other enzymes can be involved in its generation. An unpublished genome-wide association study recently showed a statistically significant association between the hepatic gene Orosomucoid 2 (ORM2, or α-1-acid glycoprotein) and DMG in humans. Moreover, ORM2 can play an anti-inflammatory role in the brain and bind small molecules[215,216]. ORM2 is highly and mainly expressed in the liver, and it is released in the bloodstream[217]. Therefore, α-dicarbonyl measurements in the plasma of *Orm2* knockout mice can elucidate its role in the metabolism of dimethylglyoxal.

5.4. The role of dimethylglyoxal in diabetic complications

At this stage, we know that DMG is upregulated under diabetic or ischemic conditions and is generated from glucose in mammalian cells. Dicarbonyl stress is caused by a substantial accumulation of α-dicarbonyls in blood and tissues, causing diabetic complications[218]. So far, dicarbonyl stress has been mainly associated with MG, in addition to 3-DG and Gx. Consequently, dicarbonyl stress is

characterized by the upregulation of glycated amino acids and AGEs, generated by the interaction of α-dicarbonyls with amino acids or proteins. Rhein and I found that DMG interacts with lysine, generating HBL[54]. Rhein detected HBL in the plasma of acutely dimethylglyoxal-treated mice, whereas I identified HBL in the brain of acute hyperglycemic mice[54]. HBL was identified based on its retention time, precursor ion *m/z* and fragmentation spectrum. HBL retention time was 6.72 min, passing the column faster than the internal standard d4-CEL. Since glycated amino acids were separated using a hydrophilic column, nonpolar molecules were eluted faster than polar compounds. Since HBL contains an extra methyl group compared to d4-CEL, it is less polar than the internal standard, which explains why HBL is less retained by the stationary phase and elutes faster than d4-CEL. The precursor ion was detected with *m/z* of 233.14956, suggesting a molecule structure generated by a nucleophilic reaction between the lysine amino group and a carbonyl group of DMG (**Fig. 5.2**). Moreover, the fragmentation spectrum elucidated the structure of HBL by detecting two fragments. The first fragment is characterized by *m/z* of 84.0810, associated with only lysine structure, while the second fragment includes DMG and partial lysine structures (**Fig. 4.12b**). Importantly, *Ilvbl* deficiency lowered levels of HBL in the brain of acute hyperglycemic mice, confirming the importance of ILVBL in DMG formation *in vivo*.

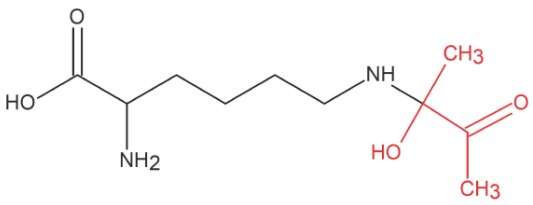

Nε-3-hydroxy-2-butanonelysine (HBL)
$[M+H]^+$ = 233.14956

Fig. 5.2| Proposed molecular structure of HBL.

The molecule was created by ChemSketch and published in Rhein, S., Costalunga, R., Inderhees, J., *et al.*, 2024[55].

Rhein detected further dimethylglyoxal-based glycated amino acids in the plasma of DMG-injected mice, based on the interaction between DMG with lysine or arginine[54]. However, my measurements did not detect other glycated amino acids. An explanation is that DMG injection markedly increased plasma DMG levels, increasing the possibility of DMG interacting with amino acids and increasing the amount of these adducts above the limit of detection[55].

In summary, our findings showed that DMG can interact with amino acids like 3-DG, Gx and MG. Thus, DMG is a reactive glucose metabolite, and its role in dicarbonyl stress has to be investigated. Notably, the reactivity of α-dicarbonyls occurs in non-hydrated form because water molecules can interact with the carbonyl groups, generating two hydrophilic groups per carbonyl group and preventing a

nucleophilic addition. Since this organic reaction occurs under acid or basic conditions, further studies could verify the impact of the hydration of dicarbonyls *in vivo*. However, DMG has the highest non-hydrated fraction compared to MG and Gx (27 % versus 1 % and 0.005 %, respectively) in aqueous solutions due to the highest number of methyl groups[219,220]. This fact suggests that DMG could be crucial in diabetic complications, theoretically contributing more to dicarbonyl stress than other α-dicarbonyls. In this thesis, I confirmed that DMG generates oxidative stress in brain endothelial cells[54]. Endothelial cells are characterized by RAGE expression, and its binding with AGEs causes oxidative stress[102,103]. Thus, the current data suggest that DMG can react with proteins, causing oxidative stress in endothelial cells. Rhein *et al.* found that DMG causes higher oxidative stress than MG in bEnd.3 cells and in macrophages[55]. Moreover, the current thesis shows that DMG also induced ROS generation in hippocampal neuronal cells and liver cells, suggesting that DMG can cause dicarbonyl stress in neurons and peripherical organs. As discussed in the introduction, neurons can generate chemical energy from glucose via glycolysis or lactate generated in glial cells and released in the intracellular space[72,73]. In a review published in 2013, Felipe Barros reported that neurons are protected from dicarbonyl stress since glycolysis occurs in astrocytes and neurons consume lactate without generating MG[221]. Our latest findings show that DMG is a reactive glucose metabolite that can be generated in neurons from extracellular lactate, and it is responsible for inducing oxidative stress, probably through the interaction of its adducts with neuronal RAGEs[222]. Thus, the binding of DMG-based AGEs to RAGEs may activate the enzyme NADPH oxidase[223]. Indeed, both AGE-RAGE engagement and NADPH oxidase cause cytokine and chemokine overexpression and activate the NF-κB cascade, besides ROS enhancement[103,105,222,224]. Moreover, this study shows that DMG induced the expression of neuronal pro-inflammatory genes *Pla2g4a*, *Ptgs2,* and *Ptges,* encoding enzymes involved in the anabolism of prostaglandins. *Pla2g4a* expression increases arachidonic acid formation, which is subsequently converted to PGH_2 by COXs. In particular, *Ptgs2* is an inducible COX isoform under inflammatory conditions, even though constitutive *Ptgs2* is present in the brain[225]. Subsequently, PGH_2 is converted to PGE_2 by *Ptges*. Interestingly, PGE_2 levels are higher in patients with diabetes and positively correlated with hyperglycemic conditions[226]. In particular, upregulation of PGE_2 has been observed in patients with diabetic retinopathy, which may be caused and worsened by accumulation of AGEs[227,228]. Moreover, neuroinflammatory effects of DMG have been confirmed *in vivo*[54,55]. DMG also induced the expression of the pro-apoptotic gene *Bim* in hippocampal neuronal cells. Neuronal *Bim* has been associated with neuron death in Alzheimer's Disease (AD), and AGEs have been linked to neuronal dysfunction and pathogenesis of neurological diseases[229,230]. Thus, glycation of protein with DMG may play a role in cognitive impairment and the development of neurological diseases.

Since diabetic and hyperglycemic conditions increase the risk of vascular dementia, a mouse model of chronic DMG upregulation had to be developed to investigate its role in developing neuronal diabetic

complications[231-233]. Chronic DMG concentration can be potentially increased by the long-term consumption of drinking water containing DMG. First, to evaluate whether DMG can cross the intestinal barrier is crucial, mice were treated with [$^{13}C_4$] DMG via oral gavage and sacrificed 20 min after the treatment. The current study showed that [$^{13}C_4$] DMG was detected in the plasma of treated mice, proving that DMG can cross the intestine. Moreover, this experiment shows that DMG can cross the BBB and be distributed to peripherical organs since [$^{13}C_4$] DMG was detected in the brain and liver. Based on these findings, mice were treated with 100 mg kg^{-1} day^{-1} native DMG in drinking water for 15 weeks. Plasma DMG concentrations were upregulated in a mouse model of long-term treatment with DMG, similar to the plasma concentrations of DMG in type-1 diabetic mice. However, brain DMG concentrations did not differ between DMG-treated mice and controls, suggesting that the dose of DMG in drinking water should be increased in future experiments in order to replicate brain DMG concentration of type-1 mice. Anyhow, long-term treatment with DMG caused cognitive impairment and BBB damage, similar to neurological complications in type-1 diabetic mice[55]. Since diabetic conditions increase DMG concentrations and long-term DMG treatment induces cognitive deficits, DMG may play an important role in the development of dementia in diabetes. Thus, future studies must be implemented to develop strategies focused on DMG reduction or the hindrance of protein glycation caused by DMG. Besides lifestyle improvement and dietary correction, pharmacological strategies may be investigated for DMG-mediated dicarbonyl stress reduction. For example, combining insulin and metformin lowered DMG levels in patients with diabetes[55]. Metformin mainly affects the liver, reducing gluconeogenic flux and blood glucose concentrations[234]. Thus, this drug increases the conversion of pyruvate to lactate, possibly causing the reduction of DMG levels. On the other hand, its mechanism of action causes lactate accumulation, which can rarely lead to lactic acidosis[235]. Even though metformin is considered safe, it can develop further side effects such as nausea, vomiting, headache and metallic taste[235]. Nevertheless, the role of metformin in reducing DMG generation and mitigating the consequence of dicarbonyl stress should be further investigated in experimental and clinical diabetes. As mentioned in the introduction, acetylsalicylic acid may compete with DMG and other α-dicarbonyls in post-translational protein modification, reducing the glycation of proteins[236]. Indeed, acetylsalicylic acid and paracetamol prevent cataract development in type-1 diabetic rats[108]. Therefore, acetylsalicylic acid effects could be investigated in preventing diabetic complications in experimental models of diabetes and/or long-term DMG intake. Moreover, the reverse strategy consists of reducing α-dicarbonyl availability to decrease protein glycation. So far, the investigational drug pimagedine has been studied in the reduction of protein glycation through its interaction with α-dicarbonyls[110]. However, pimagedine has not been approved for therapeutical use[109].

Then, pharmacological strategies can be investigated to reduce DMG production and/or stimulate DMG degradation. Previously, this thesis has shown that DMG is generated from pyruvate via ILVBL.

ILVBL is a druggable enzyme since its orthologue ALS is inhibited in other species. Since the 1980s, several classes of herbicides have been used as antagonists of ALS to suppress weed growth[237]. This pesticide class inhibits the BCAA synthesis, causing a reduction of cell division and cell death[237]. However, preliminary data showed that ALS-inhibitor treatment does not affect the generation of labeled DMG in bEnd.3 cells treated with [$^{13}C_6$] glucose[238]. Therefore, further research has to be conducted to discover proper ILVBL antagonists. However, *Ilvbl* deficiency did not reduce the infarct volume or BBB damage compared to *Ilvbl*$^{+/+}$ 2 days after pMCAO[55]. Moreover, DMG reduction in *Ilvbl*$^{-/-}$ mice did not influence BBB proprieties or neuroinflammatory states in type-1 diabetic mice (data not shown). Thus, these findings suggest addressing resources to other strategies in lowering dicarbonyl stress mediated by DMG.

Detoxification of Gx and MG is regulated by the glyoxalase system, based on their aldehyde structure[21,40]. On the other hand, DMG is an α-diketone and, therefore, is not metabolized by the glyoxalase system. Actually, brain glyoxalase I activity is inhibited by DMG[239]. Thus, the downregulation of glyoxalase I under hyperglycemic conditions may also be explained by the upregulation of DMG, worsening dicarbonyl stress states[182]. In bacteria, DMG is catabolized to acetoin by diacetyl reductase (dicarbonyl/L-xylulose reductase, DR or DCXR), followed by acetoin reduction to 2,3-butanediol by acetoin reductase (AR)[48]. A previous study found that mammal diacetyl reductase could metabolize DMG to acetoin, and that this enzyme can catalyze the oxidoreduction reaction between L-xylulose and xylitol[240]. DR deficiency has been observed in 1 in 3,300 people with Ashkenazi Jewish ancestry due to genetic mutations, causing pentosuria due to accumulation of L-xylulose in the urine[241-243]. Regarding the role of AR, a research group found that 2,3-butanediol is a metabolite of acetoin in mammalian liver homogenates in 1971[244]. Therefore, the role of DR and AR in DMG elimination should be investigated by downregulation and/or overexpression. Future research can further explore the formation of [$^{13}C_4$] acetoin and [$^{13}C_4$] 2,3-butanediol from [$^{13}C_4$] DMG in mammal cell lines.

Moreover, my unpublished preliminary data suggest that Hep G2 cells are able to lower DMG concentrations in the media. Since the liver plays a crucial role in the detoxification and metabolism of drugs, the Hep G2 cell line is suitable for the evaluation of DMG degradation. If these assumptions are confirmed, one could try to stimulate DMG elimination by upregulation of DR and AR activities in liver cells.

5.5 Conclusions

This research has investigated the α-dicarbonyl DMG in several mouse models under pathological conditions. Importantly, the current thesis has demonstrated that DMG concentrations are upregulated in mouse models of type-1 and type-2 diabetes (**Fig. 5.3**). Moreover, the current study has shown that acute hyperglycemia and ischemic stroke markedly increased DMG levels in the ischemic

hemisphere of the brain, whereas plasma DMG levels were only slightly increased in this experimental model (**Fig. 5.3**). The current work has confirmed that DMG is a post-glycolytic metabolite in mammals, and its production is higher under hypoxic conditions (**Fig. 5.3**). Therefore, the post-glycolytic DMG generation explains why cells consuming lactate – such as neurons and brain endothelial cells – are subjected to dicarbonyl stress, even though the pyruvate generation is not exclusively based on glycolysis. Importantly, this research has demonstrated that *Ilvbl* is involved in the generation of DMG in the brain of mice under chronic or ischemic hyperglycemia. Notably, the current study has identified HBL, a glycated amino acid generated by nucleophilic addition between the lysine amino group and the carbonyl group of DMG. Thus, this finding suggests the ability of DMG to interact with proteins, generating AGEs. The engagement of DMG-based AGEs with RAGE causes oxidative stress, neuroinflammation, BBB damage and development of cognitive impairment, mimicking neurological complications of diabetes (**Fig. 5.3**)[55].

In summary, DMG is crucial in developing dicarbonyl stress under diabetic or ischemic conditions. The discovery of DMG as a reactive pyruvate metabolite significantly contributes to a better understanding of dicarbonyl stress in neurological diabetic complications and the development of potential therapeutic strategies to reduce dicarbonyl effects.

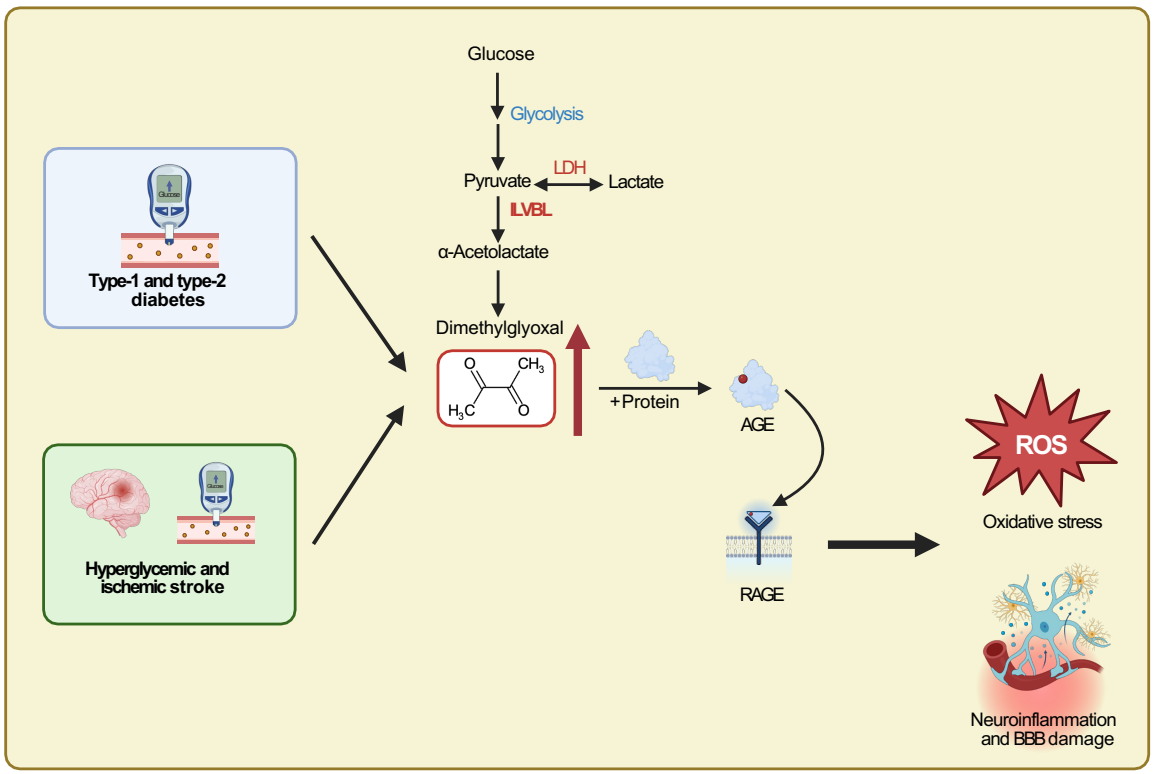

Fig. 5.3| Schematic illustration of dimethylglyoxal generation in mammal cells and its role in diabetic or ischemic complications.

This illustration was created with Biorender.com and Adobe Photoshop 2024 and modified after Inderhees, J., *et al.*, submitted[245]. LDH = lactate dehydrogenase, ILVBL = ilvB acetolactate synthase-like, AGE = advanced glycation end product, RAGE = receptor for advanced glycation end product, ROS = reactive oxygen species, BBB = blood-brain barrier.

Statistical table

Table 6.1| Statistical Table

Figure	Sample size (n)	Statistical test	Values	Comments
1b	13 mice/group	Two-tailed Mann-Whitney U test	$p < .001$	
1c	50 time points/group, 4-6 cages/group	Mixed-effects model (REML)	Time: F (4.5,44.2) = 13.0, $p <$ .001 Treatment: F (1,10) = 147.7, $p <$ .001	
1d	**3-DG, MG** and **DMG:** Control: 12 mice STZ: 11 mice **Gx:** 11 mice/group	**3-DG** and **Gx:** Two-tailed Mann-Whitney U test **MG** and **DMG:** Two-tailed unpaired t test	**3-DG:** $p < .001$ **Gx:** $p = .076$ **MG:** T (21) = 4.0, $p < .001$ **DMG:** T (21) = 2.3, $p = .030$	Value excluded: **Gx:** 1 outlier (Control)
1e	**Gx:** 11 mice/group **MG and DMG:** Control: 13 mice STZ: 12 mice	**Gx:** Two-tailed Mann-Whitney U test **MG** and **DMG:** Two-tailed unpaired t test	**Gx:** $p = .797$ **MG:** T (23) = 1.3, $p = .219$ **DMG:** T (23) = 2.3, $p = .028$	Values excluded: **Gx:** 2 outliers (Control) and 1 outlier (STZ)
1f	Control: 12 mice STZ: 11 mice	Two-tailed Mann-Whitney U test	$p = .023$	
1g	12 mice/group	Two-tailed Mann-Whitney U test	$p = .160$	Value excluded: 1 outlier (Control)
2b	12 mice/group	2-way RM ANOVA	Time: F (2.2,47.5) = 457.6, $p <$ .001 Genotype: F (1,22) = 75.8, $p <$ .001 Interaction: F (6,132) = 109.0, $p <$ .001	
2c	11 mice/group	Two-tailed Mann-Whitney U test	$p < .001$	
2d	**3-DG:** *db/+*: 11 mice *db/db*: 10 mice **Gx, MG** and **DMG**: 11 mice/group	Two-tailed Mann-Whitney U test	**3-DG:** $p = .003$ **Gx:** $p = .078$ **MG:** $p < .001$ **DMG**: $p = .010$	
2e	11 mice/group	Two-tailed unpaired t test	T (20) = 0.4, $p = .664$	
2f	*db/+*: 11 mice *db/db*: 12 mice	Two-tailed unpaired t test	**Gx:** T (21) = 0.6, $p = .543$ **MG:** T (21) = 1.1, $p = .273$ **DMG:** T (21) = 0.9, $p = .403$	
2g	*db/+*: 9 mice *db/db*: 10 mice	Two-tailed Mann-Whitney U test	$p = .905$	Values excluded: 1 outlier (*db/+*) and 2 outliers (*db/db*)
2h	*db/+*: 11 mice *db/db*: 12 mice	Two-tailed unpaired t test	**3-DG:** T (21) = 0.4, $p = .673$ **Gx:** T (21) = 2.2, $p = .036$ **MG:** T (21) = 2.2, $p = .040$ **DMG:** T (21) = 0.5, $p = .634$	
2i	*db/+*: 11 mice *db/db*: 12 mice	Two-tailed unpaired t test	T (21) = 3.1, $p = .005$	
3a	Standard Diet: 8 mice High-Fat Diet: 7 mice	Two-tailed unpaired t test	T (13) = 2.5, $p = .029$	
3b	Standard Diet: 8 mice High-Fat Diet: 7 mice	Two-tailed Mann-Whitney U test	$p < .001$	
3c	**3-DG** and **MG**: 8 mice/group **Gx** and **DMG:** Standard Diet: 8 mice High-Fat Diet: 7 mice	**3-DG** and **MG:** Two-tailed unpaired t test **Gx** and **DMG:** Two-tailed Mann-Whitney U test	**3-DG***:* T (14) = 0.1, $p = .883$ **Gx:** $p < .001$ **MG:** T (14) = 0.9, $p = .383$ **DMG:** $p = .694$	Values excluded: **Gx:** 1 outlier (HFD) **DMG:** 1 outlier (HFD)
4b	4 wells/group	Native glucose: Descriptive only Labeled glucose: Two-tailed Mann-Whitney U test	$p = .029$	
4c	4 wells/group	Cells: Descriptive only Supernatant: Two-tailed Mann-Whitney U test	$p = .029$	
4d	4 wells/group	Native glucose: Descriptive only Labeled glucose: Two-tailed Mann-Whitney U test	**MG (M+2):** $p = .029$ **MG (M+3):** $p = .029$	

Statistical table

4e	4 wells/group	Native glucose: Descriptive only Labeled glucose: Two-tailed Mann-Whitney U test	p = .029	
4f	4 wells/group	**DMG (M+2):** Native glucose: Descriptive only Labeled glucose: Two-tailed Mann-Whitney U test, Bonferroni-Holm correction Supernatant: Two-tailed Mann-Whitney U test, Bonferroni-Holm correction Cells: Descriptive only **DMG (M+4):** Descriptive only	**DMG (M+2):** Labeled glucose: p = .029 Supernatant: p = .020	
5b	Scramble siRNA: 8 wells (Normoxia) and 7 wells (Hypoxia) *Ilvbl* siRNA: 8 wells/group	Scheirer-Ray-Hare test with Mann-Whitney post hoc tests, Bonferroni-Holm correction	Oxygen: χ^2 (1) = 5.1, p = .577 siRNA: χ^2 (1) = 21.0, p < .001 Interaction: χ^2 (1) = 0.2, p = .697 Normoxia: Scramble siRNA vs *Ilvbl* siRNA: p < .001 Hypoxia: Scramble siRNA vs *Ilvbl* siRNA: p < .001	
5c	8 wells/group	Scheirer-Ray-Hare test	Oxygen: χ^2 (1) = 0.7, p = .407 siRNA: χ^2 (1) = 0.02, p = .880 Interaction: χ^2 (1) = 0.5, p = .498	
5d	8 wells/group	2-way ANOVA	Oxygen: F (1,28) = 2.0, p = .165 siRNA: F (1,28) = 1.5, p = .224 Interaction: F (1,28) = 0.01, p = .982	
5e	8 wells/group	Scheirer-Ray-Hare test	Oxygen: χ^2 (1) = 23.3, p < .001 siRNA: χ^2 (1) = 0.3, p = .598 Interaction: χ^2 (1) = 0.3, p = .598	
5f	8 wells/group	2-way ANOVA followed by Sidak´s post-hoc tests (p-values adjusted for multiple comparisons)	Oxygen: F (1,28) = 60.6, p < .001 siRNA: F (1,28) = 14.4, p < .001 Interaction: F (1,28) = 1.1, p = .312 Normoxia: Scramble siRNA vs *Ilvbl* siRNA: p = .117 Hypoxia: Scramble siRNA vs *Ilvbl* siRNA: p = .004	
5g	8 wells/group	**DMG (M+2):** 2-way ANOVA **DMG (M+4):** Scheirer-Ray-Hare test	**DMG (M+2):** Oxygen: F (1,28) = 9.2, p = .005 siRNA: F (1,28) = 1.5, p = .236 Interaction: F (1,28) = 1.2, p = .291 **DMG (M+4):** Oxygen: χ^2 (1) = 13.4, p < .001 siRNA: χ^2 (1) = 0.2, p = .678 Interaction: χ^2 (1) = 0.7, p = .407	
6b	10 wells/group	Scheirer-Ray-Hare test	Oxygen: χ^2 (1) = 0.4, p = .512 siRNA: χ^2 (1) = 0.1, p = .725 Interaction: χ^2 (1) = 0.001, p = .978	
6c	10 wells/group	Scheirer-Ray-Hare test	**DMG (M+2):** Oxygen: χ^2 (1) = 29.3, p < .001 siRNA: χ^2 (1) = 1.1, p = .304 Interaction: χ^2 (1) = 0.0, p > .999 **DMG (M+4):** Oxygen: χ^2 (1) = 29.3, p < .001 siRNA: χ^2 (1) = 0.0, p > .999 Interaction: χ^2 (1) = 0.2, p = .626	
7a	3 mice/group	Descriptive only		
7b	*Ilvbl*$^{+/+}$: 4 mice *Ilvbl*$^{-/-}$: 6 mice	Two-tailed unpaired t test	T (8) = 0.8, p = .448	

Statistical table

7c	3 mice/group	Two-tailed unpaired t test	T (4) = 0.7, p = .533	
7d	7 mice/group	Two-tailed unpaired t test	T (12) = 1.5, p = .170	
7e	3 mice/group	Two-tailed Mann-Whitney U test	p = .700	
7f	3 mice/group	Two-tailed unpaired t test	T (4) = 0.1, p = .954	
8b	Saline Injection: 12 mice/group Glucose injection: 11 mice/group	Scheirer-Ray-Hare test	**DMG (M):** Genotype: χ^2 (1) = 0.03, p = .866 Injection: χ^2 (1) = 13.5, p < .001 Interaction: χ^2 (1) = 0.01, p = .916 **DMG (M+2):** Genotype: χ^2 (1) = 0.5, p = .501 Injection: χ^2 (1) = 29.3, p < .001 Interaction: χ^2 (1) = 0.003, p = .954 **DMG (M+4):** Genotype: χ^2 (1) = 0.4, p = .468 Injection: χ^2 (1) = 29.5, p < .001 Interaction: χ^2 (1) = 0.01, p = .917	
8c	Saline Injection: 12 mice/group Glucose injection: 11 mice/group	Scheirer-Ray-Hare test	Genotype: χ^2 (1) = 2.1, p = .150 Injection: χ^2 (1) = 11.2, p < .001 Interaction: χ^2 (1) = 0.3, p = .578	
8d	11 mice/group	2-way RM ANOVA	**DMG (M+2):** Genotype: F (1,20) = 0.3, p = .608 Side: F (1,20) = 0.003, p = .959 Interaction: F (1,20) = 0.1, p = .727 **DMG (M+4):** Genotype: F (1,20) = 0.01, p = .935 Side: F (1,20) = 2.3, p = .143 Interaction: F (1,20) = 0.1, p = .753	
9b	Sham – *Ilvbl*$^{+/+}$: 11 mice Sham – *Ilvbl*$^{-/-}$: 14 mice pMCAO – *Ilvbl*$^{+/+}$: 9 mice pMCAO – *Ilvbl*$^{-/-}$: 5 mice	Scheirer-Ray-Hare test followed by two -tailed Mann -Whitney U post hoc tests, Bonferroni - Holm correction	**DMG (M):** Treatment: χ^2 (1) = 2.7, p = .100 Genotype: χ^2 (1) = 1.0, p = .310 Interaction: χ^2 (1) = 0.3, p = .580 **DMG (M+2):** Treatment: χ^2 (1) = 14.8, p < .001 Genotype: χ^2 (1) = 1.6, p = .201 Interaction: χ^2 (1) = 0.5, p = .480 *Ilvbl*$^{+/+}$:Sham vs MCAO: p = .002 *Ilvbl*$^{-/-}$: Sham vs MCAO: p = .014 **DMG (M+4):** Treatment: χ^2 (1) = 11.7, p < .001 Genotype: χ^2 (1) = 2.3 p = .131 Interaction: χ^2 (1) = 0.6, p = .445 *Ilvbl*$^{+/+}$:Sham vs MCAO: p = .004 *Ilvbl*$^{-/-}$: Sham vs MCAO: p = .070	
9c	Sham – *Ilvbl*$^{+/+}$: 11 mice Sham – *Ilvbl*$^{-/-}$: 14 mice pMCAO – *Ilvbl*$^{+/+}$: 9 mice pMCAO – *Ilvbl*$^{-/-}$: 5 mice	Scheirer-Ray-Hare test	**MG:** Treatment: χ^2 (1) = 5.5, p = .020 Genotype: χ^2 (1) = 0.3, p = .560 Interaction: χ^2 (1) = 0.8, p = .365 **MG (M+3):** Treatment: χ^2 (1) = 0.9, p = .331 Genotype: χ^2 (1) = 0.3, p = .593 Interaction: χ^2 (1) = 1.8, p = .178	
9d	Sham – *Ilvbl*$^{+/+}$: 11 mice Sham – *Ilvbl*$^{-/-}$: 14 mice pMCAO – *Ilvbl*$^{+/+}$: 9 mice	**Gx (M):** 2-way ANOVA **Gx (M+2):** Scheirer-Ray-Hare test	**Gx (M):** Treatment: F (1,35) = 3.2, p = .081	

	pMCAO – *Ilvbl*$^{-/-}$: 5 mice		Genotype: F (1,35) = 0.1, p = .779 Interaction: F (1,35) = 0.4, p = .542 **Gx (M+2):** Treatment: χ^2 (1) = 2.9, p = .090 Genotype: χ^2 (1) = 2.9, p = .089 Interaction: χ^2 (1) = 0.6, p = .438	
9e	Sham – *Ilvbl*$^{+/+}$: 11 mice Sham – *Ilvbl*$^{-/-}$: 14 mice pMCAO – *Ilvbl*$^{+/+}$: 9 mice pMCAO – *Ilvbl*$^{-/-}$: 5 mice	**3-DG (M):** 2-way ANOVA **3-DG (M+6):** Scheirer-Ray-Hare test	**3-DG (M):** Treatment: F (1,35) = 0.01, p = .942 Genotype: F (1,35) = 0.2, p = .628 Interaction: F (1,35) = 0.04, p = .836 **3-DG (M+6):** Treatment: χ^2 (1) = 1.7, p = .194 Genotype: χ^2 (1) = 0.01, p = .929 Interaction: χ^2 (1) = 1.0, p = .326	
9f	Sham – *Ilvbl*$^{+/+}$: 11 mice Sham – *Ilvbl*$^{-/-}$: 14 mice pMCAO – *Ilvbl*$^{+/+}$: 9 mice pMCAO – *Ilvbl*$^{-/-}$: 5 mice	2-way ANOVA	**Pyruvate (M):** Treatment: F (1,35) = 1.0, p = .323 Genotype: F (1,35) = 0.1, p = .323 Interaction: F (1,35) = 6.7, p = .014 Sham: *Ilvbl*$^{+/+}$ vs *Ilvbl*$^{-/-}$: p = .120 MCAO: *Ilvbl*$^{+/+}$ vs *Ilvbl*$^{-/-}$: p = .637 *Ilvbl*$^{+/+}$: Sham vs MCAO: p = .794 *Ilvbl*$^{-/-}$: Sham vs MCAO: p = .132 **Pyruvate (M+3):** Treatment: F (1,35) = 19.9, p < .001 Genotype: F (1,35) = 0.4, p = .539 Interaction: F (1,35) = 2.7, p = .106	
9g	Sham – *Ilvbl*$^{+/+}$: 14 mice Sham – *Ilvbl*$^{-/-}$: 17 mice pMCAO – *Ilvbl*$^{+/+}$: 12 mice pMCAO – *Ilvbl*$^{-/-}$: 10 mice	3-way RM ANOVA followed by Sidak´s post hoc tests (p-values adjusted for multiple comparisons)	**DMG (M):** Side: F (1,49) = 25.1, p < .001 Treatment: F (1,49) = 157.8, p < .001 Genotype: F (1,49) = 10.0, p = .003 Contralateral side – *Ilvbl*$^{+/+}$: Sham vs MCAO: p < .001 Contralateral side – *Ilvbl*$^{-/-}$: Sham vs MCAO: p < .001 Ipsilateral side – *Ilvbl*$^{+/+}$: Sham vs MCAO: p < .001 Ipsilateral side – *Ilvbl*$^{-/-}$: Sham vs MCAO: p < .001 Contralateral side – Sham: *Ilvbl*$^{+/+}$ vs *Ilvbl*$^{-/-}$: p > .999 Contralateral side – MCAO: *Ilvbl*$^{+/+}$ vs *Ilvbl*$^{-/-}$: p = .017 Ipsilateral side – Sham: *Ilvbl*$^{+/+}$ vs *Ilvbl*$^{-/-}$: p > .999 Ipsilateral side – MCAO: *Ilvbl*$^{+/+}$ vs *Ilvbl*$^{-/-}$: p < .001 Sham – *Ilvbl*$^{+/+}$: Contralateral side vs ipsilateral side: p > .999 Sham – *Ilvbl*$^{-/-}$: Contralateral side vs ipsilateral side: p = .978 pMCAO – *Ilvbl*$^{+/+}$: Contralateral side vs ipsilateral side: p < .001 pMCAO – *Ilvbl*$^{-/-}$: Contralateral side vs ipsilateral side: p = .007	

			DMG (M+2): Side: F (1,49) = 29.8, p < .001 Treatment: F (1,49) = 144.2, p < .001 Genotype: F (1,49) = 5.3, p = .025 Contralateral side – *Ilvbl*$^{+/+}$: Sham vs MCAO: p < .001 Contralateral side – *Ilvbl*$^{-/-}$: Sham vs MCAO: p < .001 Ipsilateral side – *Ilvbl*$^{+/+}$: Sham vs MCAO: p < .001 Ipsilateral side – *Ilvbl*$^{-/-}$: Sham vs MCAO: p < .001 Contralateral side – Sham: *Ilvbl*$^{+/+}$ vs *Ilvbl*$^{-/-}$: p > .999 Contralateral side – MCAO: *Ilvbl*$^{+/+}$ vs *Ilvbl*$^{-/-}$: p = .184 Ipsilateral side – Sham: *Ilvbl*$^{+/+}$ vs *Ilvbl*$^{-/-}$: p > .999 Ipsilateral side – MCAO: *Ilvbl*$^{+/+}$ vs *Ilvbl*$^{-/-}$: p = .007 Sham – *Ilvbl*$^{+/+}$: Contralateral side vs ipsilateral side: p > .999 Sham – *Ilvbl*$^{-/-}$: Contralateral side vs ipsilateral side: p > .999 pMCAO – *Ilvbl*$^{+/+}$: Contralateral side vs ipsilateral side: p < .001 pMCAO – *Ilvbl*$^{-/-}$: Contralateral side vs ipsilateral side: p = .030 **DMG (M+4):** Side: F (1,49) = 54.6, p < .001 Treatment: F (1,49) = 126.4, p < .001 Genotype: F (1,49) = 0.4, p = .524 Contralateral side – *Ilvbl*$^{+/+}$: Sham vs MCAO: p < .001 Contralateral side – *Ilvbl*$^{-/-}$: Sham vs MCAO: p < .001 Ipsilateral side – *Ilvbl*$^{+/+}$: Sham vs MCAO: p < .001 Ipsilateral side – *Ilvbl*$^{-/-}$: Sham vs MCAO: p < .001 Sham – *Ilvbl*$^{+/+}$: Contralateral side vs ipsilateral side: p > .999 Sham – *Ilvbl*$^{-/-}$: Contralateral side vs ipsilateral side: p > .999 pMCAO – *Ilvbl*$^{+/+}$: Contralateral side vs ipsilateral side: p < .001 pMCAO – *Ilvbl*$^{-/-}$: Contralateral side vs ipsilateral side: p < .001	
9h	Sham-*Ilvbl*$^{+/+}$: 14 mice Sham-*Ilvbl*$^{-/-}$: 17 mice pMCAO-*Ilvbl*$^{+/+}$: 12 mice pMCAO-*Ilvbl*$^{-/-}$: 10 mice	3-way RM ANOVA followed by Sidak´s post hoc tests (p-values adjusted for multiple comparisons)	**MG (M):** Side: F (1,49) = 3.9, p = .055 Treatment: F (1,49) = 150.3, p < .001 Genotype: F (1,49) = 0.1, p = .776 Contralateral side – *Ilvbl*$^{+/+}$: Sham vs MCAO: p < .001 Contralateral side – *Ilvbl*$^{-/-}$: Sham vs MCAO: p < .001 Ipsilateral side – *Ilvbl*$^{+/+}$: Sham vs MCAO: p < .001 Ipsilateral side – *Ilvbl*$^{-/-}$: Sham vs MCAO: p < .001	

			MG (M+3): Side: F (1,49) = 40.4, p < .001 Treatment: F (1,49) = 14.1, p < .001 Genotype: F (1,49) = 1.2, p = .287 Contralateral side – *Ilvbl*$^{+/+}$: Sham vs MCAO: p < .001 Contralateral side – *Ilvbl*$^{-/-}$: Sham vs MCAO: p = .016 Ipsilateral side – *Ilvbl*$^{+/+}$: Sham vs MCAO: p = .278 Ipsilateral side – *Ilvbl*$^{-/-}$: Sham vs MCAO: p > .999 Sham – *Ilvbl*$^{+/+}$: Contralateral side vs ipsilateral side: p > .999 Sham – *Ilvbl*$^{-/-}$: Contralateral side vs ipsilateral side: p > .999 pMCAO – *Ilvbl*$^{+/+}$: Contralateral side vs ipsilateral side: p < .001 pMCAO – *Ilvbl*$^{-/-}$: Contralateral side vs ipsilateral side: p < .001	
9i	Sham-*Ilvbl*$^{+/+}$: 11 mice Sham-*Ilvbl*$^{-/-}$: 15 mice MCAO-*Ilvbl*$^{+/+}$: 9 mice MCAO-*Ilvbl*$^{-/-}$: 10 mice	3-way RM ANOVA followed by Sidak´s post hoc tests (p-values adjusted for multiple comparisons)	Side: F (1,41) = 0.002, p = .969 Treatment: F (1,41) = 8.0, p = .007 Genotype: F (1,41) = 0.2, p = .639 Contralateral side – *Ilvbl*$^{+/+}$: Sham vs MCAO: p > .999 Contralateral side – *Ilvbl*$^{-/-}$: Sham vs MCAO: p > .999 Ipsilateral side – *Ilvbl*$^{+/+}$: Sham vs MCAO: p = .013 Ipsilateral side – *Ilvbl* $^{-/-}$: Sham vs MCAO: p = .076	Values excluded: Sham-*Ilvbl*$^{+/+}$: 3 mice (outliers) Sham-*Ilvbl*$^{-/-}$: 2 mice (outliers) MCAO-*Ilvbl*$^{+/+}$: 3 mice (outliers)
9j	Sham-*Ilvbl*$^{+/+}$: 14 mice Sham-*Ilvbl*$^{-/-}$: 17 mice MCAO-*Ilvbl*$^{+/+}$: 12 mice MCAO-*Ilvbl*$^{-/-}$: 10 mice	3-way RM ANOVA followed by Sidak´s post hoc tests (p-values adjusted for multiple comparisons)	**Pyruvate (M):** Side: F (1,49) = 2.9, p = .095 Treatment: F (1,49) = 6.9, p = .012 Genotype: F (1,49) = 0.5, p = .481 Contralateral side – *Ilvbl*$^{+/+}$: Sham vs MCAO: p = .939 Contralateral side – *Ilvbl*$^{-/-}$: Sham vs MCAO: p > .999 Ipsilateral side – *Ilvbl*$^{+/+}$: Sham vs MCAO: p = .074 Ipsilateral side – *Ilvbl*$^{-/-}$: Sham vs MCAO: p = .002 **Pyruvate (M+3):** Side: F (1,49) = 0.1, p = .711 Treatment: F (1,49) = 0.6, p = .429 Genotype: F (1,49) = 1.2, p = .274	
10b	*Ilvbl*$^{+/+}$: 18 mice *Ilvbl*$^{-/-}$: 14 mice	2-way RM ANOVA	Time: F (1,30) = 97.3, p < .001 Genotype: F (1,30) = 0.2, p = .688 Interaction: F (1,30) < 0.01, p = .933	
10c	**3-DG, MG** and **DMG:** *Ilvbl*$^{+/+}$: 16 mice *Ilvbl*$^{-/-}$: 10 mice **Gx:** *Ilvbl*$^{+/+}$: 16 mice *Ilvbl*$^{-/-}$: 9 mice	2-way RM ANOVA	**3-DG:** Time: F (1,24) = 89.7, p < .001 Genotype: F (1,24) = 0.1, p = .759 Interaction: F (1,24) = 0.6, p = .455 **Gx:**	Value excluded: **Gx:** 1 outlier at 12 weeks (value was also excluded at baseline)

Statistical table

			Time: F (1,23) = 48.4, p < .001 Genotype: F (1,23) = 1.6, p = .223 Interaction: F (1,23) = 1.3, p = .265 **MG:** Time: F (1,24) = 1.1, p = .302 Genotype: F (1,24) = 0.1, p = .779 Interaction: F (1,24) = 1.5, p = .240 **DMG:** Time: F (1,24) = 9.4, p = .005 Genotype: F (1,24) = 0.5, p = .494 Interaction: F (1,24) = 0.7, p = .406	
10d	*Ilvbl*$^{+/+}$: 18 mice *Ilvbl*$^{-/-}$: 14 mice	**3-DG, Gx** and **MG:** Two-tailed unpaired t test **DMG:** Two-tailed Mann-Whitney U test	**3-DG:** T (30) = 1.5, p = .155 **Gx:** T (30) = 0.6, p = .568 **MG:** T (30) = 0.7, p = .519 **DMG:** p = .640	
10e	*Ilvbl*$^{+/+}$: 18 mice *Ilvbl*$^{-/-}$: 12 mice	**Gx** and **MG:** Two-tailed unpaired t test **DMG:** Two-tailed Mann-Whitney U test	**Gx:** T (28) = 1.7, p = .100 **MG:** T (28) = 0.569, p = .574 **DMG:** p = .003	
11	SPF: 5 mice Germ-free: 6 mice	Two-tailed unpaired t test	**3-DG:** T (9) = 1.7, p = .130 **Gx:** T (9) = 0.4, p = .675 **MG:** T (9) = 1.1, p = .305 **Pyruvate:** T (9) = 0.8, p = .418 **DMG:** T (9) = 0.1, p = .897	
12c	*Ilvbl*$^{+/+}$: 14 mice *Ilvbl*$^{-/-}$: 17 mice	Two-tailed unpaired t test	T (29) = 2.4, p = .025	
13b	3 mice/group	Descriptive only		
13c	3 mice/group	Descriptive only		
13d	3 mice/group	Descriptive only		
14b	Control: 13 mice DMG: 14 mice	Two-tailed Mann-Whitney U test	p = .243	
14c	50 time points/group, 4-6 cages/group	Mixed-effects model (REML)	Time: F (49,482) = 6.5, p < .001 Treatment: F (1,10) = 0.8, p = 381	
14d	**3-DG, MG** and **DMG:** Control: 12 mice DMG: 13 mice **Gx:** Control: 11 mice DMG: 13 mice	**3-DG** and **MG:** Two-tailed unpaired t test **Gx** and **DMG:** Two-tailed Mann-Whitney U test	**3-DG:** T (23) = 0.4, p = .718 **Gx:** p = .392 **MG:** T (23) = 0.4, p = .718 **DMG**: p = .001	Value excluded: **Gx:** 1 outlier (Control)
14e	Control: 12 mice DMG: 13 mice	Two-tailed unpaired t test	T (23) = 1.7, p = .096	
14f	Control: 12 mice DMG: 14 mice	Two-tailed unpaired t test	T (24) = 0.6, p = .581	Value excluded: 1 outlier (Control)
14g	**Gx:** Control: 11 mice DMG: 14 mice **MG** and **DMG:** Control: 13 mice DMG: 14 mice	**Gx** and **DMG:** Two-tailed Mann-Whitney U test **MG:** Two-tailed unpaired t test	**Gx:** p = .893 **MG:** T (25) = 0.4, p = .696 **DMG:** p = .350	Values excluded: **Gx:** 2 outliers (Control)
15a	24 wells (0 µM DMG), 11 wells (5 µM DMG and 10 µM H_2O_2) and 12 wells (20 µM DMG, 50 µM DMG, 100 µM DMG, 200 µM DMG, 500 µM DMG and no cells)	Kruskal-Wallis followed by Dunn´s post hoc tests (p-values adjusted for multiple comparisons)	χ^2 (9) = 101.0, p < .001 0 µM DMG vs 5 µM DMG: p > .999 0 µM DMG vs 20 µM DMG: p > .999 0 µM DMG vs 50 µM DMG: p = .021 0 µM DMG vs 100 µM DMG: p < .001 0 µM DMG vs 200 µM DMG: p < .001 0 µM DMG vs 500 µM DMG: p < .001	

Statistical table

			0 µM DMG vs 10 µM H_2O_2: p < .001 0 µM DMG vs no cells: p = .287	
15b	12 wells (0 µM DMG) and 6 wells (5 µM DMG, 20 µM DMG, 50 µM DMG, 100 µM DMG, 200 µM DMG, 500 µM DMG, 10 µM H_2O_2 and no cells	Kruskal-Wallis followed by Dunn´s post hoc tests (p-values adjusted for multiple comparisons)	χ^2 (9) = 45.9, p < .001 0 µM DMG vs 5 µM DMG: p > .999 0 µM DMG vs 20 µM DMG: p > .999 0 µM DMG vs 50 µM DMG: p > .999 0 µM DMG vs 100 µM DMG: p = .068 0 µM DMG vs 200 µM DMG: p = .003 0 µM DMG vs 500 µM DMG: p < .001 0 µM DMG vs 10 µM H_2O_2: p > .999 0 µM DMG vs no cells: p = .431	
15c	16 wells (0 µM DMG), 8 wells (5 µM DMG, 50 µM DMG and 500 µM), and 12 wells (10 µM H_2O_2 and no cells)	Kruskal-Wallis followed by Dunn´s post hoc tests (p-values adjusted for multiple comparisons)	χ^2 (6) = 53.1, p < .001 0 µM DMG vs 5 µM DMG: p > .999 0 µM DMG vs 50 µM DMG: p > .999 0 µM DMG vs 500 µM DMG: p < .001 0 µM DMG vs 10 µM H_2O_2: p = .003 0 µM DMG vs no cells: p = .043	
15d	5 wells/group	***Pla2g4a*** and ***Ptges***: One-way ANOVA followed by Dunnett´s post-hoc tests (p-values adjusted for multiple comparisons) ***Ptgs2*** and ***Bim***: Kruskal-Wallis followed by Dunn´s post hoc tests (p-values adjusted for multiple comparisons)	*Pla2g4a:* F (2,12) = 7.15, p = .009 0 µM vs 100 µM DMG: p = .429 0 µM vs 500 µM DMG: p = .006 *Ptgs2*: χ^2 (2) = 12.0, p < .001 0 µM vs 100 µM DMG: p = .207 0 µM vs 500 µM DMG: p = .001 *Ptges:* F (2,12) = 87.44, p < .001 0 µM vs 100 µM DMG: p = .001 0 µM vs 500 µM DMG: p < .001 *Bim*: χ^2 (2) = 8.4, p = .007 0 µM vs 100 µM DMG: p > .999 0 µM vs 500 µM DMG: p = .017	

List of figures

List of tables

Abbreviations

(d4-)CEL	(Deuterated) N_{ε}-(1-carboxyethyl)-L-lysine
3-DG	3-Deoxyglucosone
3-DG-H1	Glycated 3-deoxyglucosone in histone 1
ACC1	Acetyl-CoA carboxylases 1
ACLY	Adenosine triphosphate-citrate lyase
ACN	Aconitase
AD	Alzheimer's Disease
ADP	Adenosine diphosphate
AGC	Automatic gain control
AGE	Advanced glycation end product
ALD	Fructose-biphosphate aldolase
ALDC	Acetolactate decarboxylase
ALS	Acetolactate synthase
AMPA	α-Amino-3-hydroxy-5-methyl-4-isoxazole propionic acid
AR	Acetoin reductase
ATP	Adenosine triphosphate
BBB	Blood-brain barrier
bEnd.3 cells	Mouse brain endothelial cells
Bim	BCL2 Like 11
BSA	Bovine serum album
cDNA	Complementary Deoxyribonucleic acid
CID	Collision-induced dissociation
CML	*N*-ε-carboxymethyllysine
CNS	Central nervous system
COX, or PTGS	Cyclooxygenase, or prostaglandin-endoperoxide synthase
CS	Citrate synthase
Ct	Threshold cycle
d8-DB	Deuterated o-phenylenediamine
Db/db	Leptin receptor-deficient
DETAPAC	Diethylenetriaminepentaacetic acid
DMEM	Dulbecco´s Modified Eagle's Medium
DMG	Dimethylglyoxal
DMSO	Dimethyl sulfoxide
DNA	Deoxyribonucleic acid
dNTP	Nucleoside triphosphate
DOLD	3-deoxyglucosone lysine dimer
DPBS	Dulbecco´s phosphate buffered saline
DR, or DCXR	Diacetyl reductase, or dicarbonyl/L-xylulose reductase
e^-	Electron
EDTA	Ethylenediaminetetraacetic acid
EI	Electron ionization
ESI	Electrospray ionization
FAD(H_2)	(Reduced) flavine adenine dinucleotide
FASN	Fatty acid synthase

Abbreviations

FCS	Fetal Calf Serum
FM	Fumarase
FT	Fourier Transformation
G3P	Glyceraldehyde 3-phosphate
G6PD	Glucose 6-phosphate dehydrogenase
GDP	Guanosine diphosphate
GLUT	Glucose transporter type
GOLD	Glyoxal-derived lysine dimer
GPI	Glucose 6-phosphate isomerase
GTP	Guanosine triphosphate
Gx	Glyoxal
HbA_{1c}	Glycated hemoglobin
HBL	N_{ε}-3-hydroxy-2-butanonelysine
HCD	High-energy collisional dissociation
Hep G2 cells	Human liver cancer cells
HESI-II	Heated-electrospray ionization
HFD	High-fat diet
HIF-1	Hypoxia-inducible factor 1
HK	Hexokinase
HPLC	High-performance mass spectrometry, or high-pressure mass spectrometry
HT-22 cells	Mouse hippocampal neuronal cells
I.p.	Intraperitoneal injection
IDH	Isocitrate dehydrogenase
ILVBL	IlvB acetolactate synthase like, or 2-hydroxyacyl-CoA lyase 2
IRS-1	Insulin receptor substrate
IT	Injection time
LC	Liquid chromatography
LDH	Lactate dehydrogenase
LDL	Low density lipoprotein
M-MLV	Mouse Moloney murine leukemia virus
m/z	Mass-to-charge ratio
MCT	Monocarboxylate transporter
MDH	Malate dehydrogenase
MG	Methylglyoxal
MOLD	Methylglyoxal-lysine dimer
MRM	Multiple reaction monitoring
MS	Mass spectrometry
MS^2	Tandem mass spectrometry
NaCl 0.9 %	Saline solution
NAD(H)	(Reduced) nicotinamide adenine dinucleotide
NCE	Normalized collision energy
NF-κB	Nuclear factor kappa-light-chain-enhancer of activated B cells
NMDA	*N*-methyl-D-aspartate
NOS	Nitric oxide synthases
nSREBP-1c	Sterol regulatory element-binding protein-1c
OAD	Oxaloacetate decarboxylase
OGDC	α-Ketoglutarate dehydrogenase
ORM2	Orosomucoid 2

Abbreviations

PBK, or AKT	Protein kinase B
PC	Prohormone convertase
PCR	Polymerase Chain Reaction
PDC	Pyruvate dehydrogenase complex
PDH	Pyruvate dehydrogenase
PDK1	Pyruvate dehydrogenase kinase 1
PFK-1	Phosphofructokinase-1
PG	Prostaglandin
PI3K	Phosphatidylinositol 3-kinase
PIP	Phosphatidylinositol 4,5-biphosphate
Pla2g4a	Phospholipase A2 Group IVA
pMCAO	Permanent middle cerebral artery occlusion
Ppia	Cyclophilin A
PPP	Pentose Phosphate Pathway
PRM	Parallel Reaction Monitoring
Ptges	Prostaglandin E synthase
Q1	First quadrupole
Q2	Second quadrupole
Q3	Third quadrupole
R	Resolution
RAGE	Receptor for advanced glycation end product
RNA	Ribonucleic acid
RNS	Reactive nitrogen species
ROS	Reactive oxygen species
RPE	Ribulose 5-phosphate 3-epimerase
RPI	Ribose 5-phosphate isomerase
S-Lens	Stacked ring ion guide
SCD1	Stearoyl-CoA desaturase-1
SCS	Succinyl-CoA dehydrogenase
SDH	Succinyl dehydrogenase
siRNA	Small interfering ribonucleic acid
SPF	Specific-pathogen-free
STZ	Streptozotocin
TALDO	Ribose 5-phosphate isomerase, transaldolase
TCA	Tricarboxylic acid cycle, citric acid cycle, or Krebs cycle
TCAA	Trichloroacetic acid
TK	Thiamine-dependent enzyme transketolase
TNF	Tumor necrosis factor-α
TPI	Triose phosphate isomerase
WHO	World Health Organization

Literature

1 Kreitzman SN, Coxon AY & KF. Szaz. Glycogen storage: illusions of easy weight loss, excessive weight regain, and distortions in estimates of body composition. *Am J Clin Nutr.* **56**, 292S-293S. (1992 Jul). https://doi.org/10.1093/ajcn/56.1.292S.

2 TeSlaa T, Ralser M, Fan J & JD. Rabinowitz. The pentose phosphate pathway in health and disease (Review). *Nature Metabolism* **5(8)**, 1275-1289 (2023 Aug). https://doi.org/doi: 10.1038/s42255-023-00863-2.

3 Haddad A & SS. Mohiuddin. *Biochemistry, Citric Acid Cycle*. (StatPearls Publishing, 2023 May).

4 Dashty M. A quick look at biochemistry: Carbohydrate metabolism (Review). *Clin Biochem* **46(15)**, 1339-1352 (2013 Oct). https://doi.org/10.1016/j.clinbiochem.2013.04.027

5 Wu JT. Advanced glycosylation end products: A new disease marker for diabetes and aging. *J Clin Lab Anal* **7(5)**, 252-255 (1993). https://doi.org/10.1002/jcla.1860070503

6 Glomb MA & Monnier VM. Mechanism of Protein Modification by Glyoxal and Glycolaldehyde, Reactive Intermediates of the Maillard Reaction. *Journal of Biological Chemistry* **270(17)**, 10017-10026. (1995 Apr 28). https://doi.org/10.1074/jbc.270.17.10017

7 Bum Shin D, Hayase F & Kato H. Polymerization of Proteins Caused by Reaction with Sugars and the Formation of 3-Deoxyglucosone under Physiological Conditions. *Agricultural and Biological Chemistry* **52(6)**, 1451–1458 (1988). https://doi.org/10.1080/00021369.1988.10868884

8 Portero-Otin M, Nagaraj RH & Monnier VM. Chromatographic evidence for pyrraline formation during protein glycation in vitro and in vivo *Biochim Biophys Acta* **1247(1)**, 74-80 (1995 Feb 22). https://doi.org/10.1016/0167-4838(94)00209-y

9 Skovsted IC, Christensen M, Breinholt J & Mortensen SB. Characterisation of a novel AGE-compound derived from lysine and 3-deoxyglucosone. *Cell Mol Biol* **44(7)**, 1159-1163 (1998 Nov).

10 Ashraf JM, Rabbani G, Ahmad S, Hasan Q, Khan RH, Alam K & Choi I. Glycation of H1 Histone by 3-Deoxyglucosone: Effects on Protein Structure and Generation of Different Advanced Glycation End Products. *PLoS One* **10(6)** (2015 Jun 29). https://doi.org/10.1371/journal.pone.0130630

11 Sakiyama H, Takahashi M, Yamamoto T, Teshima T, Lee SH, Miyamoto Y, Misonou Y & Taniguchi N. The Internalization and Metabolism of 3-Deoxyglucosone in Human Umbilical Vein Endothelial Cells. *Biochem* **139(2)**, 245-253 (2006 Feb). https://doi.org/10.1093/jb/mvj017

12 Kato H, van Chuyen N, Shinoda T, Sekiya F & Hayase F. Metabolism of 3-deoxyglucosone, an intermediate compound in the Maillard reaction, administered orally or intravenously to rats. *Biochim Biophys Acta* **1035(1)**, 71-76 (1990 Jul 20). https://doi.org/10.1016/0304-4165(90)90175-v

13 Wang XJ, Gao F, Li LC, Hui X, Li H & Gao WY. Quantitative analyses of α-dicarbonyl compounds in food samples by HPLC using 4-(2,3-dimethyl-6-quinoxalinyl)-1,2-benzenediamine as a derivatizing reagent. *Microchemical Journal* **141**, 64-70 (2018). https://doi.org/10.1016/j.microc.2018.05.006

14 Niwa T, Takeda N, Yoshizumi H, Tatematsu A, Ohara M, Tomiyama S & Niimura K. Presence of 3-Deoxyglucosone, a Potent Protein Crosslinking Intermediate of Maillard Reaction, in Diabetic Serum. *Biochem Biophys Res Commun* **196(2)**, 837-843 (1993 Oct 29). https://doi.org/10.1006/bbrc.1993.2325

15 Niwa T, Katsuzaki T, Momoi T, Miyazaki T, Ogawa H, Saito A, Miyazaki S, Maeda K, Tatemichi N & Y. Takei. Modification of β2m with advanced glycation end products as observed in dialysis-related amyloidosis by 3-DG accumulating in uremic serum. *Kidney Int* **49(3)**, 861-867 (1996 Mar). https://doi.org/10.1038/ki.1996.119

16 Yamada H, Miyata S, Igaki N, Yataben H, Miyauchill Y, Ohara T, Sakai M, Shoda H, Oimomi M & Kasuga M. Increase in 3-deoxyglucosone levels in diabetic rat plasma. Specific in vivo determination of intermediate in advanced Maillard reaction. *The Journal of Biology Chemistry* **269(32)** 20275-20280 (1994 Aug 12). https://doi.org/10.1016/S0021-9258(17)31987-7

17 Niwa T, Miyazaki T, Katsuzaki T, Tatemichi N & Takei Y. Serum Levels of 3-Deoxyglucosone and Tissue Contents of Advanced Glycation End Products Are Increased in Streptozotocin-Induced Diabetic Rats with Nephropathy. *Nephron* **74(3)**, 580-585 (1996). https://doi.org/10.1159/000189456.

18 Mlakar A & Spiteller G. Reinvestigation of lipid peroxidation of linolenic acid *Biochim Biophys Acta* **1214(2)**, 209-220 (1994 Sep 15). https://doi.org/10.1016/0005-2760(94)90046-9

19 O'Brien PJ, Siraki AG & Shangari N. Aldehyde Sources, Metabolism, Molecular Toxicity Mechanisms, and Possible Effects on Human Health (Review). *Crit Rev Toxicol* **35(7)**, 609-662 (2005 Aug). https://doi.org/10.1080/10408440591002183

20 Kim Y, Ahn H & Lee KG. Analysis of glyoxal, methylglyoxal and diacetyl in soy sauce. *Food Sci Biotechnol* **30(11)**, 1403-1408 (2021 Jun 8). https://doi.org/10.1007/s10068-021-00918-8

21 Abordo EA, Minhas HS & Thornalley PJ. Accumulation of α-oxoaldehydes during oxidative stress: a role in cytotoxicity. *Biochem Pharmacol* **58(4)**, 641-648 (1999 Aug 15). https://doi.org/10.1016/s0006-2952(99)00132-x

22 Knight J, Assimos DG, Easter L & Holmes RP. Metabolism of fructose to oxalate and glycolate. *Horm Metab Res* **42(12)**, 868-873 (2010 Nov). https://doi.org/10.1055/s-0030-1265145

23 Holmes RP, Knight J & Assimos DG. Lowering urinary oxalate excretion to decrease calcium oxalate stone disease (Review). *Urolithiasis* **44(1)**, 27-32 (2016 Feb). https://doi.org/10.1007/s00240-015-0839-4.

24 Han Y, Randell E, Vasdev S, Gill V, Gadag V, Newhook LA, Grant M & Hagerty D. Plasma methylglyoxal and glyoxal are elevated and related to early membrane alteration in young, complication-free patients with Type 1 diabetes. *Mol Cell Biochem* **305(1-2)**, 123-131 (. 2007 Nov). https://doi.org/10.1007/s11010-007-9535-1

25 Shangari N & O'Brien PJ. The cytotoxic mechanism of glyoxal involves oxidative stress. *Biochem Pharmacol* **68(7)**, 1433-1442 (2004 Oct 1). https://doi.org/10.1016/j.bcp.2004.06.013

26 Yamawaki H & Hara Y. Glyoxal causes inflammatory injury in human vascular endothelial cells. *Biophys Res Commun.* **369(4)**, 1155-1159 (2008 May 16). https://doi.org/10.1016/j.bbrc.2008.03.020.

27 Sugawa H, Ikeda T, Tominaga Y, Katsuta N & Nagai R. Rapid formation of Nε-(carboxymethyl)lysine (CML) from ribose depends on glyoxal production by oxidation. *RSC Chem Biol* **5(11)**, 1140–1146 (2024 Sep 18). https://doi.org/10.1039/d4cb00183d

28 Richard John P. Kinetic Parameters for the Elimination Reaction Catalyzed by Triosephosphate Isomerase and an Estimation of the Reaction's Physiological Significance. *Biochemistry* **30(18)**, 4581-4585 (1991 May 7). https://doi.org/10.1021/bi00232a031

29 Sato J, Wang YM & Eys J van. Methylglyoxal formation in rat liver cells. *J Biol Chem* **255(5)**, 2046-2050 (1980 Mar 10).

30 Casazza JP, Felver ME & Veech RL. The metabolism of acetone in rat. *J Biol Chem* **259(1)**, 231-236 (1984 Jan 10).

31 Ray S & M Ray. Formation of methylglyoxal from aminoacetone by amine oxidase from goat plasma. *J Biol Chem* **258(6)**, 3461-3462 (1983 Mar 25).

32 Tressel T, Thompson R, Zieske LR, Menendez MI & Davis L. Interaction between L-threonine dehydrogenase and aminoacetone synthetase and mechanism of aminoacetone production. *J Biol Chem* **261(35)**, 16428-16437 (1986 Dec 15).

33 Ye H, Miao Y, Zhao C & Yuan Y. Acrylamide and methylglyoxal formation in potato chips by microwaving and frying heating. *International Journal of Food Science and Technology* **46(9)**, 1921–1926 (2011 Sep). https://doi.org/10.1111/j.1365-2621.2011.02702.x

34 Atrott J & Henle T. Methylglyoxal in Manuka Honey – Correlation with Antibacterial Properties. *Czech J. Food Sci* **27**, S163-S165 (2009).

35 Cokcetin NN, Pappalardo M, Campbell LT, Brooks P, Carter DA, Blair SE & Harry EJ. The Antibacterial Activity of Australian Leptospermum Honey Correlates with Methylglyoxal Levels. *PLOS One* **11(12)** (2016 Dec 28). https://doi.org/10.1371/journal.pone.0167780

36 Frye EB, Degenhardt TP, Thorpe SR & Baynes JW. Role of the Maillard Reaction in Aging of Tissue Proteins. *The Journal of Biochemistry* **273(30)**, 18714-18719 (1998 Jul 24). https://doi.org/10.1074/jbc.273.30.18714

37 Shipanova IN, Glomb MA & Nagaraj RH. Protein Modification by Methylglyoxal: Chemical Nature and Synthetic Mechanism of a Major Fluorescent Adduct *Arch Biochem Biophys* **344(1)**, 29-36 (1997 Aug 1). https://doi.org/10.1006/abbi.1997.0195

38 Sena CM, Matafome P, Crisóstomo J, Rodrigues L, Fernandes R, Pereira P & Seiça RM. Methylglyoxal promotes oxidative stress and endothelial dysfunction. *Pharmacol Res.* **65(5)**, 497-506 (2012 May). https://doi.org/10.1016/j.phrs.2012.03.004

39 Sellin S & Mannervik B. Reversal of the reaction catalyzed by glyoxalase I. Calculation of the equilibrium constant for the enzymatic reaction. *Biol Chem.* **258(14)**, 8872-8875 (1983 Jul 25).

40 Thornalley PJ. The glyoxalase system in health and disease (Review). *Mol Aspects Med* **14(4)**, 287-371 (1993). https://doi.org/10.1016/0098-2997(93)90002-u

41 Burdock GA. *Fenaroli's Handbook of Flavor Ingredients*. (2001).

42 Kreiss K, Gomaa A, Kullman G, Fedan K, Simoes EJ & Enright PL. Clinical Bronchiolitis Obliterans in Workers at a Microwave-Popcorn Plant. *N Engl J Med* **347(5)**, 330-338 (2002 Aug 1). https://doi.org/10.1056/NEJMoa020300

43 Baranowska M. Intensification of the synthesis of flavour compounds in yogurt by milk enrichment with their precursor. *Pol. J. Food Nutr. Sci.* **15/56**, 5-11 (2006).

44 Macciola V, Candela G & Leonardis A De. Rapid gas-chromatographic method for the determination of diacetyl in milk, fermented milk and butter. *Food Control* **19(9)**, 873-878 (2008 Sep). https://doi.org/10.1016/j.foodcont.2007.08.014

45 Drake MA, Miracle RE & McMahon DJ. Impact of fat reduction on flavor and flavor chemistry of Cheddar cheeses. *J Dairy Sci* **93(11)**, 5069-5081 (2010 Nov). https://doi.org/10.3168/jds.2010-3346

46 Fornachon JC & Lloyd B. Bacterial production of diacetyl and acetoin in wine. *J Sci Food Agric* **16(12)**, 710-716 (1965 Dec). https://doi.org/10.1002/jsfa.2740161204

47 Li P, Zhu Y, He S, Fan J, Hu Q & Cao Y. Development and Validation of a High-Performance Liquid Chromatography Method for the Determination of Diacetyl in Beer Using 4-Nitro-o-phenylenediamine as the Derivatization Reagent. *J Agric Food Chem* **60(12)**, 3013-3019 (2012 Mar 28). https://doi.org/10.1021/jf3007163

48 Quintans NG, Blancato V, Repizo G, Magni C & López P. *Citrate metabolism and aroma compound production in lactic acid bacteria* (Research Signpost., 2008 Jan).

49 Umbarger HE & Brown B. Isoleucine and Valine Metabolism in *Escherichia coli*. *J Biol Chem* **233(5)**, 1156-1160 (1958 Nov).

50 RG Duggleby & Pang SS. Acetohydroxyacid Synthase. *Journal of Biochemistry and Molecular Biology* **33(1)**, 1-36 (2000 Jan).

51 Yu S, Zheng B, Chen Z & Huo YX. Metabolic engineering of Corynebacterium glutamicum for producing branched chain amino acids (Review). *Microb Cell Fact* **20(1)**, 230 (2021 Dec 24). https://doi.org/10.1186/s12934-021-01721-0

52 Tian H, Jing Y, Yu H, Huang J, Yuan H, Lou X, Wang B, Xu Z & Chen C. Effect of alsD deletion and overexpression of nox and alsS on diacetyl and acetoin production by Lacticaseibacillus casei during milk fermentation. *Journal of Dairy Science* **105(4)**, 2868-2879 (2022 Apr). https://doi.org/10.3168/jds.2021-21163

53 Lerm E, Engelbrecht L & Toit M Du. Malolactic fermentation : the ABC's of MLF. *South African Journal of Enology and Viticulture* **31(2)** (2010). https://doi.org/10.21548/31-2-1417

54 Rhein S. *Die Bedeutung von α-Dicarbonylen in zerebrovaskulaeren Erkrankungen*, (2018).

55 Rhein S, Costalunga R, Inderhees J, Gürtzgen T, Faupel TC, Shaheryar Z, Arrulo Pereira A, Othman A, Begemann K, Binder S, Stölting I, Dorta V, Nawroth PP, Fleming T, Oexle K, Prevot V, Nogueiras R, Meyhöfer S, Meyhöfer SM & Schwaninger M. The reactive pyruvate metabolite

dimethylglyoxal mediates neurological consequences of diabetes. *Nat Commun* **15(1)**, 5745 (2024 Jul 10). https://doi.org/10.1038/s41467-024-50089-3

56 Kitamura T, Seki N & Kihara A. Phytosphingosine degradation pathway includes fatty acid α-oxidation reactions in the endoplasmic reticulum. *Proc Natl Acad Sci U S A* **114(13)**, E2616-E2623 (2017 Mar 28). https://doi.org/10.1073/pnas.1700138114

57 Mori K, Naganuma T & Kihara A. Role of 2-hydroxy acyl-CoA lyase HACL2 in odd-chain fatty acid production via α-oxidation in vivo. *Mol Biol Cell* **34(9)** (2023 Aug 1). https://doi.org/10.1091/mbc.E23-02-0042

58 Asimov A. *The Human Brain - Its Capacities and Functions* (1963).

59 Karamanou M, Protogerou A, Tsoucalas G, Androutsos G & Poulakou-Rebelakou E. Milestones in the history of diabetes mellitus: The main contributors. *World J Diabetes* **7(1)**, 1-7 (2016 Jan 10). https://doi.org/10.4239/wjd.v7.i1.1.

60 Diabetes. (ed World Health Organization) (2024).

61 The top 10 causes of death. (ed World Health Organization) (2024).

62 Bennett DL, Bailyes EM, Nielsen E, Guest PC, Rutherford NG, Arden SD & Hutton JC. Identification of the type 2 proinsulin processing endopeptidase as PC2, a member of the eukaryote subtilisin family. *J Biol Chem* **267(21)**, 15229-15236 (1992 Jul 25).

63 Bailyes EM, Shennan KI, Seal AJ, Smeekens SP, Steiner DF, Hutton JC & Docherty K. A member of the eukaryotic subtilisin family (PC3) has the enzymic properties of the type 1 proinsulin-converting endopeptidase. *Biochem J* **285 (Pt 2)**, 391-394 (1992 Jul 15). https://doi.org/10.1042/bj2850391

64 Insulin. *PubChem*.

65 Mathews CK, Van Holde KE, Dean R, Appling & Anthony-Cahill SJ. *Biochemistry* 4th edn, (Addison Wesley, 2012).

66 Leto D & Saltiel AR. Regulation of glucose transport by insulin: traffic control of GLUT4 (Review). *Nat Rev Mol Cell Biol* **13(6)**, 383-396 (2012 May 23). https://doi.org/10.1038/nrm3351

67 Jumpertz R, Thearle MS, Bunt JC & Krakoff J. Assessment of non-insulin-mediated glucose uptake: association with body fat and glycemic status. *Metabolism* **59(10)**, 1396-1401 (2010 Oct). https://doi.org/10.1016/j.metabol.2010.01.006

68 Pessin JE & Bell GI. Mammalian facilitative glucose transporter family: structure and molecular regulation (Review). *Annu Rev Physiol* **54**, 911-930 (1992). https://doi.org/10.1146/annurev.ph.54.030192.004403

69 Simpson IA, Dwyer D, Malide D, Moley KH, Travis A & Vannucci SJ. The facilitative glucose transporter GLUT3: 20 years of distinction (Review). *Am J Physiol Endocrinol Metab* **295(2)**, E242-253 (2008 Aug). https://doi.org/10.1152/ajpendo.90388.2008

70 Shah K, Desilva S & Abbruscato T. The role of glucose transporters in brain disease: diabetes and Alzheimer's Disease (Review). *Int J Mol Sci* **13(10)**, 12629-12655 (2012 Oct 3). https://doi.org/10.3390/ijms131012629

71 Bakker W, Eringa EC, Sipkema P & Hinsbergh VW van. Endothelial dysfunction and diabetes: roles of hyperglycemia, impaired insulin signaling and obesity (Review). *Cell Tissue Res* **335(1)**, 165-189 (2009 Jan). https://doi.org/10.1007/s00441-008-0685-6

72 Li H, Guglielmetti C, Sei YJ, Zilberter M, Le Page LM, Shields L, Yang J, Nguyen K, Tiret B, Gao X, Bennett N, Lo I, Dayton TL, Kampmann M, Huang Y, Rathmell JC, Vander Heiden M, Chaumeil MM & Nakamura K. Neurons require glucose uptake and glycolysis in vivo. *Cell Rep* **42(4)**, 112335 (2023 Apr 25). https://doi.org/10.1016/j.celrep.2023.112335

73 Bélanger M & Magistretti PJ. The role of astroglia in neuroprotection. *Dialogues Clin Neurosci* **11(3)**, 281-295 (2009). https://doi.org/10.31887/DCNS.2009.11.3/mbelanger

74 Magistretti PJ. Role of glutamate in neuron-glia metabolic coupling. *Am J Clin Nutr.* **90(3)**, 875S-880S (2009 Sep). https://doi.org/10.3945/ajcn.2009.27462CC

75 Mean fasting blood glucose. (ed World Health Organization) (2025).

76 Gillett MJ. International Expert Committee report on the role of the A1c assay in the diagnosis of diabetes: Diabetes Care; 32(7): 1327-1334. *Clin Biochem Rev.* **30(4)**, 197-200 (2009 Nov).

77 American Diabetes Association. Diagnosis and Classification of Diabetes Mellitus (Position Statement). *Diabetes Care* (2010).

78 Katsarou A, Gudbjörnsdottir S, Rawshani A, Dabelea D, Bonifacio E, Anderson BJ, Jacobsen LM, Schatz DA & Lernmark Å. Type 1 diabetes mellitus (Review). *Nat Rev Dis Primers* **3**, 17016 (2017 Mar 30). https://doi.org/10.1038/nrdp.2017.16

79 Thomas NJ, Jones SE, Weedon MN, Shields BM, Oram RA & Hattersley AT. Frequency and phenotype of type 1 diabetes in the first six decades of life: a cross-sectional, genetically stratified survival analysis from UK Biobank. *Lancet Diabetes Endocrinol* **6(2)**, 122-129 (2018 Feb). https://doi.org/10.1016/S2213-8587(17)30362-5

80 Simon K & Wittmann I. Can blood glucose value really be referred to as a metabolic parameter? (Review). *Rev Endocr Metab Disord* **20(2)**, 151-160 (2019 Jun). https://doi.org/10.1007/s11154-019-09504-0

81 2. Classification and Diagnosis of Diabetes (Position Statement). *Diabetes Care* (2014).

82 Martin BC, Warram JH, Krolewski AS, Bergman RN, Soeldner JS & Kahn CR. Role of glucose and insulin resistance in development of type 2 diabetes mellitus: results of a 25-year follow-up study. *Lancet* **340(8825)**, 925-929 (1992 Oct 17). https://doi.org/10.1016/0140-6736(92)92814-v

83 Turner R, Cull C, Stratton I, Manley S, Kohner E, Matthews D, Haw. N, Levy J & Holman R. U.K. Prospective Diabetes Study 16: Overview of 6 Years' Therapy of Type II Diabetes: A Progressive Disease. *Diabetes* **44**, 1249-1258 (1995 Nov 1). https://doi.org/10.2337/diab.44.11.1249

84 Drivsholm T, de Fine Olivarius N, Nielsen AB & Siersma V. Symptoms, signs and complications in newly diagnosed type 2 diabetic patients, and their relationship to glycaemia, blood pressure and weight. *Diabetologia* **48(2)**, 210-214 (2005 Feb). https://doi.org/10.1007/s00125-004-1625-y

85 Diabetes. (World Health Organization, 2013).

86 Wannamethee SG & Shaper AG. Weight change and duration of overweight and obesity in the incidence of type 2 diabetes. *Diabetes Care* **22(8)**, 1266-1272 (1999 Aug). https://doi.org/10.2337/diacare.22.8.1266

87 Ahmad E, Lim S, Lamptey R, Webb DR & Davies MJ. Type 2 diabetes (Review). *The Lancet* **400(10365)**, 1803-1820 (2022 Nov 19). https://doi.org/10.1016/S0140-6736(22)01655-5

88 DeFronzo RA & Goodman AM. Efficacy of metformin in patients with non-insulin-dependent diabetes mellitus. The Multicenter Metformin Study Group. *N Engl J Med* **333(9)** 541-549 (1995 Aug 31). https://doi.org/10.1056/NEJM199508313330902

89 Deshpande AD, Harris-Hayes M & Schootman M. Epidemiology of diabetes and diabetes-related complications (Review). *Phys Ther* **88(11)**, 1254-1264 (2008 Nov). https://doi.org/10.2522/ptj.20080020

90 Fowler MJ. Microvascular and Macrovascular Complications of Diabetes (Review). *Clin Diabetes* **26(2)**, 77–82 (2008 Apr 1). https://doi.org/10.2337/diaclin.26.2.77

91 Vlassara H & Palace MR. Diabetes and advanced glycation endproducts (Review). *J Intern Med* **251(2)**, 87-101 (2002 Feb). https://doi.org/10.1046/j.1365-2796.2002.00932.x

92 Lopes-Virella MF, Klein RL, Lyons TJ, Stevenson HC & Witztum JL. Glycosylation of low-density lipoprotein enhances cholesteryl ester synthesis in human monocyte-derived macrophages. *Diabetes* **37(5)**, 550-557 (1988 May). https://doi.org/10.2337/diab.37.5.550

93 Huijberts MS, Wolffenbuttel BH, Boudier HA, Crijns FR, Kruseman AC, Poitevin P & Lévy BI. Aminoguanidine treatment increases elasticity and decreases fluid filtration of large arteries from diabetic rats. *J Clin Invest* **92(3)**, 1407-1411 (1993 Sep). https://doi.org/10.1172/JCI116716

94 Stracke H, Hammes HP, Werkmann D, Mavrakis K, Bitsch I, Netzel M, Geyer J, Köpcke W, Sauerland C, Bretzel RG & Federlin KF. Efficacy of benfotiamine versus thiamine on function and glycation products of peripheral nerves in diabetic rats. *Exp Clin Endocrinol Diabetes* **109(6)**, 330-336 (2001). https://doi.org/10.1055/s-2001-17399

95 Karachalias N, Babaei-Jadidi R, Ahmed N & Thornalley PJ. Accumulation of fructosyl-lysine and advanced glycation end products in the kidney, retina and peripheral nerve of streptozotocin-

induced diabetic rats (Review). *Biochem Soc Trans* **31(Pt 6)**, 1423-1425 (2003 Dec). https://doi.org/10.1042/bst0311423

96 Vlassara H, Brownlee M & Cerami A. Nonenzymatic glycosylation of peripheral nerve protein in diabetes mellitus. *Proc Natl Acad Sci U S A* **78(8)**, 5190-5192 (1981 Aug). https://doi.org/10.1073/pnas.78.8.5190

97 Sugimoto K, Nishizawa Y, Horiuchi S & Yagihashi S. Localization in human diabetic peripheral nerve of Ne-carboxymethyllysine-protein adducts, an advanced glycation endproduct. *Diabetologia* **40(12)**, 1380-1387 (1997 Dec). https://doi.org/10.1007/s001250050839

98 Allaman I, Bélanger M & Magistretti PJ. Methylglyoxal, the dark side of glycolysis (Review). *Front Neurosci* **9**, 23 (2015 Feb 9). https://doi.org/10.3389/fnins.2015.00023

99 Newington JT, Harris RA & Cumming RC. Reevaluating Metabolism in Alzheimer's Disease from the Perspective of the Astrocyte-Neuron Lactate Shuttle Model (Review). *J Neurodegener Dis* **2013**, 234572 (2013). https://doi.org/10.1155/2013/234572

100 Takeuchi M, Bucala R, Suzuki T, Ohkubo T, Yamazaki M, Koike T, Kameda Y & Makita Z. Neurotoxicity of advanced glycation end-products for cultured cortical neurons. *J Neuropathol Exp Neurol* **59(12)**, 1094-1105 (2000 Dec). https://doi.org/10.1093/jnen/59.12.1094

101 Hiromi Sekido Takeshi Suzuki, Takahito Jomori, Masayoshi Takeuchi, Chihiro Yabe-Nishimura, Soroku Yagihashi. Reduced cell replication and induction of apoptosis by advanced glycation end products in rat Schwann cells. *Biochemical and Biophysical Research Communications* (2004).

102 Xiong F, Leonov S, Howard AC, Xiong S, Zhang B, Mei L, McNeil P, Simon S & Xiong WC. Receptor for Advanced Glycation End Products (RAGE) Prevents Endothelial Cell Membrane Resealing and Regulates F-actin Remodeling in a β-Catenin-dependent Manner. *J Biol Chem* **286(40)**, 35061-35070 (2011 Oct 7). https://doi.org/10.1074/jbc.M111.261073

103 Yan SD, Schmidt AM, Anderson GM, Zhang J, Brett J, Zou YS, Pinsky D & Stern D. Enhanced cellular oxidant stress by the interaction of advanced glycation end products with their receptors/binding proteins. *J Biol Chem* **269(13)**, 9889-9897 (1994 Apr 1).

104 Seno K, Sase S, Ozeki A, Takahashi H, Ohkuchi A, Suzuki H, Matsubara S, Iwata H, Kuwayama T & Shirasuna K. Advanced glycation end products regulate interleukin-1β production in human placenta. *J Reprod Dev* **63(4)**, 401-408 (2017 Aug 19). https://doi.org/10.1262/jrd.2017-032

105 Rashid G, Benchetrit S, Fishman D & Bernheim J. Effect of advanced glycation end-products on gene expression and synthesis of TNF-alpha and endothelial nitric oxide synthase by endothelial cells. *Kidney Int* **66(3)**, 1099-1106 (2004 Sep). https://doi.org/10.1111/j.1523-1755.2004.00860.x

106 Jin X, Yao T, Zhou Z, Zhu J, Zhang S, Hu W & Shen C. Advanced Glycation End Products Enhance Macrophages Polarization into M1 Phenotype through Activating RAGE/NF-κB Pathway. *Biomed Res Int* **2015**, 732450 (2015). https://doi.org/10.1155/2015/732450

107 Kim J, Waldvogel HJ, Faull RL, Curtis MA & Nicholson LF. The RAGE receptor and its ligands are highly expressed in astrocytes in a grade-dependant manner in the striatum and subependymal layer in Huntington's disease. *J Neurochem* **134(5)**, 927-942 (2015 Sep). https://doi.org/10.1111/jnc.13178.

108 Blakytny R & Harding JJ. Prevention of cataract in diabetic rats by aspirin, paracetamol (acetaminophen) and ibuprofen. *Experimental Eye Research* **54(4)**, 509-518 (1992 Apr). https://doi.org/10.1016/0014-4835(92)90129-g

109 Thornalley PJ. Use of aminoguanidine (Pimagedine) to prevent the formation of advanced glycation endproducts (Review). *Arch Biochem Biophys* **419(1)**, 31-40 (2003 Nov 1). https://doi.org/10.1016/j.abb.2003.08.013

110 Hirsch J & Feather MS. Aminoguanidine as an Inhibitor of the Maillard Reaction. *Maillard Reactions in Chemistry, Food and Health*, 325-328 (2005). https://doi.org/10.1533/9781845698393.4.325

111 Lo TW, Selwood T & Thornalley PJ. The reaction of methylglyoxal with aminoguanidine under physiological conditions and prevention of methylglyoxal binding to plasma proteins. *Biochem Pharmacol* **48(10)**, 1865-1870 (1994 Nov 16). https://doi.org/10.1016/0006-2952(94)90584-3

112 Saraiva MA, Borges CM & Florêncio MH. Reactions of Aminoguanidine with α-Dicarbonyl Compounds Studied by Electrospray Ionization Mass Spectrometry. *Eur J Mass Spectrom (Chichester)* **18(4)**, 385-397 (2012). https://doi.org/10.1255/ejms.1191

113 Collaborators GBD 2016 Stroke. Global, regional, and national burden of stroke, 1990-2016: a systematic analysis for the Global Burden of Disease Study 2016. *Lancet Neurol* **18(5)**, 439-458 (2019 May). https://doi.org/10.1016/S1474-4422(19)30034-1

114 Unnithan AKA, Das JM & Mehta P. *Hemorrhagic Stroke*. (StatPearls Publishing, 2023).

115 Lui F, Hui C, Khan Suheb MZ & Patti L. *Ischemic Stroke*. (StatPearls Publishing, 2024).

116 O'Donnell MJ, Xavier D, Liu L, Zhang H, Chin SL, Rao-Melacini P, Rangarajan S, Islam S, Pais P, McQueen MJ, Mondo C, Damasceno A, Lopez-Jaramillo P, Hankey GJ, Dans AL, Yusoff K, Truelsen T, Diener HC, Sacco RL, Ryglewicz D, Czlonkowska A, Weimar C, Wang X, Yusuf S & investigators INTERSTROKE. Risk factors for ischaemic and intracerebral haemorrhagic stroke in 22 countries (the INTERSTROKE study): a case-control study. *Lancet* **376(9735)**, 112-123 (2010 Jul 10). https://doi.org/10.1016/S0140-6736(10)60834-3

117 Melamed E. Reactive hyperglycaemia in patients with acute stroke. *J Neurol Sci* **29(2-4)**, 267-275 (1976 Oct). https://doi.org/ 10.1016/0022-510x(76)90176-3

118 Rhein S, Inderhees J, Herrmann O, Othman A, Begemann K, Fleming T, Nawroth PP, Klika KD, Isa R, König IR, Royl G & Schwaninger M. Glyoxal in hyperglycaemic ischemic stroke - a cohort study. *Cardiovasc Diabetol* **22(1)**, 173 (2023 Jul 12). https://doi.org/10.1186/s12933-023-01892-7

119 Christensen H, Boysen G & Johannesen HH. Serum-cortisol reflects severity and mortality in acute stroke. *J Neurol Sci* **217(2)**, 175-180 (2004 Feb 15). https://doi.org/10.1016/j.jns.2003.09.013

120 Gustavson SM, Chu CA, Nishizawa M, Farmer B, Neal D, Yang Y, Donahue EP, Flakoll P & Cherrington AD. Interaction of glucagon and epinephrine in the control of hepatic glucose production in the conscious dog. *Am J Physiol Endocrinol Metab* **284(4)**, E695-707 (2003 Apr). https://doi.org/10.1152/ajpendo.00308.2002

121 Iversen J. Adrenergic Receptors and the Secretion of Glucagon and Insulin from the Isolated, Perfused Canine Pancreas. *J Clin Invest* **52(9)**, 2102-2116 (1973 Sep). https://doi.org/10.1172/JCI107395

122 Brott T & Bogousslavsky J. Treatment of Acute Ischemic Stroke (Review). *N Engl J Med* **343(10)**, 710-722 (2000 Sep 7). https://doi.org/10.1056/NEJM200009073431007

123 Bruick RK & McKnight SL. A Conserved Family ofProlyl-4-Hydroxylases ThatModify HIF. *Science* **294(5545)**, 1337-1340 (2001 Nov 9). https://doi.org/10.1126/science.1066373

124 Wang GL, Jiang BH, Rue EA & Semenza GL. Hypoxia-inducible factor 1 is a basic-helix-loop-helix-PASheterodimer regulated by cellular 02 tension. *Proc Natl Acad Sci U S A* **92(12)**, 5510-5514 (1995 Jun 6). https://doi.org/10.1073/pnas.92.12.5510

125 Kim JW, Tchernyshyov I, Semenza GL & Dang CV. HIF-1-mediated expression of pyruvate dehydrogenase kinase: A metabolic switch required for cellular adaptation to hypoxia. *Cell Metab* **3(3)**, 177-185 (2006 Mar). https://doi.org/10.1016/j.cmet.2006.02.002

126 Holness MJ & Sugden MC. Regulation of pyruvate dehydrogenase complex activity by reversible phosphorylation (Review). *Biochem Soc Trans* **31(Pt 6)**, 1143-1151 (2003 Dec). https://doi.org/10.1042/bst0311143

127 Gourdin M & Dubois P. *Impact of ischemia on Cellular Metabolism (Chapter 1, Artery Bypass)*. (2013).

128 Abramov AY, Scorziello A & Duchen MR. Three Distinct Mechanisms Generate Oxygen Free Radicals in Neurons and Contribute to Cell Death during Anoxia and Reoxygenation. *J Neurosci* **27(5)**, 1129-1138 (2007 Jan 31). https://doi.org/10.1523/JNEUROSCI.4468-06.2007

129 Zweier JL & Talukder MA. The role of oxidants and free radicals in reperfusion injury (Review). *Cardiovasc Res* **70(2)**, 181-190 (2006 May 1). https://doi.org/10.1016/j.cardiores.2006.02.025

130 Doyle KP, Simon RP & Stenzel-Poore MP. Mechanisms of ischemic brain damage (Review). *Neuropharmacology* **55(3)**, 310-318 (2008 Sep). https://doi.org/10.1016/j.neuropharm.2008.01.005

131 Lipton P. Ischemic cell death in brain neurons (Review). *Physiol Rev* **79(4)**, 1431-1568 (1999 Oct). https://doi.org/10.1152/physrev.1999.79.4.1431

132 Kuehl FA Jr & Egan RW. Prostaglandins, Arachidonic Acid,and Inflammation. *Science* **210(4473)**, 978-984 (1980 Nov 28). https://doi.org/10.1126/science.6254151

133 Hedi H & Norbert G. 5-Lipoxygenase Pathway, Dendritic Cells, and Adaptive Immunity (Review). *J Biomed Biotechnol* **2004(2)**, 99-105 (2004). https://doi.org/10.1155/S1110724304310041

134 Sifat AE, Vaidya B & Abbruscato TJ. Blood-Brain Barrier Protection as a Therapeutic Strategy for Acute Ischemic Stroke (Review). *AAPS J* **19(4)**, 957-972 (2017 Jul). https://doi.org/10.1208/s12248-017-0091-7

135 Jensen AW, Mohanty DK & Dilling WL. The growing relevance of biological ene reactions (Review). *Bioorg Med Chem* **27(5)**, 686-691 (2019 Mar 1). https://doi.org/10.1016/j.bmc.2019.01.020

136 Squadrito GL & Pryor WA. Oxidative chemistry of nitric oxide: the roles of superoxide, peroxynitrite, and carbon dioxide. *Free Radic Biol Med* **25(4-5)**, 392-403 (1998 Sep). https://doi.org/10.1016/s0891-5849(98)00095-1

137 Patel RP, McAndrew J, Sellak H, White CR, Jo H, Freeman BA & Darley-Usmar VM. Biological aspects of reactive nitrogen species (Review). *Biochim Biophys Acta* **1411(2-3)**, 385-400 (1999 May 5). https://doi.org/10.1016/s0005-2728(99)00028-6

138 Salgo MG Squadrito GL & Pryor WA. Peroxynitrite causes apoptosis in rat thymocytes. *Biochem Biophys Res Commun* **215(3)**, 1111-1118 (1995 Oct 24). https://doi.org/10.1006/bbrc.1995.2578

139 Gawdi R Shumway KR & Emmady PD. *Physiology, Blood Brain Barrier*. (2023).

140 Correale J & Villa A. Cellular Elements of the Blood-Brain Barrier (Review). *Neurochem Res* **34(12)**, 2067-2077 (2009 Dec). https://doi.org/10.1007/s11064-009-0081-y

141 Yuan Y, Sun J, Dong Q & Cui M. Blood-brain barrier endothelial cells in neurodegenerative diseases: Signals from the "barrier" (Review). *Front Neurosci* **17**, 1047778 (2023 Feb 24). https://doi.org/10.3389/fnins.2023.1047778

142 Jiao H, Wang Z, Liu Y, Wang P & Xue Y. Specific role of tight junction proteins claudin-5, occludin, and ZO-1 of the blood-brain barrier in a focal cerebral ischemic insult. *J Mol Neurosci* **44(2)**, 130-139 (2011 Jun). https://doi.org/10.1007/s12031-011-9496-4

143 Takata F, Nakagawa S, Matsumoto J & Dohgu S. Blood-Brain Barrier Dysfunction Amplifies the Development of Neuroinflammation: Understanding of Cellular Events in Brain Microvascular Endothelial Cells for Prevention and Treatment of BBB Dysfunction (Review). *Front Cell Neurosci* **15**, 661838 (2021 Sep 13). https://doi.org/10.3389/fncel.2021.661838

144 Puig-Pijoan A, Jimenez-Balado J, Fernández-Lebrero A, García-Escobar G, Navalpotro-Gómez I, Contador J, Manero-Borràs RM, Puente-Periz V, Suárez A, Muñoz FJ, Grau-Rivera O, Suárez-Calvet M, de la Torre R, Roquer J & Ois A. Risk of cognitive decline progression is associated to increased blood-brain-barrier permeability: A longitudinal study in a memory unit clinical cohort. *Alzheimers Dement* **20(1)**, 538-548 (2024 Jan). https://doi.org/10.1002/alz.13433

145 Ettre LS. Nomenclature for chromatography (IUPAC Recommendations 1993). *Pure & Appl. Chem* **65(4)**, 819-872 (1993).

146 Ardrey B. *Liquid Chromatography - Mass Spectrometry: An Introduction* (Wiley, 2003).

147 Kostiainen R & Kauppila TJ. Effect of eluent on the ionization process in liquid chromatography–mass spectrometry (Review). *J Chromatogr A* **1216(4)**, 685-699 (2009 Jan 23). https://doi.org/10.1016/j.chroma.2008.08.095

148 Konermann L, Ahadi E, Rodriguez AD & Vahidi S. Unraveling the Mechanism of Electrospray Ionization. *Anal Chem* **85(1)**, 2-9 (2013 Jan 2). https://doi.org/10.1021/ac302789c

149 Covey TR, Thomson BA & Schneider BB. Atmospheric pressure ion sources (Review). *Mass Spectrom Rev* **28(6)**, 870-897 (2009 Nov-Dec). https://doi.org/10.1002/mas.20246

150 Banerjee S & Mazumdar S. Electrospray Ionization Mass Spectrometry: A Technique to Access the Information beyond the Molecular Weight of the Analyte (Review). *Int J Anal Chem* **2012**, 282574 (2012). https://doi.org/10.1155/2012/282574.

151 Murray KK, Boyd RK, Eberlin MN, Langley GJ, Li L & YNaito. Definitions of terms relating to massspectrometry (IUPAC Recommendations 2013). *Pure Appl. Chem* **85(7)**, 1515–1609 (2013 Jun 6).

152 KM. Wooding & Auchus RJ. Mass spectrometry theory and application to adrenal diseases (Review). *Mol Cell Endocrinol* **371(1-2)**, 201-207 (2013 May 22). https://doi.org/10.1016/j.mce.2012.12.026

153 Yost RA. The triple quadrupole: Innovation, serendipity and persistence *J Mass Spectrom Adv Clin Lab* **24**, 90-99 (2022 May 10). https://doi.org/10.1016/j.jmsacl.2022.05.001

154 Michalski A, Damoc E, Hauschild JP, Lange O, Wieghaus A, Makarov A, Nagaraj N, Cox J, Mann M & Horning S. Mass Spectrometry-based Proteomics Using Q Exactive, a High-performance Benchtop Quadrupole Orbitrap Mass Spectrometer. *Mol Cell Proteomics* **10(9)**, M111.011015 (2011 Sep). https://doi.org/10.1074/mcp.M111.011015

155 Olsen JV, Schwartz JC, Griep-Raming J, Nielsen ML, Damoc E, Denisov E, Lange O, Remes P, Taylor D, Splendore M, Wouters ER, Senko M, Makarov A, Mann M & Horning S. A Dual Pressure Linear Ion Trap Orbitrap Instrument with Very High Sequencing Speed. *Mol Cell Proteomics* **8(12)**, 2759-2769 (2009 Dec). https://doi.org/10.1074/mcp.M900375-MCP200

156 Improved Sensitivity Through Enhanced Ion Transmission Using an S-Lens on the LTQ Velos Linear Ion Trap. (ed Thermo Fischer) (2009).

157 Olsen JV, Macek B, Lange O, Makarov A, Horning S & Mann M. Higher-energy C-trap dissociation for peptide modification analysis. *Nat Methods* **4(9)**, 709-712 (2007 Sep). https://doi.org/10.1038/nmeth1060

158 Zubarev RA & Makarov A. Orbitrap Mass Spectrometry. *Anal Chem* **85(11)**, 5288-5296 (2013 Jun 4). https://doi.org/10.1021/ac4001223

159 Rauniyar N. Parallel Reaction Monitoring: A Targeted Experiment Performed Using High Resolution and High Mass Accuracy Mass Spectrometry (Review). *Int J Mol Sci* **16(12)**, 28566-28581 (2015 Dec 2). https://doi.org/10.3390/ijms161226120

160 Beisswenger PJ, Howell SK, Smith K & Szwergold BS. Glyceraldehyde-3-phosphate dehydrogenase activity as an independent modifier of methylglyoxal levels in diabetes. *Biochim Biophys Acta* **1637(1)** 98-106 (2003 Jan 20). https://doi.org/10.1016/s09254439(02)00219-3

161 Khan MA, Schultz S, Othman A, Fleming T, Lebrón-Galán R, Rades D, Clemente D, Nawroth PP & Schwaninger M. Hyperglycemia in Stroke Impairs Polarization of Monocytes/Macrophages to a Protective Noninflammatory Cell Type. *J Neurosci* **36(36)**, 9313-9325 (2016 Sep 7). https://doi.org/10.1523/JNEUROSCI.0473-16.2016

162 Aden DP, Fogel A, Plotkin S, Damjanov I & Knowles BB. Controlled synthesis of HBsAg in a differentiated human liver carcinoma-derived cell line. *Nature* **282(5739)**, 615-616 (1979 Dec 6). https://doi.org/10.1038/282615a0

163 Rossini AA, Like AA, Chick WL, Appel MC & Cahill GF. Studies of streptozotocin-induced insulitis and diabetes. *Proc Natl Acad Sci U S A* **74(6)**, 2485-2489 (1977 Jun). https://doi.org/10.1073/pnas.74.6.2485

164 Bolzán AD & Bianchi MS. Genotoxicity of Streptozotocin. *Mutat Res* **512(2-3)**, 121-134 (2002 Dec). https://doi.org/10.1016/s1383-5742(02)00044-3

165 Furman BL. Streptozotocin-Induced Diabetic Models in Mice and Rats. *Curr Protoc Pharmacol* **70**, 5.47.41-45.47.20 (2015 Sep 1). https://doi.org/10.1002/0471141755.ph0547s70

166 Fujii J, Homma T, Miyata S & Takahashi M. Pleiotropic Actions of Aldehyde Reductase (AKR1A). *Metabolites* **11(6)**, 343 (2021 May 26). https://doi.org/10.3390/metabo11060343

167 Sachdeva R, Schlotterer A, Schumacher D, Matka C, Mathar I, Dietrich N, Medert R, Kriebs U, Lin J, Nawroth P, Birnbaumer L, Fleming T, Hammes HP & Freichel M. TRPC proteins contribute to development of diabetic retinopathy and regulate glyoxalase 1 activity and methylglyoxal accumulation. *Mol Metab* **9**, 156-167 (2018 Mar). https://doi.org/10.1016/j.molmet.2018.01.003

168 Kobayashi K, Forte TM, Taniguchi S, Ishida BY, Oka K & Chan L. The db/db mouse, a model for diabetic dyslipidemia: Molecular characterization and effects of western diet feeding. *Metabolism* **49(1)**, 22-31 (2000 Jan). https://doi.org/10.1016/s0026-0495(00)90588-2

169 Lang P, Hasselwander S, Li H & Xia N. Effects of different diets used in diet-induced obesity models on insulin resistance and vascular dysfunction in C57BL/6 mice. *Sci Rep* **9(1)**, 19556 (2019 Dec 20). https://doi.org/10.1038/s41598-019-55987-x

170 Henderson AR. Biochemistry of hypoxia: current concepts. I. An introduction to biochemical pathways and their control. *Br J Anaesth* **41(3)**, 245-250 (1969 Mar). https://doi.org/10.1093/bja/41.3.245

171 Greijer AE, van der Groep P, Kemming D, Shvarts A, Semenza GL, Meijer GA, van de Wiel MA, Belien JA, van Diest PJ & Wall E van der. Up-regulation of gene expression by hypoxia is mediated predominantly by hypoxia-inducible factor 1 (HIF-1). *J Pathol* **206(3)**, 291-304 (2005 Jul). https://doi.org/10.1002/path.1778

172 Wang Y, Sun W, Zheng S, Zhang Y & Bao Y. Genetic engineering of Bacillus sp. and fermentation process optimizing for diacetyl production. *J Biotechnol* **301**, 2-10 (2019 Aug 10). https://doi.org/10.1016/j.jbiotec.2019.05.308

173 Chellan P & Nagaraj RH. Protein crosslinking by the Maillard reaction: dicarbonyl-derived imidazolium crosslinks in aging and diabetes. *Arch Biochem Biophys* **368(1)**, 98-104 (1999 Aug 1). https://doi.org/10.1006/abbi.1999.1291

174 Thornalley PJ. Protein and nucleotide damage by glyoxal and methylglyoxal in physiological systems--role in ageing and disease. *Drug Metabol Drug Interact* **23(1-2)**, 125-150 (2008). https://doi.org/10.1515/dmdi.2008.23.1-2.125

175 Lawless HT, Antinone MJ, Ledford RA & Johnston M. Olfactory responsiveness to diacetyl. *Journal of Sensory Studies* **9(1)**, 47-56 (1993). https://doi.org/10.1111/j.1745-459X.1994.tb00229.x

176 Seals RG & Hammond EG. Diacetyl as the Buttery Flavor Component in Soybean Oil. *Journal of the American Oil Chemists Society* **43**, 401-402 (1966).

177 Seo K, Ki SH & Shin SM. Methylglyoxal Induces Mitochondrial Dysfunction and Cell Death in Liver. *Toxicol Res* **30(3)**, 193-198 (2014 Sep). https://doi.org/10.5487/TR.2014.30.3.193

178 Wada R & Yagihashi S. Role of advanced glycation end products and their receptors in development of diabetic neuropathy (Review). *Ann N Y Acad Sci* **1043**, 598-604 (2005 Jun). https://doi.org/10.1196/annals.1338.067

179 Beisswenger PJ, Makita Z, Curphey TJ, Moore LL, Jean S, Brinck-Johnsen T, Bucala R & Vlassara H. Formation of Immunochemical Advanced Glycosylation End Products Precedes and Correlates With Early Manifestations of Renal and Retinal Disease in Diabetes. *Diabetes* **44(7)**, 824–829 (1995 Jul 01). https://doi.org/https://doi.org/10.2337/diab.44.7.824

180 Oliveira AL, Medeiros ML, Ghezzi AC, Dos Santos GA, Mello GC, Mónica FZ & Antunes E. Evidence that methylglyoxal and receptor for advanced glycation end products are implicated in bladder dysfunction of obese diabetic ob/ob mice. *Am J Physiol Renal Physiol* **325(4)**, F436-F447 (2023 Oct 1). https://doi.org/10.1152/ajprenal.00089.2023

181 Sullivan MA & Forbes JM. Glucose and glycogen in the diabetic kidney: Heroes or villains? (Review). *EBioMedicine* **47**, 590-597 (2019 Sep). https://doi.org/10.1016/j.ebiom.2019.07.067

182 Cortizo FG, Pfaff D, Wirth A, Schlotterer A, Medert R, Morgenstern J, Weber T, Hammes HP, Fleming T, Nawroth PP, Freichel M & Teleman AA. The activity of glyoxylase 1 is regulated by glucose-responsive phosphorylation on Tyr136. *Mol Metab* **55**, 101406 (2022 Jan). https://doi.org/10.1016/j.molmet.2021.101406

183 Reyaz A, Alam S, Chandra K, Kohli S & Agarwal S. Methylglyoxal and soluble RAGE in type 2 diabetes mellitus: Association with oxidative stress. *J Diabetes Metab Disord* **19(1)**, 515-521 (2020 May 12). https://doi.org/10.1007/s40200-020-00543-y

184 Chen J, Feng Q, Qiao Y, Pan S, Liang L, Liu Y, Zhang X, Liu D, Liu Z & Liu Z. ACSF2 and lysine lactylation contribute to renal tubule injury in diabetes. *Diabetologia* **67(7)**, 1429-1443 (2024). https://doi.org/10.1007/s00125-024-06156-x

185 Ma YL, Ke JF, Wang JW, Wang YJ, Xu MR & Li LX. Blood lactate levels are associated with an increased risk of metabolic dysfunction-associated fatty liver disease in type 2 diabetes: a real-world study. *Front Endocrinol (Lausanne)* **14**, 1133991 (2023 May 8). https://doi.org/10.3389/fendo.2023.1133991

186 Zhang F, Xu X, Zhang Y, Zhou B, He Z & Zhai Q. Gene Expression Profile Analysis of Type 2 Diabetic Mouse Liver. *PLoS One* **8(3)**, e57766 (2013). https://doi.org/10.1371/journal.pone.0057766

187 Ghimenti S, Tabucchi S, Lomonaco T, Di Francesco F, Fuoco R, Onor M, Lenzi S & Trivella MG. Monitoring breath during oral glucose tolerance tests. *J Breath Res* **7(1)**, 017115 (2013 Mar). https://doi.org/10.1088/1752-7155/7/1/017115

188 Van den Eynde MDG, Kusters YHAM, Houben AJHM, Scheijen JLJM, van Duynhoven J, Fazelzadeh P, Joris PJ, Plat J, Mensink RP, Hanssen NMJ, Stehouwer CDA & Schalkwijk CG. Diet-induced weight loss reduces postprandial dicarbonyl stress in abdominally obese men: Secondary analysis of a randomized controlled trial. *Clin Nutr* **40(5)**, 2654-2662 (2021 May). https://doi.org/10.1016/j.clnu.2021.03.042

189 Winzell MS & Ahrén B. The high-fat diet-fed mouse: a model for studying mechanisms and treatment of impaired glucose tolerance and type 2 diabetes. *Diabetes* **53(3)** (2004 Dec). https://doi.org/10.2337/diabetes.53.suppl_3.s215

190 INRAE-CIRAD-AFZ. *Lard - Feed table*, <https://www.feedtables.com/content/lard> (2025).

191 Watanabe T, Shirai N, Okada H, Honda Y & Kuwahara M. Production and chemiluminescent free radical reactions of glyoxal in lipid peroxidation of linoleic acid by the ligninolytic enzyme, manganese peroxidase. *Eur J Biochem* **268(23)**, 6114-6122 (2001 Dec). https://doi.org/10.1046/j.0014-2956.2001.02557.x

192 Finkielstein VA & Goldfarb DS. Strategies for preventing calcium oxalate stones. *CMAJ* **174(10)**, 1407-1409 (2006 May 9). https://doi.org/10.1503/cmaj.051517

193 Guo T, Kong J, Zhang L, Zhang C & Hu S. Fine Tuning of the Lactate and Diacetyl Production through Promoter Engineering in Lactococcus lactis. *PLoS One* **7(4)**, e36296 (2012). https://doi.org/10.1371/journal.pone.0036296

194 Lasik-Kurdyś M, Majcher M & Nowak J. Effects of Different Techniques of Malolactic Fermentation Induction on Diacetyl Metabolism and Biosynthesis of Selected Aromatic Esters in Cool-Climate GrapeWines. *Molecules* **23(10)**, 2549 (2018 Oct 6). https://doi.org/10.3390/molecules23102549

195 Gao X, Xu N, Li S & Liu L. Metabolic Engineering of Candida glabrata for Diacetyl Production. *PLoS One* **9(3)**, e89854 (2014 Mar 10). https://doi.org/10.1371/journal.pone.0089854

196 Berends E, van Oostenbrugge RJ, Foulquier S & Schalkwijk CG. Methylglyoxal, a highly reactive dicarbonyl compound, as a threat for blood brain barrier integrity (Review). *Fluids Barriers CNS* **20(1)**, 75 (2023 Oct 24). https://doi.org/10.1186/s12987-023-00477-6

197 Kim ES, Kim KS, Lee CH, Jeon MT, Lee SB, Lee JH & Kim DG. Brain Endothelial Cells Utilize Glycolysis for the Maintenance of the Transcellular Permeability. *Mol Neurobiol* **59(7)**, 4315-4333 (2022 Jul). https://doi.org/10.1007/s12035-022-02778-7

198 Manosalva C, Quiroga J, Hidalgo AI, Alarcón P, Anseoleaga N, Hidalgo MA & Burgos RA. Role of Lactate in Inflammatory Processes: Friend or Foe (Review). *Front Immunol* **12**, 808799 (2022 Jan 14). https://doi.org/10.3389/fimmu.2021.808799

199 Patet C, Suys T, Carteron L & Oddo M. Cerebral Lactate Metabolism After Traumatic Brain Injury (Review). *Curr Neurol Neurosci Rep* **16(4)**, 31 (2016 Apr). https://doi.org/10.1007/s11910-016-0638-5

200 Yamagata K. Lactate Supply from Astrocytes to Neurons and its Role in Ischemic Stroke-induced Neurodegeneration (Review). *Neuroscience* **481**, 219-231 (2022 Jan 15). https://doi.org/10.1016/j.neuroscience.2021.11.035

201 Jourdain P, Allaman I, Rothenfusser K, Fiumelli H, Marquet P & PJMagistretti. L-Lactate protects neurons against excitotoxicity: implication of an ATP-mediated signaling cascade. *Sci Rep* **6**, 21250 (2016 Feb 19). https://doi.org/10.1038/srep21250

202 Ruan L, Wang Y, Chen SC, Zhao T, Huang Q, Hu ZL, Xia NZ, Liu JJ, Chen WJ, Zhang Y, Cheng JL, Gao HC, Yang YJ & Sun HZ. Metabolite changes in the ipsilateral and contralateral cerebral hemispheres in rats with middle cerebral artery occlusion. *Neural Regen Res* **12(6)**, 931-937 (2017 Jun). https://doi.org/10.4103/1673-5374.208575

203 Hu ZL, Xia HH, Yang YJ, Zheng H, Zhao LC, Chen YC, Zhuge QC, Xia NZ, Gao HC & Chen WJ. Metabolic alterations in the rat cerebellum following acute middle cerebral artery occlusion, as determined by 1H NMR spectroscopy. *Mol Med Rep* **17(1)**, 531-541 (2018 Jan). https://doi.org/10.3892/mmr.2017.7918

204 Dorau R, Chen L, Liu J, Jensen PR & Solem C. Efficient production of α-acetolactate by whole cell catalytic transformation of fermentation-derived pyruvate. *Microb Cell Fact* **18(1)**, 217 (2019 Dec 29). https://doi.org/10.1186/s12934-019-1271-1

205 Fan Y & Pedersen O. Gut microbiota in human metabolic health and disease (Review). *Nat Rev Microbiol* **19(1)**, 55-71 (2021 Jan). https://doi.org/10.1038/s41579-020-0433-9

206 Arrieta MC, Walter J & Finlay BB. Human Microbiota-Associated Mice: A Model with Challenges (Forum). *Cell Host Microbe* **19(5)**, 575-578 (2016 May 11). https://doi.org/10.1016/j.chom.2016.04.014

207 Hou K, Wu ZX, Chen XY, Wang JQ, Zhang D, Xiao C, Zhu D, Koya JB, Wei L, Li J & Chen ZS. Microbiota in health and diseases (Review). *Signal Transduct Target Ther* **7(1)**, 135 (2022 Apr 23). https://doi.org/10.1038/s41392-022-00974-4

208 Zhang L, Zhang Y, Liu Q, Meng L, Hu M, Lv M, Li K, Gao C, Xu P & Ma C. Production of diacetyl by metabolically engineered Enterobacter cloacae. *Sci Rep* **5**, 9033 (2015 Mar 12). https://doi.org/10.1038/srep09033

209 Lindsay T.W. Keenan and R.C. Diacetyl Production and Utilization by Lactobacillus Species. *Journal of Dairy Science* (1968).

210 Speckman RA & Collins EB. Diacetyl Biosynthesis in Streptococcus diacetilactis and Leuconostoc citrovorum. *J Bacteriol* **95(1)**, 174-180 (1968 Jan). https://doi.org/10.1128/jb.95.1.174-180.1968

211 Delgado-Ocaña S & S S Cuesta. From microbes to mind: germ-free models in neuropsychiatric research (Minireview). *mBio* **15**, e02075-02024 (2024). https://doi.org/https://doi.org/10.1128/mbio.02075-24

212 Braniste V, Al-Asmakh M, Kowal C Anuar F, Abbaspour A, Tóth M, Korecka A, Bakocevic N, Ng LG, Kundu P, Gulyás B, Halldin C, Hultenby K, Nilsson H, Hebert H, Volpe BT, Diamond B & Pettersson S. The gut microbiota influences blood-brain barrier permeability in mice. *Sci Transl Med* **6(263)**, 263ra158 (2014 Nov 19). https://doi.org/10.1126/scitranslmed.3009759

213 Shin MG, Lee JW, Han JS, Lee B, Jeong JH, Park SH, Kim JH, Jang S, Park M, Kim SY, Kim S, Yang YR, Kim JY, Hoe KL, Park C, Lee KP, Kwon KS & Kwon ES. Bacteria-derived metabolite, methylglyoxal, modulates the longevity of C. elegans through TORC2/SGK-1/ DAF-16 signaling. *Proc Natl Acad Sci U S A* **117(29)**, 17142-17150 (2020 Jul 21). https://doi.org/10.1073/pnas.1915719117

214 Le Bars D & Yvon M. Formation of diacetyl and acetoin by Lactococcus lactis via aspartate catabolism. *J Appl Microbiol* **104(1)**, 171-177 (2008 Jan). https://doi.org/10.1111/j.1365-2672.2007.03539.x

215 Jo M, Kim JH, Song GJ, Seo M, Hwang EM & Suk K. Astrocytic Orosomucoid-2 Modulates Microglial Activation and Neuroinflammation. *J Neurosci* **37(11)**, 2878-2894 (2017 Mar 15). https://doi.org/10.1523/JNEUROSCI.2534-16.2017

216 Ruiz M. Into the Labyrinth of the Lipocalin α1-Acid Glycoprotein (Review). *Front Physiol* **12**, 686251 (2021 Jun 8). https://doi.org/10.3389/fphys.2021.686251

217 Zhou B, Luo Y, Ji N, Hu C & Lu Y. Orosomucoid 2 maintains hepatic lipid homeostasis through suppression of de novo lipogenesis. *Nat Metab* **4(9)**, 1185-1201 (2022 Sep). https://doi.org/10.1038/s42255-022-00627-4

218 Rabbani N, Xue M & Thornalley PJ. *Chapter 36 - Dicarbonyl stress and the glyoxalase system - Oxidative Stress*. (2020).

219 Hooper DL. Nuclear Magnetic Resonance Measurements of Equilibria involving Hydration and Hemiacetal Formation from Some Carbonyl Compounds. *J. Chem. Soc. B* **0**, 169-170 (1967). https://doi.org/10.1039/J29670000169

220 Sibbersen C & Johannsen M. Dicarbonyl derived post-translational modifications: chemistry bridging biology and aging-related disease (Review). *Essays Biochem* **64(1)**, 97-110 (2020 Feb 17). https://doi.org/10.1042/EBC20190057

221 Barros LF. Metabolic signaling by lactate in the brain. *Trends Neurosci* **36(7)**, 396-404 (2013 Jul). https://doi.org/10.1016/j.tins.2013.04.002

222 Piras S, Furfaro AL, Domenicotti C, Traverso N, Marinari UM, Pronzato MA & Nitti M. RAGE Expression and ROS Generation in Neurons: Differentiation versus Damage (Review). *Oxid Med Cell Longev* **2016**, 9348651 (2016). https://doi.org/10.1155/2016/9348651

223 Wautier MP, Chappey O, Corda S, Stern DM, Schmidt AM & Wautier JL. Activation of NADPH oxidase by AGE links oxidant stress to altered gene expression via RAGE. *Am J Physiol Endocrinol Metab* **280(5)**, E685-694 (2001 May). https://doi.org/10.1152/ajpendo.2001.280.5.E685

224 Clark RA & Valente AJ. Nuclear factor kappa B activation by NADPH oxidases. *Mech Ageing Dev* **125(10-11)**, 799-810 (2004 Oct-Nov). https://doi.org/10.1016/j.mad.2004.08.009

225 Simon LS. Role and regulation of cyclooxygenase-2 during inflammation. *The American Journal of Medicine* **106(5)**, 37S-42S (1999). https://doi.org/10.1016/S0002-9343(99)00115-1

226 Fenske R, Weeks A, Brill A, Nall R, Pabitch S, Punt M, Daniels M, Blaha S, Davis DB & Kimple M. Prostaglandin E2 (PGE2) Levels As a Predictor of Type 2 Diabetes Control in Human Subjects: A cross-sectional view of initial cohort study data. *The FASEB Journal* **31(S1)**, 675.676-675.676 (2017 Apr). https://doi.org/10.1096/fasebj.31.1_supplement.675.6

227 Ying L, Shen Y, Zhang Y, Wang Y, Liu Y, Yin J, Wang Y, Yin J, Zhu W, Bao Y & Zhou J. Association of advanced glycation end products with diabetic retinopathy in type 2 diabetes mellitus. *Diabetes Res Clin Pract* **177**, 108880 (2021 Jul). https://doi.org/10.1016/j.diabres.2021.108880

228 Zong H, Ward M & Stitt AW. AGEs, RAGE, and Diabetic Retinopathy (Review). *Curr Diab Rep* **11(4)**, 244-252 (2011 Aug). https://doi.org/10.1007/s11892-011-0198-7

229 Biswas SC, Shi Y, Vonsattel JP, Leung CL, Troy CM & Greene LA. Bim Is Elevated in Alzheimer's Disease Neurons and Is Required for β-Amyloid-Induced Neuronal Apoptosis. *J Neurosci* **27(4)**, 893-900 (2007 Jan 24). https://doi.org/10.1523/JNEUROSCI.3524-06.2007

230 Sasaki N, Fukatsu R, Tsuzuki K, Hayashi Y, Yoshida T, Fujii N, Koike T, Wakayama I, Yanagihara R, Garruto R, Amano N & Makita Z. Advanced Glycation End Products in Alzheimer's Disease and Other Neurodegenerative Diseases. *Am J Pathol* **153(4)**, 1149-1155 (1998 Oct). https://doi.org/10.1016/S0002-9440(10)65659-3

231 Cao F, Yang F, Li J, Guo W, Zhang C, Gao F, Sun X, Zhou Y & Zhang W. The relationship between diabetes and the dementia risk: a meta-analysis (Review). *Diabetol Metab Syndr* **16(1)**, 101 (2024 May 14). https://doi.org/10.1186/s13098-024-01346-4

232 Xue M, Xu W, Ou YN, Cao XP, Tan MS, Tan L & Yu JT. Diabetes mellitus and risks of cognitive impairment and dementia: A systematic review and meta-analysis of 144 prospective studies. *Ageing Res Rev* **55**, 100944 (2019 Nov). https://doi.org/10.1016/j.arr.2019.100944

233 Cheng G, Huang C, Deng H & Wang H. Diabetes as a risk factor for dementia and mild cognitive impairment: a meta-analysis of longitudinal studies. *Intern Med J* **42(5)**, 484-491 (2012 May). https://doi.org/10.1111/j.1445-5994.2012.02758.x

234 Foretz M, Guigas B & Viollet B. Metformin: update on mechanisms of action and repurposing potential (Review). *Nat Rev Endocrinol* **19(8)**, 460-476 (2023 Aug). https://doi.org/10.1038/s41574-023-00833-4

235 Ghosal S & Ghosal S. The Side Effects of Metformin - A Review. *J Diabetes Metab Disord* **6**, 030 (2019). https://doi.org/10.24966/DMD-201X/100030

236 Rendell M, Nierenberg J, Brannan C, Valentine JL, Stephen PM, Dodds S, Mercer P, Smith PK & Walder J. Inhibition of glycation of albumin and hemoglobin by acetylation in vitro and in vivo. *J Lab Clin Med* **108(4)**, 286-293 (1986 Oct).

237 Zhoua Q, Liu W, Zhanga Y & Liu KK. Action mechanisms of acetolactate synthase-inhibiting herbicides (Review). *Pesticide Biochemistry and Physiology* **89(2)** (2007 Oct). https://doi.org/10.1016/j.pestbp.2007.04.004

238 Gürtzgen T. *Ursprung und Bedeutung von Diacetyl im hyperglykämischen Stoffwechsel*, (2023).

239 Lupidi G, Bollettini M, Venardi G, Marmocchi F & Rotilio G. Functional residues on the enzyme active site of glyoxalase I from bovine brain. *Prep Biochem Biotechnol* **31(3)**, 317-329 (2001 Aug). https://doi.org/10.1081/PB-100104912

240 Nakagawa J, Ishikura S, Asami J, Isaji T, Usami N, Hara A, Sakurai T, Tsuritani K, Oda K, Takahashi M, Yoshimoto M, Otsuka N & Kitamura K. Molecular Characterization of Mammalian Dicarbonyl/l-Xylulose Reductase and Its Localization in Kidney. *The Journal of Biological Chemistry* **277(20)**, 17883-17891 (2002 May 17). https://doi.org/10.1074/jbc.M110703200

241 Pierce SB, Spurrell CH, Mandell JB, Lee MK, Zeligson S, Bereman MS, Stray SM, Fokstuen S, MacCoss MJ, Levy-Lahad E, King MC & Motulsky AG. Garrod's fourth inborn error of metabolism solved by the identification of mutations causing pentosuria. *Proc Natl Acad Sci U S A* **108(45)**, 18313-18317 (2011 Nov 8). https://doi.org/10.1073/pnas.1115888108

242 Lane AB. On the Nature of L-Xylulose Reductase Deficiency in Essential Pentosuria. *Biochem Genet* **23(1-2)**, 61-72 (1985 Feb). https://doi.org/10.1007/BF00499113

243 Ishikura S, Isaji T, Usami N, Nakagawa J, El-Kabbani O & Hara A. Identification of amino acid residues involved in substrate recognition of L-xylulose reductase by site-directed mutagenesis. *Chem Biol Interact* **143-144**, 543-550 (2003 Feb 1). https://doi.org/10.1016/s0009-2797(02)00217-x

244 Gabriel MA, Jabara H & al-Khalidi UA. Metabolism of Acetoin in Mammalian Liver Slices and Extracts. *Biochem J* **124(4)**, 793-800 (1971 Oct). https://doi.org/10.1042/bj1240793

245 Julica Inderhees Riccardo Costalunga and Markus Schwaninger. Dimethylglyoxal (diacetyl), a reactive pyruvate metabolite produced in diabetes. *Neural Regeneration Research* (Submitted).

Publications

2024 | Rhein S*, **Costalunga R***, Inderhees J*, Gürtzgen T, Faupel TC, Shaheryar Z, Arrulo Pereira A, Othman A, Begemann K, Binder S, Stölting I, Dorta V, Nawroth PP, Fleming T, Oexle K, Prevot V, Nogueiras R, Meyhöfer S, Meyhöfer SM, Schwaninger M. The reactive pyruvate metabolite dimethylglyoxal mediates neurological consequences of diabetes. Nat Commun. 2024 Jul 10;15(1):5745. doi: 10.1038/s41467-024-50089-3.

*Shared first authorship

2022 | **Costalunga R**, Tshepelevitsh S, Sepman H, Kull M, Kruve A. Sodium adduct formation with graph-based machine learning can aid structural elucidation in non-targeted LC/ESI/HRMS. Anal Chim Acta. 2022 Apr 29;1204:339402. doi: 10.1016/j.aca.2021.339402.

Eidesstattliche Erklärung

Hiermit versichere ich an Eides statt, dass ich die vorliegende Dissertation ohne fremde Hilfe und ohne Benutzung anderer als der angegebenen Quellen und Hilfsmittel angefertigt und die den benutzten Quellen wörtlich oder inhaltlich entnommenen Stellen als solche kenntlich gemacht habe. Diese Arbeit wurde in gleicher oder ähnlicher Form.

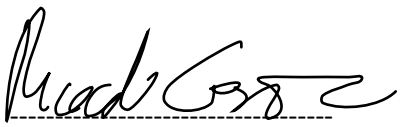

Acknowledgement

First, I sincerely thank Prof. Schwaninger for allowing me to conduct my doctoral studies in his lab and for his trust in me and support during the last four years. His insight and enthusiasm were a beacon of inspiration to me over the years, especially during the revision of our manuscript. He taught me several abilities, such as designing and managing an experiment.

I also would like to express my gratitude to Dr. Inderhees for her support and mentorship, characterized by kindness, empathy and knowledge. She taught me crucial skills, from competence in acting in the laboratory to theoretical and practical knowledge of mass spectrometry.

In addition to my supervisors, I would like to acknowledge Ines, Zaib, Teresa, Sonja, Frauke, Adriana, and Ümit for their help and support in the realization of the current thesis during these years. I also would like to thank Prof. Jöhren for his contribution to funding this project and Prof. Uetrecht for being available as a second thesis referee. Moreover, I am grateful to my friends and colleagues with whom I spent my doctoral experience, both inside the lab and during trips around the world.

In particular, I am extremely grateful to my parents, my brother Alessandro and his family, and my grandmother Vanda for their lovely support during these years, even though they are physically distant. They have always believed in my personal and professional abilities and protected me from unfairness during difficult times. I heartily thank Adriana for her support and closeness throughout the thesis writing period. I am really grateful for her daily kindness and presence.